USGS
science for a changing world

Groundwater Availability and Use Assessments

Prepared in cooperation with Santa Barbara County Water Agency and Vandenberg Space Force Base

Simulation of Groundwater and Surface-Water Resources of the San Antonio Creek Valley Watershed, Santa Barbara County, California

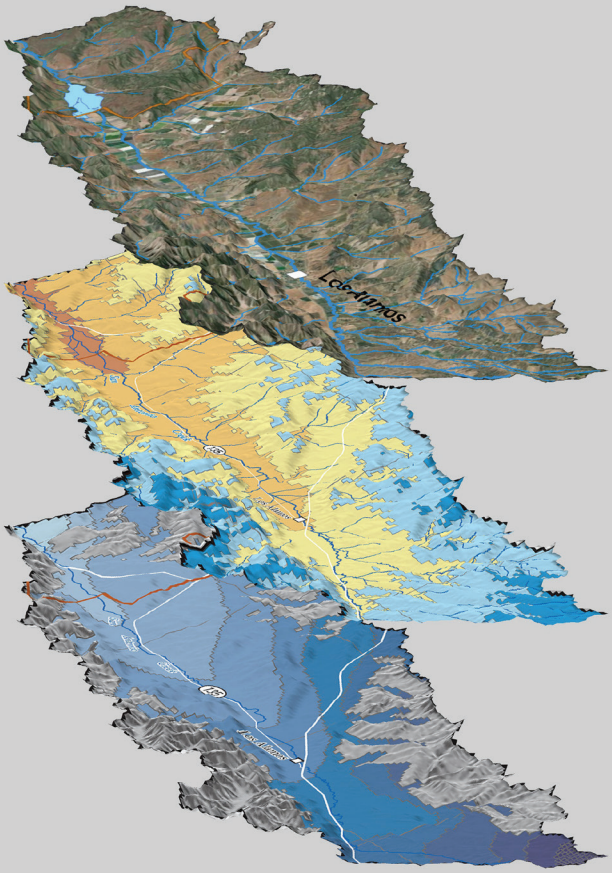

Scientific Investigations Report 2021–5139

U.S. Department of the Interior
U.S. Geological Survey

Cover: Visualization of the simulated domain and hydrologic components from the San Antonio Creek Integrated Model.

Simulation of Groundwater and Surface-Water Resources of the San Antonio Creek Valley Watershed, Santa Barbara County, California

By Linda R. Woolfenden, John A. Engott, Joshua D. Larsen, and Geoffrey Cromwell

Groundwater Availability and Use Assessments

Prepared in cooperation with Santa Barbara County Water Agency and Vandenberg Space Force Base

Scientific Investigations Report 2021–5139

U.S. Geological Survey, Reston, Virginia: 2022

For more information on the USGS—the Federal source for science about the Earth, its natural and living resources, natural hazards, and the environment—visit https://www.usgs.gov or call 1–888–ASK–USGS.

For an overview of USGS information products, including maps, imagery, and publications, visit https://store.usgs.gov/.

Suggested citation:
Woolfenden, L.R., Engott, J.A., Larsen, J.D., and Cromwell, G., 2022, Simulation of groundwater and surface-water resources of the San Antonio Creek Valley Watershed, Santa Barbara County, California: U.S. Geological Survey Scientific Investigations Report 2021–5139, 76 p., https://doi.org/10.3133/sir20215139.

Associated data for this publication:
Woolfenden, L.R., Engott, J.A., and Larsen, J.D., 2022, GSFLOW model used to evaluate the groundwater and surface-water resources of the San Antonio Creek Valley watershed, Santa Barbara County, California: U.S. Geological Survey data release, https://doi.org/10.5066/P960EOK8.

ISSN 2328-0328 (online)

Acknowledgments

The authors thank the Santa Barbara County Water Agency and Vandenberg Space Force Base for their cooperation on this project, including funding support and expertise. The authors also thank U.S. Geological Survey colleagues Sandra Bond and Whitney Seymour for assistance in data compilation and analysis and Claudia Faunt, Ayman Alzraiee, and Jon Traum for their technical assistance on model calibration.

Contents

Figures

Tables

Conversion Factors

U.S. customary units to International System of Units

Multiply	By	To obtain
	Length	
inch (in.)	2.54	centimeter (cm)
inch (in.)	25.4	millimeter (mm)
foot (ft)	0.3048	meter (m)
mile (mi)	1.609	kilometer (km)
	Area	
Acre	4,047	square meter (m^2)
Acre	0.4047	hectare (ha)
Acre	0.4047	square hectometer (hm^2)
Acre	0.004047	square kilometer (km^2)
square mile (mi^2)	259.0	hectare (ha)
square mile (mi^2)	2.590	square kilometer (km^2)
	Volume	
cubic foot (ft^3)	28.32	cubic decimeter (dm^3)
cubic foot (ft^3)	0.02832	cubic meter (m^3)
acre-foot (acre-ft)	1,233	cubic meter (m^3)
acre-foot (acre-ft)	0.001233	cubic hectometer (hm^3)

Multiply	By	To obtain
	Flow rate	
acre-foot per year (acre-ft/yr)	1,233	cubic meter per year (m^3/yr)
acre-foot per year (acre-ft/yr)	0.001233	cubic hectometer per year (hm^3/yr)
foot per day (ft/d)	0.3048	meter per day (m/d)
cubic foot per second (ft^3/s)	0.02832	cubic meter per second (m^3/s)
inch per year (in/yr)	25.4	millimeter per year (mm/yr)
	Solar radiation	
langley	1	calorie per square centimeter
	Hydraulic conductivity	
foot per day (ft/d)	0.3048	meter per day (m/d)

International System of Units to U.S. customary units

Multiply	By	To obtain
	Length	
kilometer (km)	0.6214	mile (mi)
kilometer (km)	0.5400	mile, nautical (nmi)
	Area	
square kilometer (km^2)	247.1	acre
square kilometer (km^2)	0.3861	square mile (mi^2)

Temperature in degrees Celsius (°C) may be converted to degrees Fahrenheit (°F) as follows:

$$°F = (1.8 \times °C) + 32.$$

Temperature in degrees Fahrenheit (°F) may be converted to degrees Celsius (°C) as follows:

$$°C = (°F - 32) / 1.8.$$

Datum

Vertical coordinate information is referenced to the North American Vertical Datum of 1988 (NAVD 88).

Horizontal coordinate information is referenced to the North American Datum of 1983 (NAD 83).

Altitude, as used in this report, refers to distance above the vertical datum.

Well-Numbering System

Wells are identified and numbered according to their location in the rectangular system for the subdivision of public lands. Identification consists of the township number, north or south; the range number, east or west; and the section number. Each section is divided into 16 40-acre tracts lettered consecutively (except "I" and "O"), beginning with "A" in the northeast corner of the section and progressing in a sinusoidal manner to "R" in the southeast corner. Within the 40-acre tract, wells are sequentially numbered in the order they are inventoried. The final letter refers to the base line and meridian. In California, there are three base lines and meridians: Humboldt (H), Mount Diablo (M), and San Bernardino (S). All wells in the study area are referenced to the San Bernardino base line and meridian (S). Well numbers consist of 15 characters and follow the format 008N034W16C001S. In this report, well numbers are abbreviated and written 8N/34W-16C1. The following diagram shows how the number for well 8N/34W-16C1 is derived.

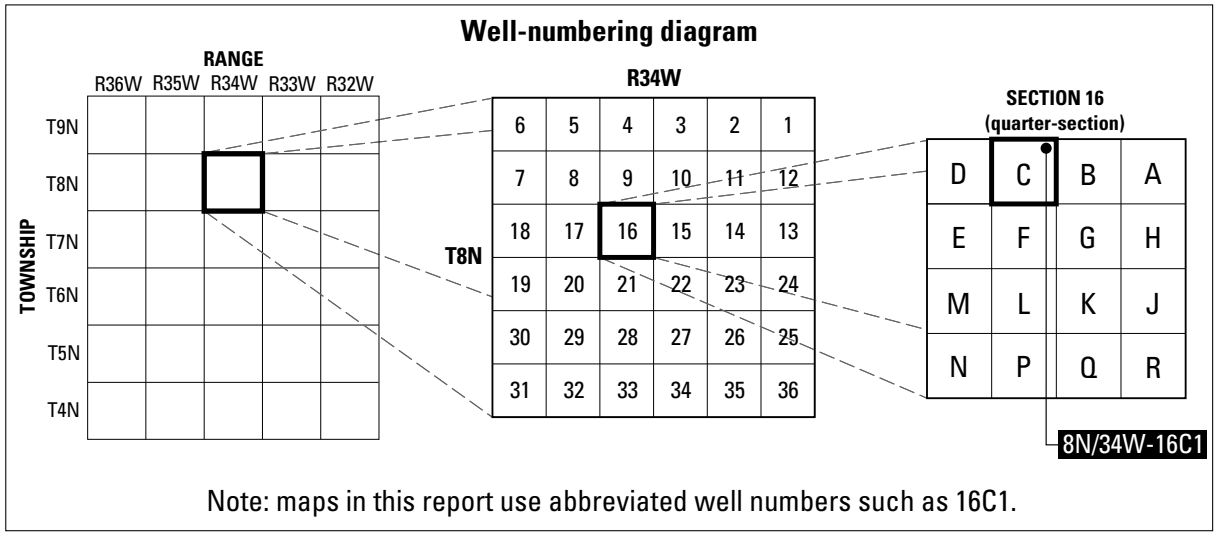

Note: maps in this report use abbreviated well numbers such as 16C1.

Abbreviations

3D HFM	Three-dimensional hydrogeologic framework model
AAEE	Absolute average estimation error
AG	Agricultural Water Use
BAS6	Basic

CRT	Cascade Routing Tool
DEM	Digital Elevation Model
ET	Evapotranspiration
GHB	General-Head Boundary
GSFLOW	Groundwater and Surface-Water Flow
HANI	Horizontal anisotropy
HK	Horizontal hydraulic conductivity
HRU	Hydrologic response unit
KC	Crop coefficient
MF-NWT	MODFLOW-NWT
MNW2	Multi-node well
NNSE	Normalized Nash-Sutcliffe efficiency
NRMSE	Normalized root mean square error
PAEE	Percent average estimation error
PET	Potential evapotranspiration
PRISM	Parameter-Estimation Regressions on Independent Slopes Model
PRMS	Precipitation Runoff Modeling System
RMSE	Root mean square error
SACC	San Antonio Creek – Cat Canyon
SACIM	San Antonio Creek Integrated Model
SACR	San Antonio Creek – Old Careaga Ranch Road
SACVGB	San Antonio Creek Valley groundwater basin
SACVW	San Antonio Creek Valley watershed
SFR2	Streamflow routing
SS	Specific storage
SURFK	Surface hydraulic conductivity
SY	Specific yield
UPW	Upstream weighting
USGS	U.S. Geological Survey
UZ	Unsaturated zone
UZF1	Unsaturated zone flow
VANI	Vertical anisotropy
VK	Vertical hydraulic conductivity
VKS	Vertical saturated hydraulic conductivity
VSFB	Vandenberg Space Force Base

Simulation of Groundwater and Surface-Water Resources of the San Antonio Creek Valley Watershed, Santa Barbara County, California

By Linda R. Woolfenden, John A. Engott, Joshua D. Larsen, and Geoffrey Cromwell

Abstract

In the San Antonio Creek Valley watershed (SACVW), western Santa Barbara County, California, groundwater is the primary source of water for agricultural irrigation, the town of Los Alamos, and supplemental water to Vandenberg Space Force Base (VSFB). Groundwater pumpage has increased since the 1970s as non-irrigated agricultural land has been converted to irrigated land and as local pumping for municipal use has increased. This increase in groundwater use has resulted in declining groundwater levels, adjustments in surface-water flows and species habitats, and changes in water quality. Water managers are addressing the challenges of meeting this increased demand while maintaining sustainable groundwater supplies. To address these challenges, Santa Barbara County Water Agency, Vandenberg Space Force Base (VSFB), and the U.S. Geological Survey (USGS) undertook a cooperative study to characterize the integrated hydrologic system of the SACVW and develop tools to better understand and manage the groundwater system. The objectives of this study were to improve the understanding of the integrated hydrologic system and incorporate the understanding into an integrated groundwater and surface-water flow model that can be used to help manage the water resources in the SACVW.

The San Antonio Creek integrated model (SACIM) was developed using the USGS coupled groundwater and surface-water flow model to simulate the hydrologic system of the SACVW and provide annual and average water budgets for 1948–2018 water years. Results from the SACIM indicated that between 1948 and 2018, total groundwater from storage (storage depletion) for the period was 453,300 acre-feet (acre-ft). Agricultural pumpage was the largest discharge and accounted for a total of 1,020,000 acre-ft of groundwater. Increased pumpage since the mid-1980s (of which agricultural pumpage is the primary component) is tied to an increased rate of storage depletion and reduced rates of groundwater evapotranspiration and surface leakage (groundwater discharge to the surface and soil zone). The increased pumpage also reduced subsurface inflow to Barka Slough, resulting in a decline in upward flow through the underlying hydrogeologic units and surface leakage. In addition to quantifying historical changes in the integrated hydrologic system, the SACIM is a tool than can be used by water managers to evaluate the effects of different climatic and hydrologic conditions and management strategies.

Introduction

The San Antonio Creek Valley watershed (SACVW) is in western Santa Barbara County, California, 15 miles (mi; 24 kilometers, km) south of Santa Maria and 55 mi (88 km) north of Santa Barbara (fig. 1). Groundwater is the primary source of water for agricultural irrigation, the town of Los Alamos, the habitat for several endangered species near Barka Slough, and an important source of supplemental water to Vandenberg Space Force Base (VSFB). Demand for groundwater has increased since the 1970s as non-irrigated pastures and hayland were converted to irrigated vineyards and from increased local municipal and military pumping; the increased demand has resulted in declining water levels. The San Antonio Creek Valley groundwater basin (SACVGB) is encompassed by the SACVW and was designated a “medium priority” groundwater basin by California Department of Water Resources (California Department of Water Resources, 2021a) as part of the Sustainable Groundwater Management Act (SGMA; California Department of Water Resources, 2021b). The act requires development of a groundwater sustainability plan for all medium and high priority groundwater basins with the goal of balancing pumping and recharge.

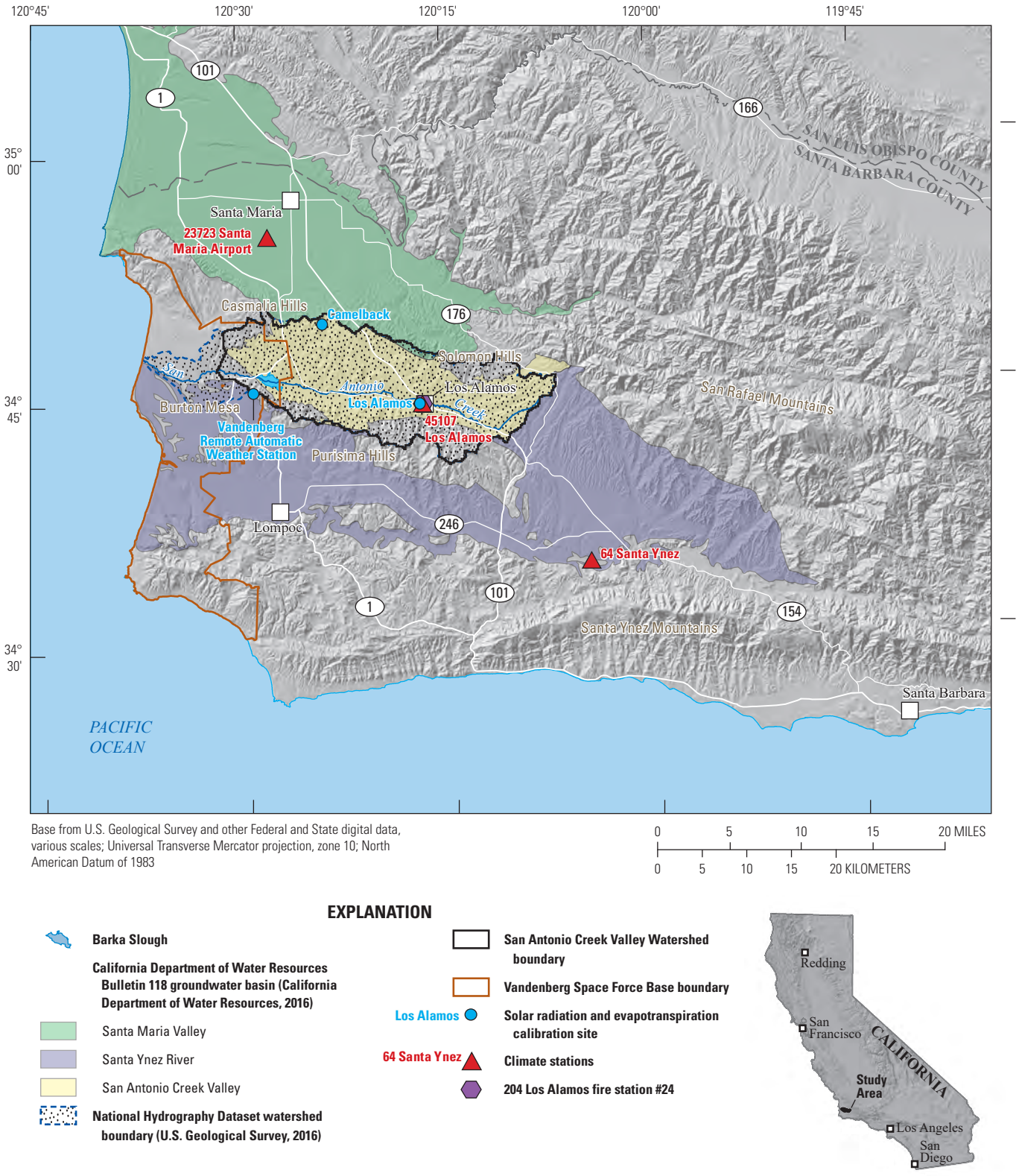

Figure 1. Location the San Antonio Creek Valley groundwater basin and the San Antonio Creek Valley watershed and climate stations, Santa Barbara County, California.

Water managers must deal with the challenge of achieving groundwater sustainability while trying to meet increased groundwater demand. The task becomes urgent when declining water levels threaten the economic viability of pumping and degrade water quality by dewatering the alluvial aquifer. To address these challenges, Santa Barbara County Water Agency (SBCWA), VSFB, and the U.S. Geological Survey (USGS) began a cooperative study to characterize the hydrology of the SACVW and develop tools to better understand and manage the groundwater system. The objectives of this study are to (1) develop an assessment of the hydrology and water chemistry of the SACVW and (2) develop an integrated surface-water and groundwater flow model for the SACVW. Cromwell and others (2022) described the hydrogeology, aquifer system, surface-water and groundwater hydrology, and groundwater chemistry of the SACVW in support of the first objective. This report describes the development of the integrated model and simulated water budgets in support of the second objective.

Purpose and Scope

The purpose of this report is to present the construction, calibration, and simulated water budgets of the integrated surface-water and groundwater-flow model for the SACVW, referred to as the San Antonio Creek Valley integrated model (SACIM). The SACIM is composed of a watershed-component model and a groundwater-component model. This report includes detailed descriptions of both models. The watershed-component model includes watershed parameters that vary over time to represent the changes in land use and potential evapotranspiration (PET). The discretization and parameterization of the groundwater-component model is derived from a three-dimensional hydrogeologic framework model (3D HFM) developed by Cromwell and others (2022) as part of this study. The SACIM was calibrated to hydrologic conditions during water years 1948–2018. A water year is the 12-month period from October 1 to September 30 and is designated by the calendar year in which it ends. Hydrologic data and information from published reports (Hutchinson, 1980; Martin, 1985; and Tetra Tech, Inc., 2013), and new data collected as part of this study, were used as calibration targets. The new data include measurements from multiple completed and shallow monitoring wells, infiltrometers, and streamgages installed for this study, and water-level and streamflow measurements for existing wells and streamgages, respectively. The new data are published in the USGS National Water Information System (NWIS; U.S. Geological Survey, 2021) or in a companion data release (Ely and others, 2022). The long-term average and annual groundwater-budget components simulated by the SACIM are presented in the "Simulated Groundwater Budgets" section of this report.

Previous Investigations

The hydrogeology of the SACVW has been described in previously published reports, for example, Muir (1964), Hutchinson (1980), and Cromwell and others (2022). Cromwell and others (2022) described the surface-water and groundwater hydrology, historical land use, hydrogeology, and water-quality characteristics of the SACVW to provide information on the conceptual model of the hydrologic system as part of this study.

Two previous groundwater-flow models were developed for the SACVGB. Martin (1985) developed the first model of the groundwater basin; the two-dimensional model was based on a comprehensive water budget for the SACVGB for calendar years 1958–77 (Hutchinson, 1980). The model was calibrated to steady-state conditions for calendar year 1943 and transient conditions during calendar years 1944–77 and used to evaluate the knowledge and concepts of the groundwater system at that time (Martin, 1985). Tetra Tech, Inc. (2013) developed the second transient model of the groundwater basin; their model was a three-dimensional groundwater-flow model based on the hydrologic conditions and historical water balance in the SACVGB described in Tetra Tech, Inc. (2012). The model was calibrated to hydrologic conditions during water years 1935–2010 and was used to update water-budget components and assess the effects of pumping on groundwater-surface-water interaction, including at Barka Slough, and groundwater storage change (Tetra Tech, Inc., 2013). The report documenting this previous model and simulation results is not available for public release.

Study Area Description

The study area for this report is the SACVW, which includes the SACVGB and the uplands of the Casmalia Hills in the north, the Solomon Hills in the northeast, and the Purisima Hills in the south and southeast (fig. 1). The SACVW is about 24 mi long and about 7 mi wide and covers about 134 square miles (mi^2). San Antonio Creek, which runs the length of the valley floor (valley floor is designated as "the valley" herein), is fed by tributaries in the uplands to the north and south (fig. 2). All streams are intermittent, except at the western end of SACVW, where shallow bedrock forms a barrier impeding the westward flow of groundwater. Upwelling of groundwater east of the barrier has created a 660-acre marshland known as Barka Slough. Barka Slough is a pristine marshland that is known or believed to be inhabited by at least nine threatened or endangered species of wildlife (Descheneaux, 1975; Martin, 1985; Cromwell and others, 2022).

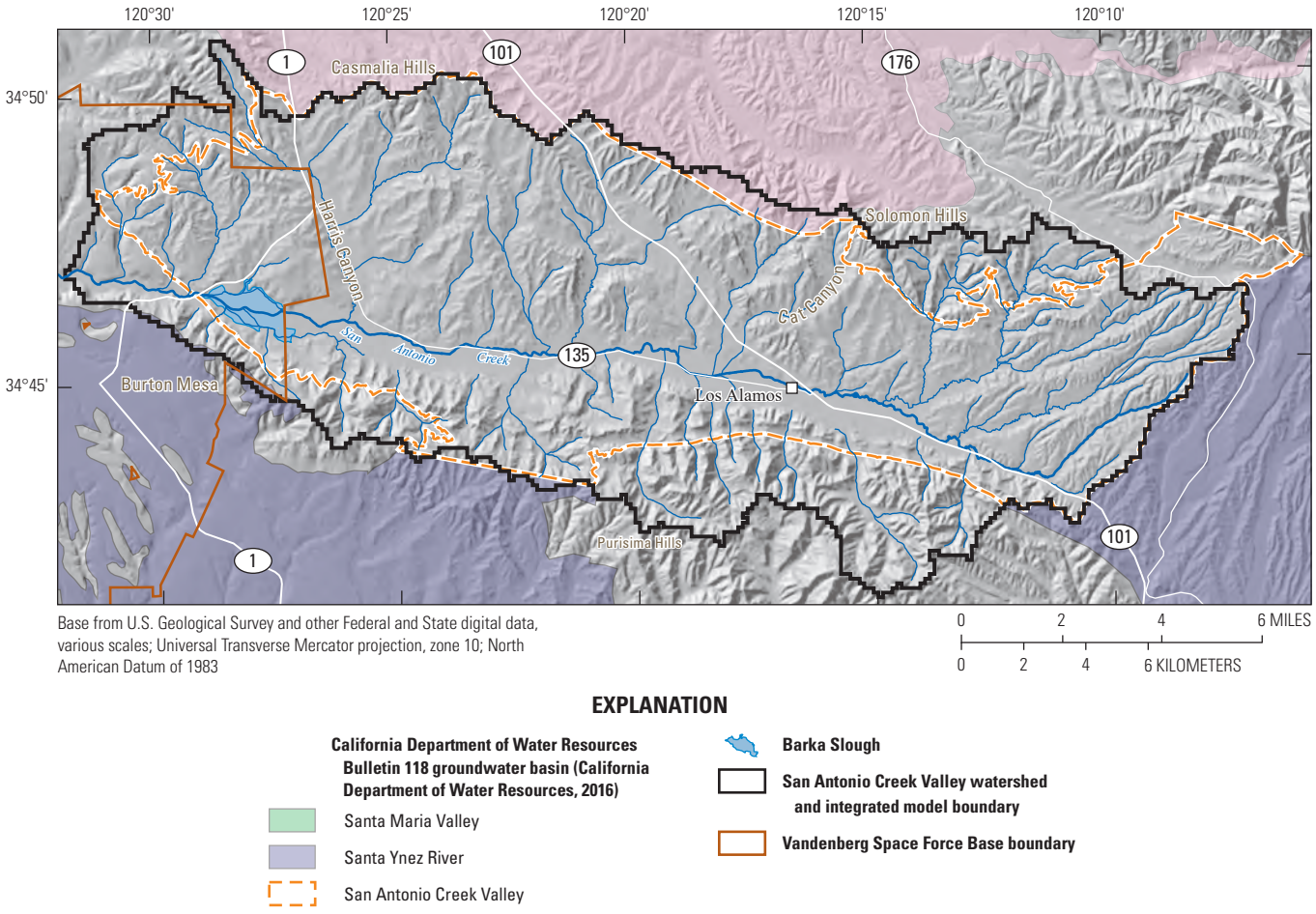

Figure 2. San Antonio Creek Valley watershed and groundwater basin, Santa Barbara County, California.

The SACVW has a semiarid climate characterized by mild temperatures and low rainfall. Rainfall generally is lower in the valley and higher in the upland areas. About 92 percent of annual rainfall recorded in the town of Los Alamos occurs from November to April. The estimated mean annual precipitation recorded in the town of Los Alamos in the SACVW for 1948–2018 was about 15 inches per year (in/yr; Cromwell and others, 2022).

Land use in the SACVW was used primarily for agriculture. Historically, the uplands were used for dry farming or pastureland, and the valley along San Antonio Creek was used for irrigated farming. Since about the 1980s, however, large sections of formerly non-irrigated pastureland in the uplands have been converted to irrigated vineyards. The western quarter of the SACVW is owned by VSFB (fig. 2), and the rest of the SACVW is privately owned. The town of Los Alamos has seen a slow, steady growth in population from about 140 people in 1935 (Tetra Tech, Inc., 2012) to about 1,890 people in 2010 (U.S. Census Bureau, 2010).

Conceptual Model

The conceptual model of the SACVW is based on known and estimated physical and hydrologic characteristics of the surface-water and groundwater systems and how these characteristics influence the flow and storage of water in the SACVW. The characterization of the SACVW hydrologic system is described in Cromwell and others (2022). Information from Cromwell and others (2022) is summarized here to provide a conceptual model of the SACVW that gives the reader the necessary background to understand the construction of the SACIM.

Precipitation

The major source of water for the SACVW is precipitation that falls as rain. Mean annual rainfall ranges from about 14.6 to 21.9 in/yr (PRISM Climate Group, 2013) and generally is lower in the western part of the valley and higher in the Solomon Hills and Purisima Hills in the eastern uplands (Cromwell and others, 2022). The precipitation in the uplands infiltrates to the soil zone or becomes runoff to tributaries of San Antonio Creek, which can contribute to streamflow and potential recharge in the downstream valley.

Streamflow

San Antonio Creek is the major stream that drains the SACVW. The main channel of San Antonio Creek originates in the Solomon Hills (fig. 2). San Antonio Creek is intermittent throughout its length east of Barka Slough and perennial at Barka Slough and downstream to the Pacific Ocean. Consolidated bedrock at Barka Slough underlies the SACVW at shallow depths and creates a subsurface flow barrier that, combined with the narrowing of the valley, causes almost all groundwater to move upward to the land surface and discharge into San Antonio Creek (Muir, 1964; Cromwell and others, 2022). All tributaries to San Antonio Creek within the SACVW are intermittent and most originate in the uplands above the valley.

Aquifer System

The aquifer system in the SACVW includes three principal basin-fill hydrogeologic units: channel alluvium, the Paso Robles Formation, and the Careaga Sandstone (fig. 3). Cromwell and others (2022) subdivided the Paso Robles Formation into upper, middle, and lower members. These basin-fill units are underlain by a consolidated bedrock unit. The thickness of the basin-fill sediments along the axis of the SACVW ranges from a few tens of feet (ft) to more than 3,200 ft (Cromwell and others, 2022). The channel alluvium occurs along San Antonio Creek in the valley and along its tributaries in the uplands. The Paso Robles Formation underlies the channel alluvium and crops out in parts of the uplands. The Careaga Sandstone underlies the Paso Robles Formation and crops out along its northern, southern, and western extents in the uplands. Consolidated bedrock underlies the Careaga Sandstone and crops out along the northeastern and southern boundaries of the SACVW (fig. 3).

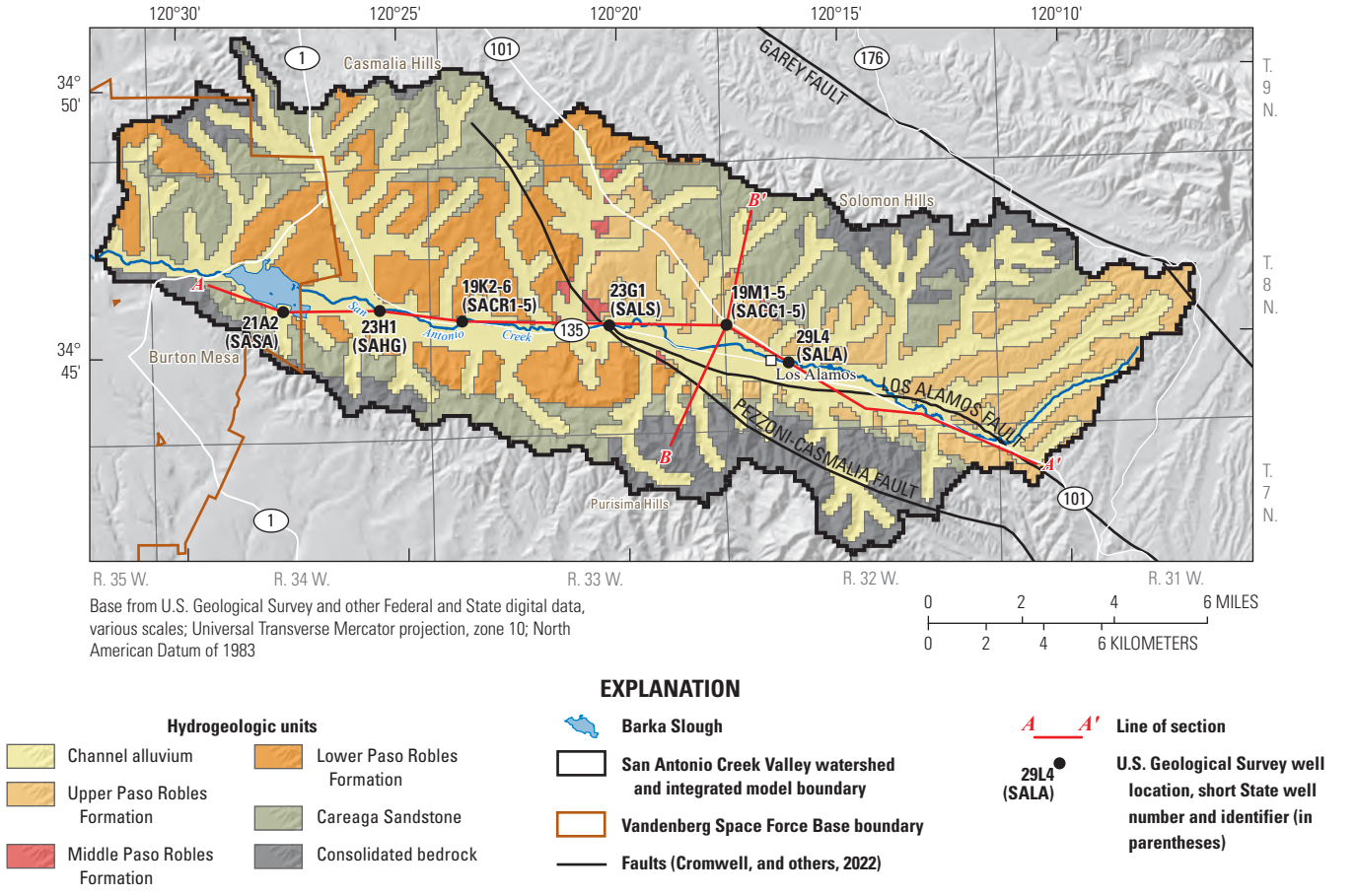

Figure 3. Hydrogeologic units of the San Antonio Creek Valley watershed, Santa Barbara County, California.

The channel alluvium is comprised of unconsolidated gravel, sand, and clay. The channel alluvium generally is unsaturated across most of the SACVW except in the valley near Barka Slough, where groundwater discharges to land surface; the channel alluvium is not considered a major aquifer (Cromwell and others, 2022). The Paso Robles Formation is non-marine in origin and is identified by Muir (1964) as the main water-bearing unit in the SACVW. The partition of the Paso Robles Formation vertically into three hydrogeologic members by Cromwell and others (2022) reflects the variability of the unit within the SACVW. The lower and upper members of the Paso Robles Formation are lithologically heterogeneous and provide most of the groundwater storage within the aquifer; the middle interval is primarily fine grained and impedes vertical groundwater flow (Cromwell and others, 2022). The Careaga Sandstone is comprised of marine and nonmarine sandstone and sand and consists of a coarse-grained upper member and a fine-grained lower member (Woodring and Bramlette, 1950). The Careaga Sandstone is tapped by a few wells, mainly in the uplands, and yields small quantities of water to these wells (Cromwell and others, 2022). The bedrock is comprised of consolidated sedimentary rocks and yields small quantities of water to wells in the eastern part of the uplands and western part of the valley where it is present at shallow depths (Muir, 1964; Cromwell and others, 2022).

Groundwater Recharge

The primary sources of recharge to the groundwater system in the SACVW are infiltration of precipitation in the uplands of the Casmalia Hills and Solomon Hills and infiltration along the main channel of San Antonio Creek (fig. 3). Annual recharge increased over time, ranging from about 5,000 acre-feet (acre-ft) to more than 15,000 acre-ft for 1948–2018 (Muir, 1964; Hutchinson, 1980; Martin, 1985; Tetra Tech, Inc., 2012). The increase in recharge over time may have been a result of the decline in groundwater levels with increased pumping in the valley; the decline in groundwater levels created more storage capacity for recharge from San Antonio Creek (Martin, 1985). Anthropogenic recharge such as return flow from agricultural irrigation, municipal water systems, and wastewater effluent, was estimated to range from about 600 acre-ft in 1948 to about 6,700 acre-ft in 2018; the increase in anthropogenic recharge primarily is due to the increase in irrigation return flow from the establishment of irrigated vineyards on previously unirrigated pasture, which ranged from 550 acre-ft in 1948 to 6,400 acre-ft in 2018 (Cromwell and others, 2022).

Natural Groundwater Discharge

Natural groundwater discharge supplies evapotranspiration and base flow to San Antonio Creek near Barka Slough. Natural discharge from evapotranspiration of phreatophytes occurs in Barka Slough and along the channel of San Antonio Creek. Martin (1985) estimated that evapotranspiration (ET) in Barka Slough was reduced from about 3,100 acre-ft/yr in pre-development conditions (1943) to about 1,000 acre-ft/yr in 1977; ET along San Antonio Creek was reduced from about 400 to 0 acre-ft/yr over the same time period (Martin, 1985). The reductions in ET in Barka Slough and along San Antonio Creek were a result of increased pumpage in the SACVW that caused declining groundwater levels and available groundwater for consumptive use by phreatophytes. Tetra Tech, Inc. (2012), estimated average total ET from marshland in Barka Slough and riparian vegetation along San Antonio Creek to be 2,900 acre-ft/yr from 1935 to 2010.

Natural discharge of deep groundwater occurs as base flow in San Antonio Creek in the western part of the SACVW. Estimates of the amount of base flow indicate that, on average, there was an overall decline in base flow from about 1,700 acre-ft/yr during 1956–69 to about 300 acre-ft/yr during 2016–18 (Cromwell and others, 2022).

Pumpage

Groundwater pumping in the SACVW is used for rural, municipal, and military water supply and agricultural irrigation. Pumpage estimates for 1948–2018 range from about 3,000 acre-ft in 1948 to about 32,600 acre-ft in 2018; pumpage for 1978, when demand for groundwater began to increase substantially, was estimated to be about 14,800 acre-ft. The increase in groundwater demand was due to establishment of irrigated agriculture on previously unirrigated land and the increase in local military pumping (Cromwell and others, 2022). The average annual amount of groundwater removed from the SACVW by pumping between 1948 and 2018 was estimated to be about 17,200 acre-ft/yr, which was 10 percent to more than 300 percent greater than most estimates of annual recharge to the valley (Cromwell and others, 2022).

Groundwater Flow

The general direction of groundwater flow is from the eastern uplands in the Solomon Hills to the west along San Antonio Creek toward Barka Slough, and from the northern uplands in the Casmalia Hills to the south toward San Antonio Creek (Cromwell and others, 2022). Groundwater also flows northward from the Purisima Hills toward San Antonio Creek. Declining groundwater levels from increased pumping over time has not altered the general direction of groundwater flow (Cromwell and others, 2022). Hydraulic data indicate that groundwater moves vertically downward near the town of Los Alamos and vertically upward about seven miles downgradient from the town. Stable and radioactive isotope data indicate that movement of deep groundwater recharged in the eastern upland areas toward the west is slow. In the western part of the SACVW, deep groundwater is forced upward by shallow bedrock near Barka Slough. Upward groundwater flow has maintained discharge to Barka Slough, although the amount of discharge has been reduced by increased pumping that has caused declining groundwater levels in the SACVW. The faults that are inferred to cross the SACVW (fig. 3) are not likely to impede groundwater flow (Cromwell and others, 2022).

Simulation of Groundwater and Surface-Water Resources

A coupled groundwater and surface-water model allows for analysis of movement of water through the SACVW by simultaneously simulating (1) flow across the land surface and within the aquifer system and (2) effects of stresses on the hydrologic system of the watershed. The USGS coupled groundwater and surface-water flow model (GSFLOW) was used to simulate the hydrologic system of the SACVW and provide annual and average groundwater budgets. The version of GSFLOW (Markstrom and others, 2008; Regan and Niswonger, 2021) used in this study includes the USGS Precipitation-Runoff Modeling System (PRMS; Regan and LaFontaine, 2017 ; Regan and others, 2020) and the Modular Groundwater Flow Model-Newton Formulation, generally referred to as MODFLOW-NWT (MF-NWT; Niswonger and others, 2011).

GSFLOW is defined by boundaries and three inter-connected regions (fig. 4); these regions are the conceptual basis for the San Antonio Creek Valley integrated model. The regions in the SACIM are (1) the plant canopy, the land surface, and the soil zone, (2) streams, and (3) the subsurface that includes the unsaturated zone (UZ) and the underlying saturated zone. PRMS simulates region 1 and MF-NWT simulates regions 2 and 3 (Markstrom and others, 2008). Water is stored in each region, and the regions are linked by the exchange of flow among them. Movement of water between the regions depends on soil-moisture conditions and hydraulic heads. The flow processes and properties specific to each region determine the flow into, out of, and within, each region.

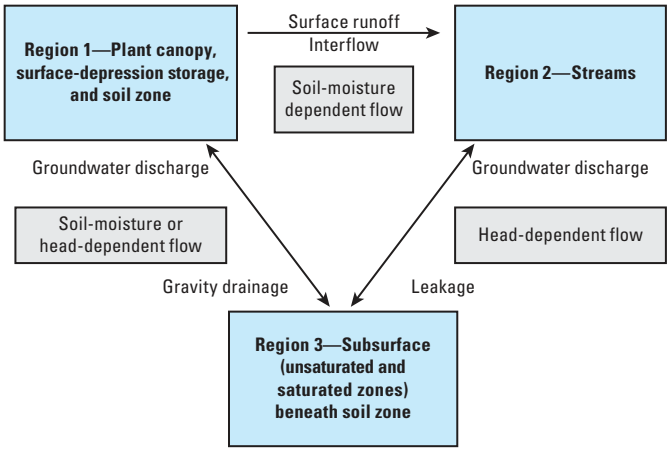

Figure 4. Exchange of flow among the three regions in GSFLOW as applied to the San Antonio Creek integrated model (modified from Markstrom and others, 2008).

The physical horizontal boundary for regions 1 and 3 is the surface-water drainage divide for the SACIM. The boundaries for region 2 are the lowest elevations of the streambeds and the horizontal extent of the stream channels in the SACVW. The only point of surface outflow from the SACVW is where San Antonio Creek exits the watershed (fig. 2). Flow across the bottom of the streambed in region 2 depends on the water-level elevation in the underlying aquifer. Flow across the lateral extent of the stream channels is a function of precipitation and channel characteristics. Flow across the unsaturated part of region 3 is assumed to be vertical and does not cross the lateral model boundary. Most of the lateral boundary for the saturated part of region 3 is a no-flow boundary, where a groundwater divide is assumed to coincide with the surface-water divide. The remaining lateral boundary of region 3 includes one small segment where there could be groundwater interaction with an adjacent groundwater subbasin. The vertical extent of the aquifer system that underlies the three regions includes the basin-fill hydrogeologic units and the shallow bedrock.

The SACVW was divided into a grid of 15,484 uniform cells of 492 ft on each side (fig. 5). In PRMS, these cells are known as hydrologic response units (HRUs). The HRUs correspond to the region where land-surface characteristics such as precipitation, temperature, slope, aspect, and soil properties are uniform. The HRUs are connected using a network of cascades and stream segments. Surface-water runoff and interflow are routed by cascades to the stream segments; the stream segments route streamflow to one outflow point on the boundary of the watershed. In MF-NWT, the subsurface is represented by a three-dimensional array of rectangular cells with the same horizontal grid spacing as the PRMS model. The MF-NWT cells correspond to regions where aquifer properties and boundary conditions are assumed homogeneous. The aquifer system is divided vertically into four layers. The SACIM is a transient model that simulates hydrologic conditions from October 1947 through September 2018 (water years 1948–2018). A decoupled PRMS-only simulation provided preliminary calibration of watershed parameters and provided net infiltration and residual potential-evapotranspiration rates for a decoupled MF-NWT-only steady-state model. The steady-state model provided preliminary calibration of aquifer properties for the transient SACIM model and was used to test the effectiveness of faults as barriers to groundwater flow. Results from the steady-state model indicate that the faults in the SACVW are not barriers to groundwater flow.

PRMS Model Description

PRMS is a deterministic, distributed-parameter model that computes energy and water balances based on the physical characteristics and processes within a watershed. The watershed structure is conceptualized as a series of interconnected reservoirs that include the plant canopy, snowpack, impervious surfaces, soil zone, groundwater reservoir, and streams (fig. 6). Flow between and storage within these reservoirs is computed on a daily time scale. The hydrologic and physical characteristics distributed to the HRUs include land-surface elevation, slope, aspect, flow direction, precipitation, solar radiation, air temperature, land use, soil properties, vegetation type, and vegetation cover. Daily minimum and maximum air temperature and precipitation are used to simulate hydrologic responses in a watershed, particularly evapotranspiration (ET), streamflow, soil-moisture storage, and groundwater recharge. A complete description of PRMS is available in Markstrom and others (2015). The following sections describe some of the key PRMS parameters for land-surface characteristics, land use, soils, topography and streams, and climate.

Land-Surface Characteristics

PRMS parameters that describe land-surface characteristics were developed using the Gsflow-ArcPy Toolkit (Gardner and others, 2018) with geospatial datasets: National Elevation Dataset (NED) 10-meter digital elevation model (DEM; U.S. Geological Survey, 2013), soil maps from the Soil Survey Geographic database (SSURGO; U.S. Department of Agriculture, 2016), a percent developed impervious map from the National Land Cover Database (NLCD; Xian and others, 2011), and land-use maps for years 1959, 1968, 1977, 1986, 1996, 2006, and 2016 from Cromwell and others (2022). The parameters used in the PRMS model that were developed from geospatial datasets unique to this study and their initial values are given in table 1. A full description of PRMS parameters is provided in Markstrom and others (2015).

Land Use

Land-use change was represented in PRMS by using seven distinct land-use periods associated with the land-use maps developed by Cromwell and others (2022). Lists of LANDFIRE 140 vegetation codes (LANDFIRE, 2014) and corresponding PRMS parameters were developed by Gardner and others (2018) and used to re-assign LANDFIRE 140 codes for each land-use period to the vegetation codes supported by PRMS (Cromwell and others, 2022). HRU-specific parameters derived from the LANDFIRE 140 codes were vegetation cover type (*cov_type*), summer and winter cover density (*covden_sum* and *covden_win*, respectively), summer and winter rain interception (*srain_intcp* and *wrain_intcp,* respectively), root depth, and short-wave radiation transmission coefficient (*rad_trncf*) through winter vegetation. For vegetation cover type (0=bare, 1=grass, 2=shrub, 3=trees), the predominant cover type within an HRU was assigned to that HRU. For the other vegetation-based parameters listed above, each HRU was assigned the area-weighted mean computed for the vegetation codes occurring within that HRU. For example, if 20 percent of the area of an HRU consisted of pasture and hay (*covden_sum* = 0.80) and the remaining 80 percent of the area consisted of low-intensity developed land cover (*covden_sum* = 0.10), then the value for *covden_sum* used for that HRU would be (0.20×0.80) + (0.80×0.10) = 0.24. Impervious land cover was derived from the NLCD percent developed impervious map (Xian and others, 2011) and used to populate the PRMS *hru_percent_imperv* parameter for each active HRU. This parameter was held constant over the simulation period because of a lack of information and the relatively small area of impervious surfaces in the SACVW.

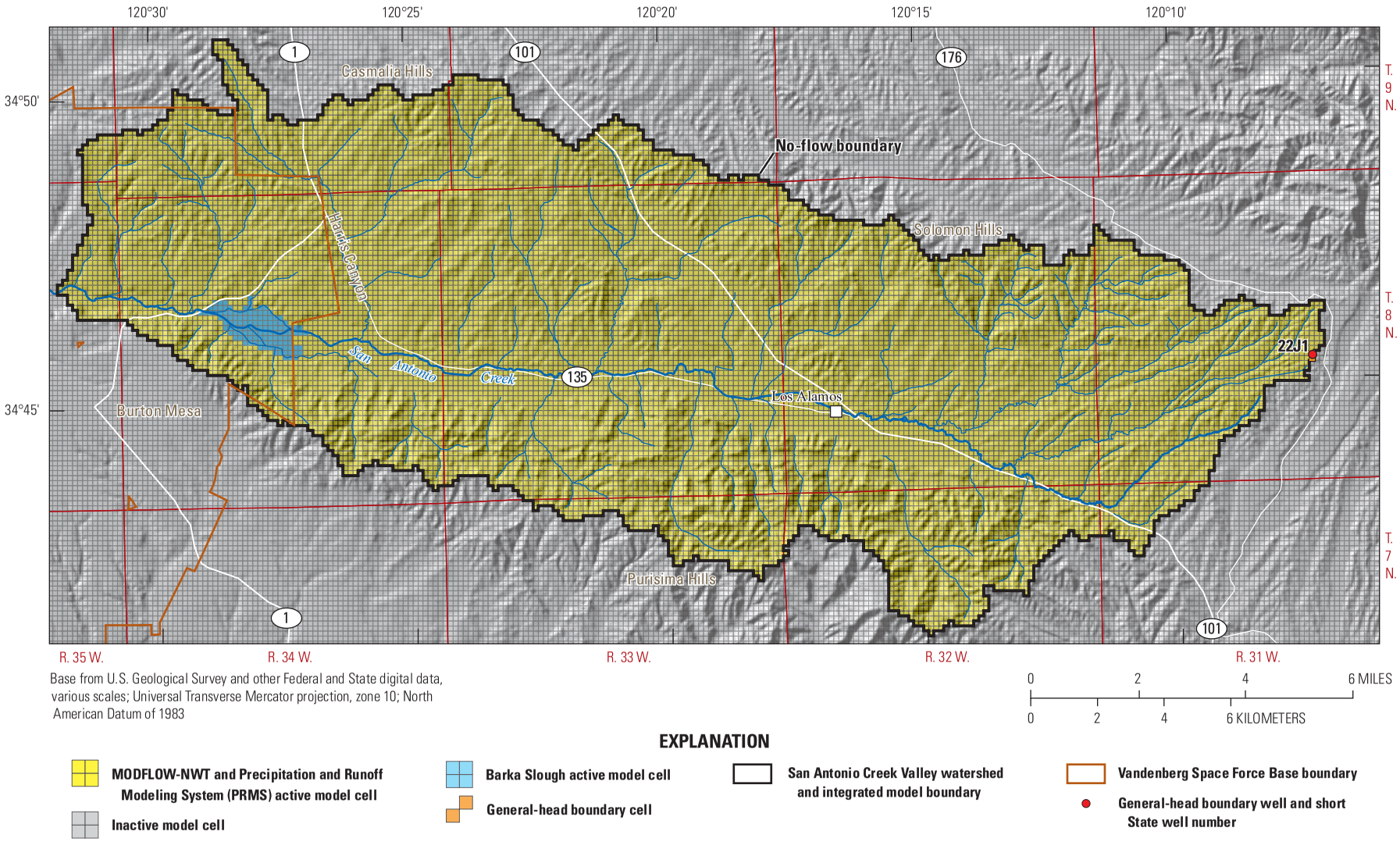

Figure 5. MODFLOW-NWT grid and boundary conditions and Precipitation-Runoff Modeling System (PRMS) hydrologic response units for the San Antonio Creek Valley integrated model, Santa Barbara County, California.

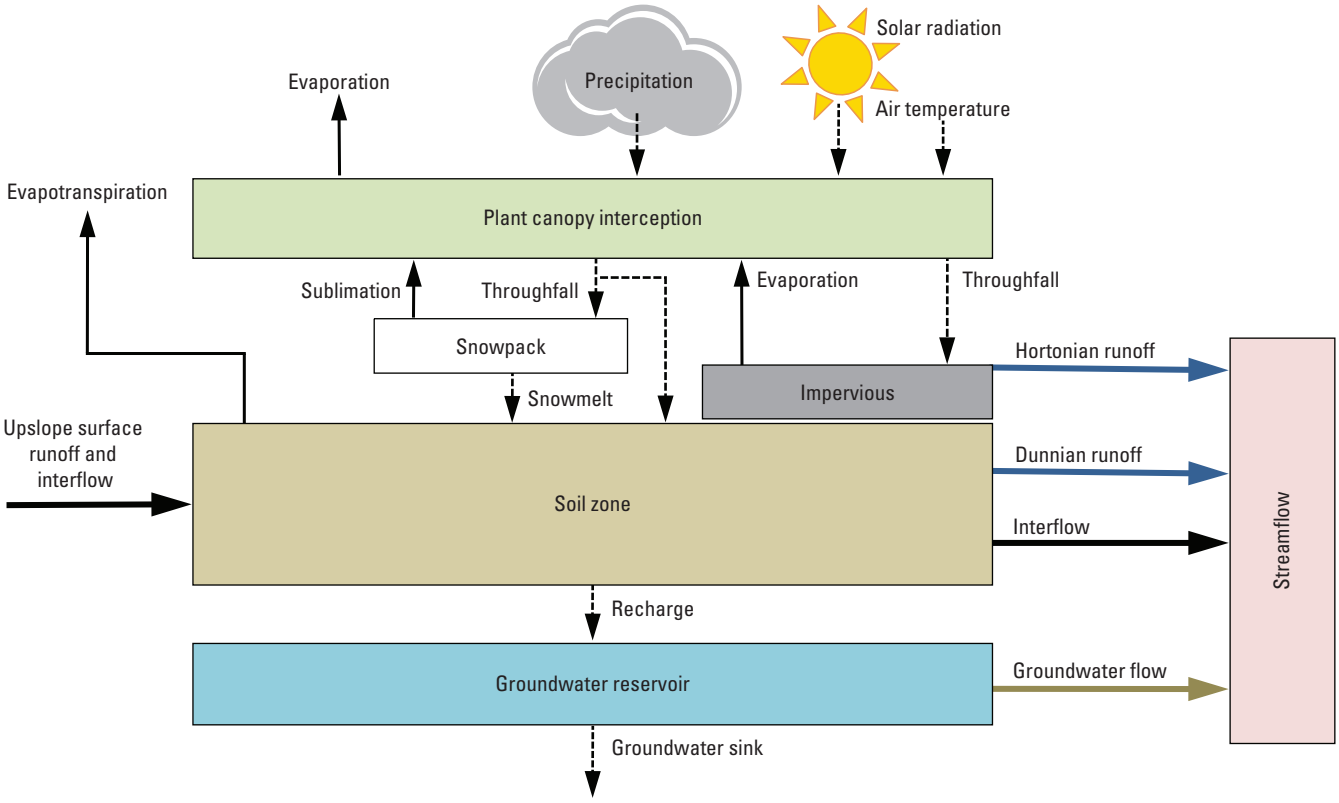

Figure 6. Precipitation-Runoff Modeling System (PRMS) climate inputs, watershed components, and flow paths (modified from Markstrom and others, 2015).

Soils

The SSURGO database was used to develop PRMS parameters that are based on soil properties. Soil texture (percent sand, clay, and silt), available water capacity, saturated hydraulic conductivity, and soil depth for each HRU were used to compute PRMS soil-zone parameters affecting storage, interflow, gravity drainage, and runoff. The PRMS parameter *soil_type* (1=sand, 2=loam, and 3=clay) was assigned on the basis of the predominant soil texture for each HRU. Initial values for other soil-zone parameters, including *soil_moist_max*, *sat_threshold*, *ssr2gw_rate*, *soil_rechr_max_frac*, and *slowcoef_lin*, were computed for each HRU using the available water capacity, soil depth, slope, and porosity data from the SSURGO database and the Gsflow-ArcPy Toolkit (table 1). These parameter values were adjusted during calibration of the decoupled PRMS-only mode model using a scaling approach that preserved the relative spatial variabilities of each parameter.

Topography and Stream Network

The mean elevation (*hru_elev*), mean aspect (*hru_aspect*), mean slope (*hru_slope*), and latitude of the centroid (*hru_lat*) were derived for each HRU from the 10-m DEM geospatial layer using the Gsflow-ArcPy Toolkit (Gardner and others, 2018). With the exception of *hru_lat*, these parameters were adjusted during the creation of the discretized stream network to ensure that individual stream segments in the model follow the natural-flow direction of the streams. Adjustment of the topographic parameters is an iterative process that required manual adjustment of HRU elevations, subsequent execution of the Cascade Routing Tool (CRT; Henson and others, 2013), and comparison of the generated stream network with the National Hydrography Dataset (NHD; U.S. Geological Survey, 2016) and satellite imagery in Google Earth (Google, Landsat/Copernicus, © 2021 Maxar Technologies). During this initial stream creation and revision process, two CRT parameters used to generate stream segments—flow-accumulation threshold and flow-length threshold—also were adjusted. The flow-accumulation threshold is the minimum number of upgradient cells required for water to flow to a particular cell for that cell to be designated a stream segment. The flow-length threshold is the minimum length (in number of cells) for all first order streams. The final values used for flow-accumulation threshold and flow-length threshold in CRT were 30 and 3, respectively. The final layout of the stream cells used in the SACIM is shown in figure 7.

Table 1. Initial Precipitation-Runoff Modeling System (PRMS) parameter values derived from geospatial data, or otherwise not at default values, for the San Antonio Creek Valley integrated model, Santa Barbara County, California.

[one, scalar parameter; nhru, a value for each hydrologic response unit in model; nmonths, number of months in a year; nmonths by hru, number of months in a year for each hru; ntemp, number of air temperature measurement stations]

Parameter	Dimension	Value		Units
		Minimum	Maximum	
hru_area	one	5.56	5.56	acres
pref_flow_den[1]	one	0.2	0.2	decimal fraction
smidx_coef[1]	one	0.01	0.01	decimal fraction
slowcoef_sq[1]	one	0.1	0.1	none
carea_max[1]	nhru	0.29	1	decimal fraction
cov_type	nhru	0	4	none
covden_sum	nhru	0	0.8	decimal fraction
covden_win	nhru	0	0.65	decimal fraction
hru_aspect	nhru	0	315	angular degrees
hru_elev	nhru	19.39	867.94	meters
hru_lat	nhru	34.67762	34.8535	angular degrees
hru_percent_imperv	nhru	0	0.71	decimal fraction
hru_psta	nhru	1	1	none
hru_slope	nhru	0	0.92	decimal fraction
hru_subbasin	nhru	0	5	none
hru_tlaps	nhru	2	4	none
hru_tsta	nhru	1	3	none
hru_type	nhru	0	1	none
jh_coef_hru	nhru	22.0861	22.0861	per degrees Fahrenheit
rad_trncf	nhru	0.165375	0.9917	decimal fraction
sat_threshold[1]	nhru	0	6.48	inches
slowcoef_lin[1]	nhru	0	0.55309	fraction/day
soil_moist_init_frac	nhru	0	0.1	decimal fraction
soil_moist_max[1]	nhru	0	4.92	inches
soil_rechr_init_frac	nhru	0	0.87143	decimal fraction
soil_rechr_max_frac[1]	nhru	0	1	decimal fraction
soil_type	nhru	1	3	none
srain_intcp	nhru	0	0.04	inches
ssr2gw_rate[1]	nhru	0	0.073735	fraction/day
tmax_adj	nhru	–1.8	1.8	degrees Celsius
tmin_adj	nhru	–1.8	1.8	degrees Celsius
wrain_intcp	nhru	0	0.04	inches
dday_intcp[1]	nmonths	–7.8	–38	degree day
dday_slope[1]	nmonths	0.31	0.65	degree day/degree Celsius
jh_coef[1]	nmonths	0.0904	0.016301	per degrees Fahrenheit
tmax_index	nmonths	16.23464	33.88191	degrees Celsius
rain_adj	nmonths by nhru	0.43705	2.95373	decimal fraction
tsta_elev	ntemp	171	868	meters

[1]Parameters modified during model calibration in decoupled PRMS-only model.

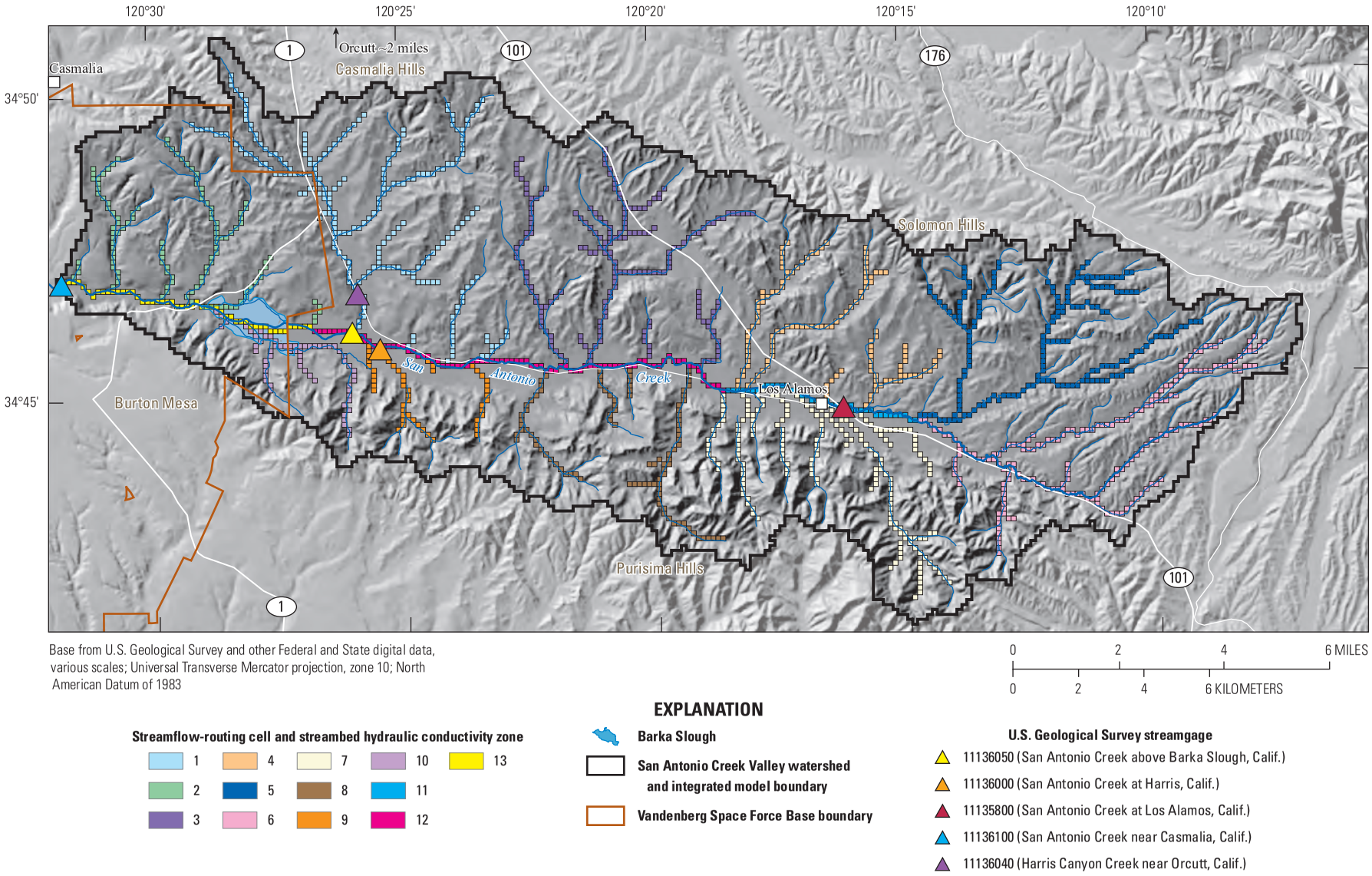

Figure 7. Streamflow-routing cells and U.S. Geological Survey streamgages in the San Antonio Creek Valley integrated model, Santa Barbara County, California.

A major limitation of PRMS is that once cascading flows are collected in the stream segments, the flow cannot subsequently infiltrate to groundwater and is instead routed directly to the end of each segment. Therefore, once flow reaches a stream segment, it accumulates (increases) as it moves downstream, resulting in unrealistically high runoff from the drainages. The runoff computed by PRMS approximates the quantity of runoff that originates from the respective drainage areas and does not consider losses that occur as water moves through ephemeral channels (Allander and others, 2014).

Daily Precipitation and Air Temperature

Climate input to the PRMS consisted of daily values of precipitation and minimum and maximum temperature (T_{min} and T_{max}, respectively) during the model simulation period, 1948–2018. Daily precipitation data came from Santa Barbara County (2019) for station 204 Los Alamos Fire Station #24 (fig. 1). The record was gap-filled by Santa Barbara County using data from nearby stations. Daily temperature data came from the National Centers for Environmental Information (NCEI; formerly the National Climatic Data Center; NCEI, 2019) for station 45107 Los Alamos and station 23723 Santa Maria Airport and from the California Irrigation Management Information System (CIMIS) station 64 Santa Ynez (California Irrigation Management Information System, 2017a; figs. 1, 8).

No long-term datasets of minimum and maximum temperature within the SACVW were available before the establishment of 45107 Los Alamos in 1995. Temperature data for this study consisted of daily adjusted values from 23723 Santa Maria Airport during 1948–86, 64 Santa Ynez during 1986–95, and 45107 Los Alamos after 1995. T_{min} and T_{max} data were adjusted by calculating the difference in mean monthly T_{min} and T_{max} between station 45107 Los Alamos, station 23723 Santa Maria Airport, or station 64 Santa Ynez, and adding (or subtracting) this difference to T_{min} and T_{max} for days in which values at 45107 Los Alamos were unavailable.

Precipitation data were distributed to each HRU using the PRMS **precip_1sta** module (Markstrom and others, 2015). The *rain_adj* parameter, which accounts for spatial variation in rainfall due to elevation and other factors, was computed as the ratio of mean monthly precipitation at the centroid of each HRU from the Parameter-Estimation Regressions on Independent Slopes Model (PRISM; PRISM Climate Group, 2013) to the mean monthly precipitation calculated from measurements made at station 204 Los Alamos Fire Station #24.

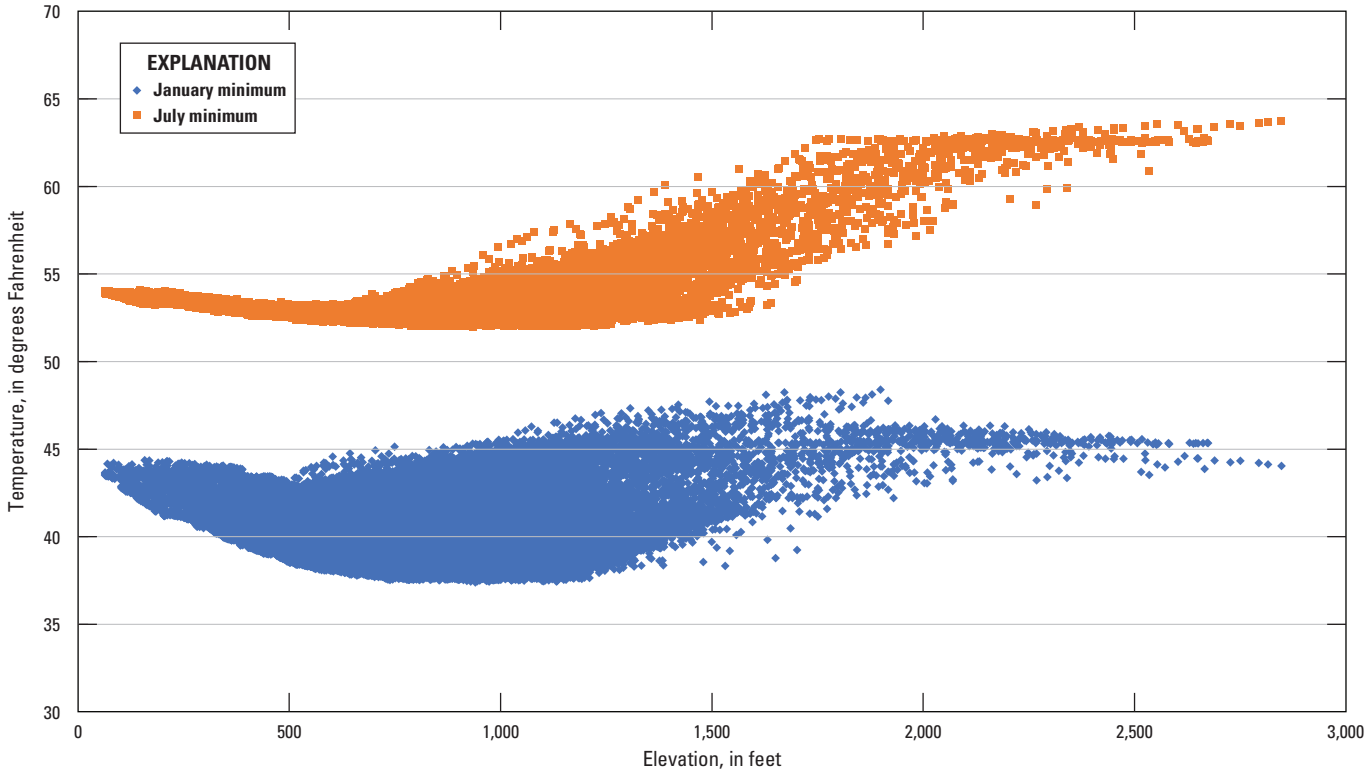

Figure 8. Mean monthly minimum temperature at each hydrologic response unit (HRU) versus elevation during January and July 1981–2010, San Antonio Creek Valley watershed, Santa Barbara County, California.

Temperature data were distributed to each HRU using the PRMS **temp_laps** module (Markstrom and others, 2015), which requires temperature data from multiple stations at different elevations. Because measured data at climate stations at different elevations are not available for the SACVW, three virtual stations at elevations of 820, 1,903, and 2,848 ft were created. The elevations of the two lower virtual stations (820 and 1,903 ft) were chosen because they correspond generally to inflection points in the plots relating mean monthly T_{min} and T_{max} (PRISM Climate Group, 2013) to elevation (figs. 8, 9). The elevation of the highest virtual station (2,848 ft) corresponds to the centroid elevation of the highest HRU in the active model area. To estimate daily T_{min} and T_{max} at each of the virtual stations, gridded mean monthly T_{min} and T_{max} data (PRISM Climate Group, 2013) were used to develop three linear regressions relating T_{min} and T_{max} to elevation for each calendar month. The first regression used data for all the HRUs between the elevation of the 45107 Los Alamos climate station (565 ft; fig. 1) and 820 ft, the second regression used data for all the HRUs between the elevations of 820 and 1,903 ft, and the third regression used data for all the HRUs between the elevations of 1,903 and 2,848 ft. The coefficients of determination (R^2) and intercepts for each regression along with the corresponding temperature lapse rates, which are the same as the slope of each regression, are given in table 2.

Potential Evapotranspiration

Potential evapotranspiration (PET) in the PRMS is calculated using the Jensen-Haise equation in the **potet_jh** module (Markstrom and others, 2015) and is directly proportional to the Jensen-Haise coefficient (*jh_coef*). The initial range of monthly values for *jh_coef* (Gardner and others, 2018) is given in table 1. PET can vary substantially according to vegetation and land-cover type. To incorporate the spatiotemporal effects of land use in the SACIM, the concept of crop coefficients is used. A monthly crop coefficient (KC) is an empirically derived monthly ratio of PET of a given land-use type to a reference ET (ET_0). A commonly used ET_0 for this purpose is derived from the Penman-Montieth equation using a grass reference surface with specific characteristics (California Irrigation Management Information System, 2020). As part of the calibration process of the decoupled PRMS-only model, monthly values for *jh_coef* were calibrated to Penman-Montieth ET_0 computed from observed data. Following this calibration, monthly values for *jh_coef* were multiplied by the KC for each HRU to produce a new *jh_coef* value for every HRU for every month.

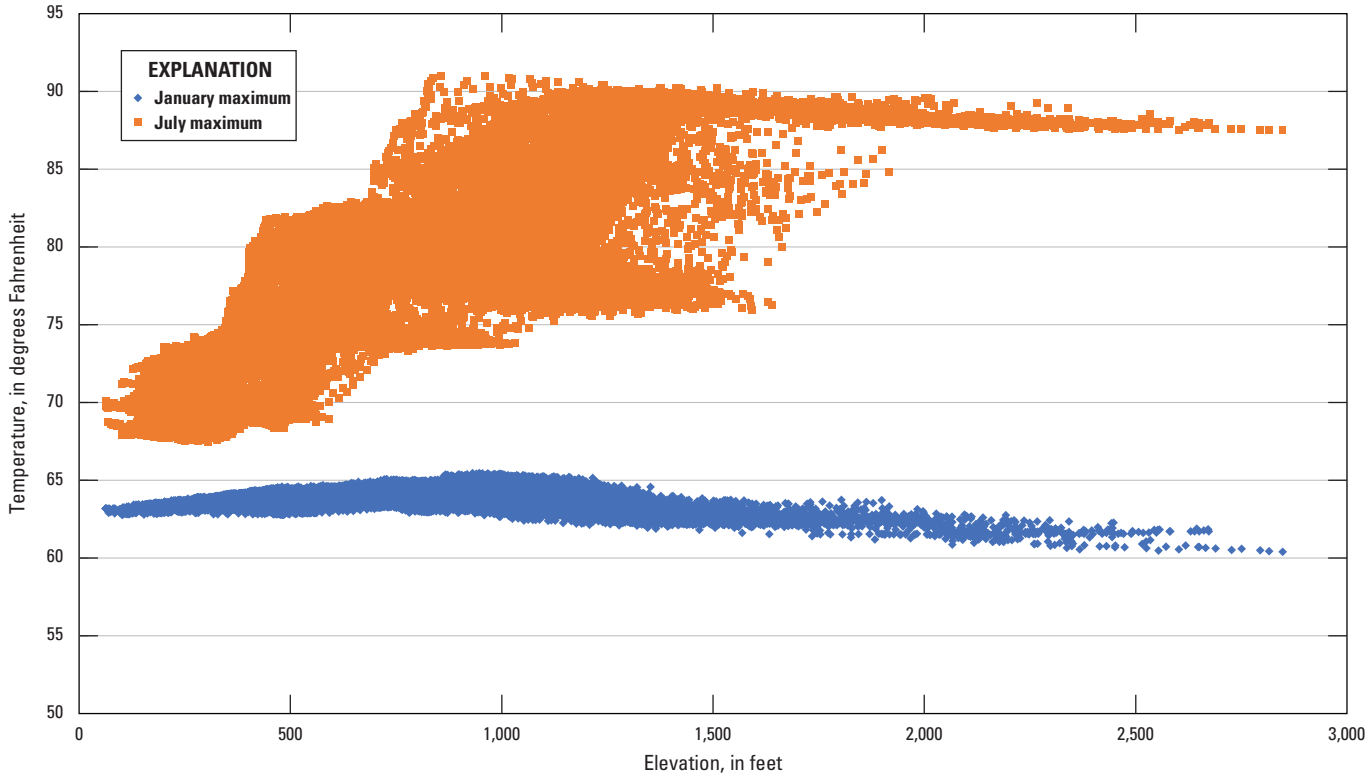

Figure 9. Mean monthly maximum temperature at each hydrologic response unit (HRU) versus elevation during January and July, San Antonio Creek Valley watershed, Santa Barbara County, California.

Table 2. Monthly temperature lapse rates used to estimate daily minimum and maximum temperatures in the San Antonio Creek Valley watershed and the coefficients of determination for the linear regressions used to estimate the temperature lapse rates from mean monthly temperature data (PRISM Climate Group, 2013).

[Low-elevation, below 820 ft.; Mid-elevation, between 820 and 1,903 ft.; High-elevation, above 1,903 ft. **Abbreviations**: °C, degrees Celsius; m, meters]

Month	Temperature lapse rate (°C/100 m)			Linear regression intercept (m)			Linear regression coefficient of determination		
	Low-elevation	Mid-elevation	High-elevation	Low-elevation	Mid-elevation	High-elevation	Low-elevation	Mid-elevation	High-elevation
Minimum temperature (T_{min})									
January	–0.5648	0.7022	–0.0873	5.8930	2.7437	7.9193	0.0968	0.1142	0.0181
February	–0.6270	0.4913	–0.1400	6.7044	4.0235	7.9487	0.1812	0.0978	0.0832
March	–0.7102	0.5131	–0.0765	7.4668	4.4352	8.3071	0.2846	0.1377	0.0195
April	–0.5574	0.3884	–0.0789	7.7459	5.4894	8.4833	0.2729	0.1612	0.0260
May	–0.4492	0.5461	0.1815	9.2394	6.7784	9.5564	0.4175	0.5612	0.0859
June	–0.4271	0.5833	0.3626	10.8706	8.3002	10.5161	0.6571	0.4883	0.2315
July	–0.3116	1.0145	0.6608	12.0876	8.7449	12.1338	0.5547	0.5558	0.2943
August	–0.5225	1.0926	0.6155	12.5601	8.4439	12.6501	0.7117	0.6406	0.2387
September	–0.2799	0.9123	0.4293	11.8129	8.7541	12.8702	0.2142	0.6238	0.1613
October	–0.4670	0.8218	0.0187	10.2423	7.0160	12.3721	0.1293	0.2617	0.0006
November	–0.7072	0.7123	–0.0282	7.9925	4.4394	9.4755	0.1836	0.1456	0.0017
December	–0.8370	0.7159	–0.0832	6.0657	2.1877	7.4777	0.1904	0.1191	0.0153
Maximum temperature (T_{max})									
January	0.2792	–0.4091	–0.2963	17.2764	19.0148	18.5310	0.3161	0.4869	0.3421
February	0.3258	–0.4219	–0.3195	17.4196	19.3611	18.7655	0.2824	0.3551	0.3752
March	0.6206	–0.3225	–0.2018	17.7250	20.0747	19.6463	0.3224	0.1331	0.3108
April	0.8509	0.5425	–0.5003	18.5399	19.0820	24.1753	0.2235	0.1072	0.3536
May	1.7036	0.7298	–0.2913	18.4647	20.5311	25.7989	0.3459	0.1226	0.3267
June	1.8783	1.4540	–0.2739	19.3866	20.1343	29.3993	0.3237	0.2002	0.2942
July	2.7548	1.8928	–0.1830	19.8341	21.3287	32.4011	0.4308	0.2679	0.2291
August	2.6671	1.8941	–0.1971	20.2048	21.2731	32.7016	0.3870	0.2282	0.1937
September	2.2495	1.4465	–0.1559	21.0393	22.4859	30.7300	0.3710	0.2365	0.2277
October	1.4360	0.6988	–0.2381	21.4158	22.8633	27.5469	0.3482	0.1379	0.3242
November	0.5190	–0.3266	–0.2568	19.9230	22.0755	21.7980	0.3789	0.2048	0.3187
December	0.3522	–0.4511	–0.3375	17.2542	19.3357	18.5885	0.4785	0.5154	0.3649

Monthly KCs were assigned to each land-use subcategory (table 3; fig. 5 in Cromwell and others, 2022). KCs take into account the growth cycle of crops and provide an index of the integrated effect of vegetation characteristics (reflectance, roughness, and plant physiology) on PET.

Seven KCs were assumed not to vary interannually. The KC for the developed subcategory is based on cool season turfgrass in Snyder and others (2014), and the dominant land cover in the subcategory is assumed to be lawns. For forest and shrubland, which are largely native areas, the assigned KC of 0.80 (table 3) was the same value used by Tetra Tech, Inc. (2012); using a KC value less than 1.0 indicated that we assumed that these native plants have a drought-tolerant adaptation. Grasslands were assigned the same KC (1.00; table 3) as annual alfalfa in Snyder and others (2014). For the water subcategory, the KC for open water surfaces (1.10) in Snyder and others (1994) was used. The orchard land-use subcategory was assumed to consist largely of mature avocado trees. Thus, the KC for avocado from Snyder and others (2014) was used. The pasture and hayland subcategory was assigned a single, annual KC consistent with grazed pasture in Snyder and others (1994).

Table 3. Initial monthly crop coefficients used for each general land-use subcategory in the San Antonio Creek Valley integrated model, Santa Barbara County, California.

General land-use subcategory	Month											
	Jan.	Feb.	Mar.	Apr.	May	June	July	Aug.	Sept.	Oct.	Nov.	Dec.
Developed	0.80	0.80	0.80	0.80	0.80	0.80	0.80	0.80	0.80	0.80	0.80	0.80
Forest	0.80	0.80	0.80	0.80	0.80	0.80	0.80	0.80	0.80	0.80	0.80	0.80
Grassland	1.00	1.00	1.00	1.00	1.00	1.00	1.00	1.00	1.00	1.00	1.00	1.00
Shrubland	0.80	0.80	0.80	0.80	0.80	0.80	0.80	0.80	0.80	0.80	0.80	0.80
Sparsely vegetated	0.90	0.60	0.40	0.20	0.20	0.20	0.20	0.20	0.20	0.40	0.60	0.85
Water	1.10	1.10	1.10	1.10	1.10	1.10	1.10	1.10	1.10	1.10	1.10	1.10
Riparian[1]	0.80	0.80	0.80	0.80	0.90	1.00	1.10	1.20	1.20	1.15	1.00	0.85
Orchard[1]	0.70	0.70	0.70	0.70	0.70	0.70	0.70	0.70	0.70	0.70	0.70	0.70
Row crop[1]	0.90	0.60	0.40	0.55	1.12	0.92	0.53	1.12	0.95	0.40	0.60	0.85
Vineyard[1]	1.00	1.00	1.00	1.00	0.47	0.63	0.64	0.63	0.55	1.00	1.00	1.00
Bush fruit and berries[1]	0.90	0.60	0.40	0.35	0.61	0.98	1.03	0.99	0.20	0.40	0.60	0.85
Pasture and hayland[1]	0.90	0.90	0.90	0.90	0.90	0.90	0.90	0.90	0.90	0.90	0.90	0.90
Fallow/Idle Cropland[1]	0.90	0.60	0.40	0.20	0.20	0.20	0.20	0.20	0.20	0.40	0.60	0.85
Wheat[1]	0.27	0.68	1.12	1.18	1.18	0.86	0.20	0.20	0.20	0.40	0.60	0.23

[1]Crop coefficients were modified during GSFLOW calibration.

Seven KCs were assumed to vary interannually. Monthly KCs for the sparsely vegetated land-use subcategory were estimated using evapotranspiration data from the CIMIS 2-km grid at Los Alamos (California Irrigation Management Information System, 2017b) and the Irrigation Scheduling Water Balance Method documentation (table 1 and figure 6 in Snyder and others, 2014). Assigned monthly KCs for riparian land use were based on values from Howes and others (2015). Dry beans were used for the row crop land-use subcategory. Double cropping was assumed to occur during April–September. KCs derived from Allen and others (1998) were used for these months. During the other months (January–March and October–December), the KCs for the sparse land-use subcategory were used to simulate fallow conditions. For vineyards, monthly KCs during May–September were calculated assuming use of vertical-shoot-positioned (VSP) trellis systems and 8-ft row spacing (Williams, 2001). The monthly KCs for vineyards during the remaining months (January–April and October–December) were assumed to correspond to a grass cover crop. Hence, the KC for the grassland land-use subcategory was used during this unirrigated period. For the bush fruit and berries subcategory, the active cultivation period was assumed to be April through August, and KCs for these months were estimated using values for truck and berry crops in Snyder and others (1994), Allen and others (1998), and Brush and others (2004). During the other months (January–March and September–December), the KCs for the sparsely vegetated land-use subcategory were used for the bush fruit and berries subcategory (table 3). Fallow/idle cropland was assigned the same monthly KCs as the sparsely vegetated land-use subcategory. Wheat was assumed to be cultivated during December–June, and the monthly KCs were derived from Allen and others (1998) for winter wheat. During the remaining months (July–November), wheat was assigned the same monthly KCs as the sparsely vegetated land-use subcategory (table 3). Initial KCs for riparian and agricultural land-cover subcategories (table 3) were adjusted during the integrated-model-calibration stage because of their importance to the SACVW water budget, specifically agricultural pumping and ET.

MODFLOW-NWT Model Description

The groundwater model in the SACIM was constructed using MF-NWT (Niswonger and others, 2011). MF-NWT is a finite-difference model that simulates unsaturated and saturated groundwater flow in a three-dimensional heterogeneous and anisotropic medium. The MF-NWT packages used in the model are the Basic (BAS6; Harbaugh, 2005), General-Head Boundary (GHB; Harbaugh, 2005); Upstream Weighting (UPW; Niswonger and others, 2011); Multi-Node Well 2 (MNW2; Konikow and others, 2009), Streamflow Routing (SFR2; Niswonger and Prudic, 2005); and Unsaturated Zone Flow (UZF1; Niswonger and others, 2006) with the Newton formulation solver (NWT; Niswonger and others, 2011). The Agricultural Water Use (AG) package (Niswonger, 2020) is used for simulating agricultural pumping in the model. This section describes model discretization and boundaries, hydraulic properties of the subsurface, and flow processes.

Spatial and Temporal Discretization

The MF-NWT model contains a rectangular grid with a uniform grid spacing that is the same as the discretization of HRUs in the PRMS model and of the hydrogeologic framework model (Cromwell and others, 2022). The grid-cell size is 492 ft by 492 ft, with a total of 124 rows and 268 columns (fig. 5) extending over 4 layers. The number of active cells in each of the four layers varies, with only the cells in model layer four covering the entire active area of the model. The hydraulic properties are assigned to each model cell of the grid.

The vertical discretization of the groundwater model initially was the same as layers 1–6 in the hydrogeologic framework model (Cromwell and others, 2022). To decrease the execution time of the model, the number of layers were reduced to four and the layers were redefined. The distributions of thickness for model layers 1–4 are shown in figures 10 and 11. Model layer 1, which is considered unconfined in the SACIM, includes the channel alluvium, and upper and middle members of the Paso Robles Formation (fig. 10); in the eastern part of the SACVW, the lateral extent of layer 1 coincides with the extent of the fine-grained middle Paso Robles Formation. Model layer 2 primarily represents the lower member of the Paso Robles Formation and some channel alluvium in the western part of the valley and parts of the uplands (fig. 10) where channel alluvium overlays the Careaga Sandstone. In the eastern part of the SACIM, model layer 2 is considered confined where it underlies the upper and middle members of the Paso Robles Formation and unconfined in the western part of the SACIM. Model layer 3 primarily represents the Careaga Sandstone and some channel alluvium in the uplands where channel alluvium overlays consolidated bedrock. Model layer 3 is considered unconfined in the upland areas and confined in the valley areas. Model layer 4 represents the upper part of the consolidated bedrock, which also crops out along the model boundaries (figs. 3, 10). The variable thickness for model layers 1–3 (fig. 11) is based on the 3D HFM described in Cromwell and others (2022). A uniform thickness of 984 ft was used throughout the SACIM in model layer 4; it was assumed that this part of the bedrock was sufficiently weathered or contained fractures through which groundwater may flow.

The model simulates transient conditions for water year 1948 through water year 2018 (October 1, 1947, through September 30, 2018). This period was divided into 852 monthly stress periods and daily time steps for consistency with the PRMS model. Simulated hydraulic heads and flows can change each day in response to the daily changes in temperature and precipitation that are specified in PRMS. Specified pumping rates and pumping rates calculated by the model changed for each monthly stress period.

Boundary Conditions

Most of the lateral boundary of the MF-NWT model represents a groundwater divide that is assumed to coincide with the surface-water divide. The boundary is a type of specified-flux boundary where no groundwater moves across the divide (no-flow boundary condition; fig. 5). The location of groundwater divides can change with changes in hydrologic stresses; however, in this model, the divide is assumed to be static and negligible. The bottom of the model also is represented by a no-flow boundary condition.

During model calibration, a GHB was added to simulate a source of water outside the model area that supplied water to two cells along the eastern boundary (fig. 5). The modified boundary condition was needed to reasonably simulate the hydraulic heads in well 8N/31W-21J1 (fig. 5), which is the only well with relatively long-term water-level data in the eastern part of the SACVW. Pumping in this well was assumed to induce groundwater flow from the Santa Ynez groundwater basin (fig. 2) through hydrologically connected aquifer material. The rate of flow of water through the GHB is proportional to the hydraulic-head differences between the external source (specified hydraulic head) and the model cell (simulated hydraulic head). The rate of flow through the GHB is regulated by a specified hydraulic conductance. The specified hydraulic head is the earliest measured water level (1,174 ft NAVD 88) in well 8N/31W-22J1 (fig. 5). Since the measured water levels in this well did not fluctuate substantially for the period of record (calendar years 1997–2018; fig. 12), the specified hydraulic head was held constant for the simulation period.

The top boundary of the model is the water table in the uppermost active layer in the model grid. This boundary is simulated as a free-surface boundary that is allowed to move vertically in response to changes in inflow, outflow, and storage of water in the aquifer system. The initial distribution of the water table was derived from reported groundwater-level contours for 1943 (Martin, 1985); the gridded data were assigned to each layer in the model. The starting hydraulic-head distributions were adjusted during model calibration because the reported water-level contours are based on scattered data, so the actual distribution is largely unknown. The final starting hydraulic-head distribution generally followed the pattern of flow of the reported contours, and the simulated contours have a similar shape. The final distributions for model layers 1–4 are shown in figure 13.

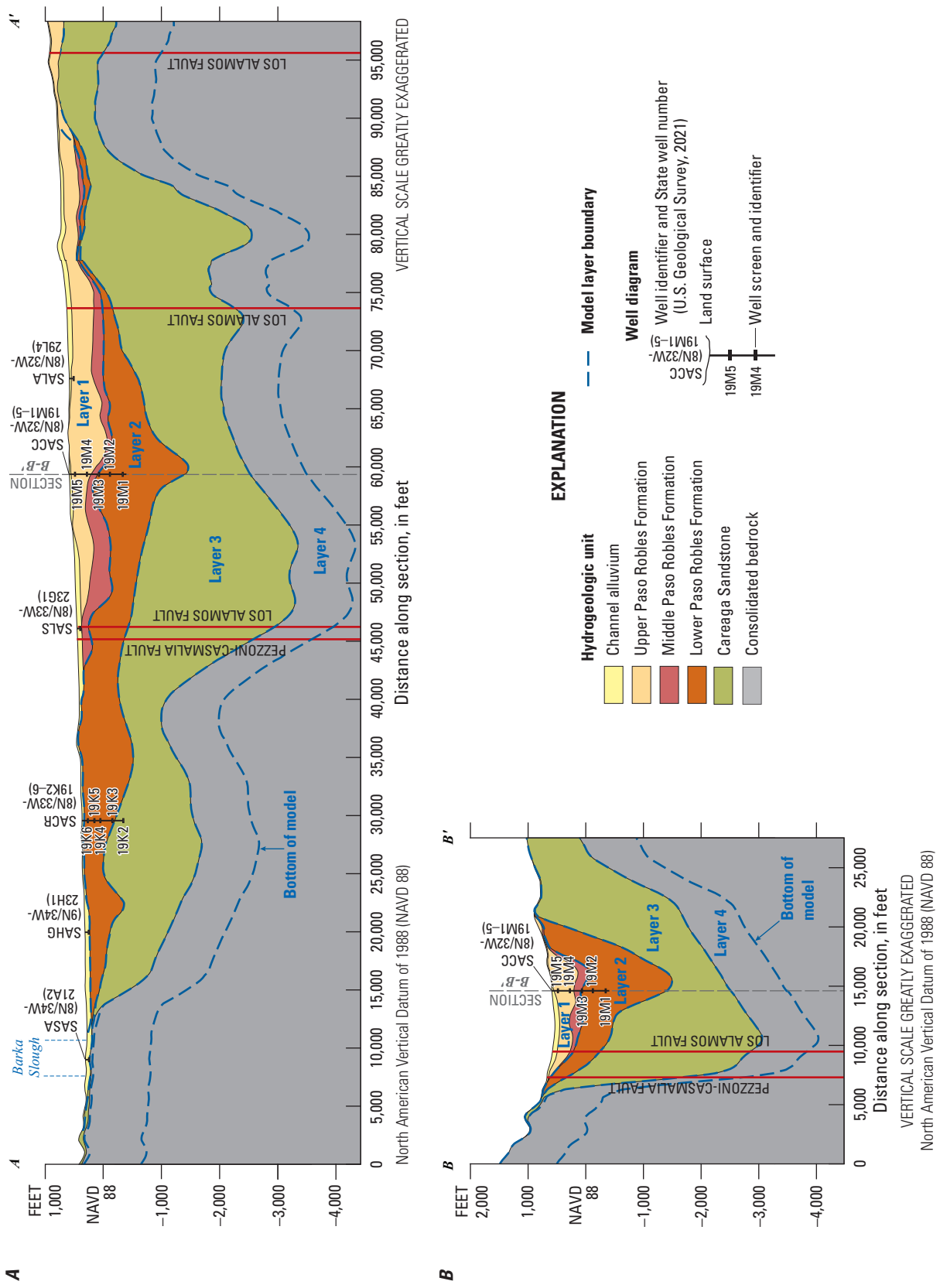

Figure 10. Cross-sectional view across San Antonio Creek Valley watershed, Santa Barbara County, California, showing hydrogeologic units and model layers along *A*, A–A'; and *B*, B–B' (cross-section locations shown in fig. 3).

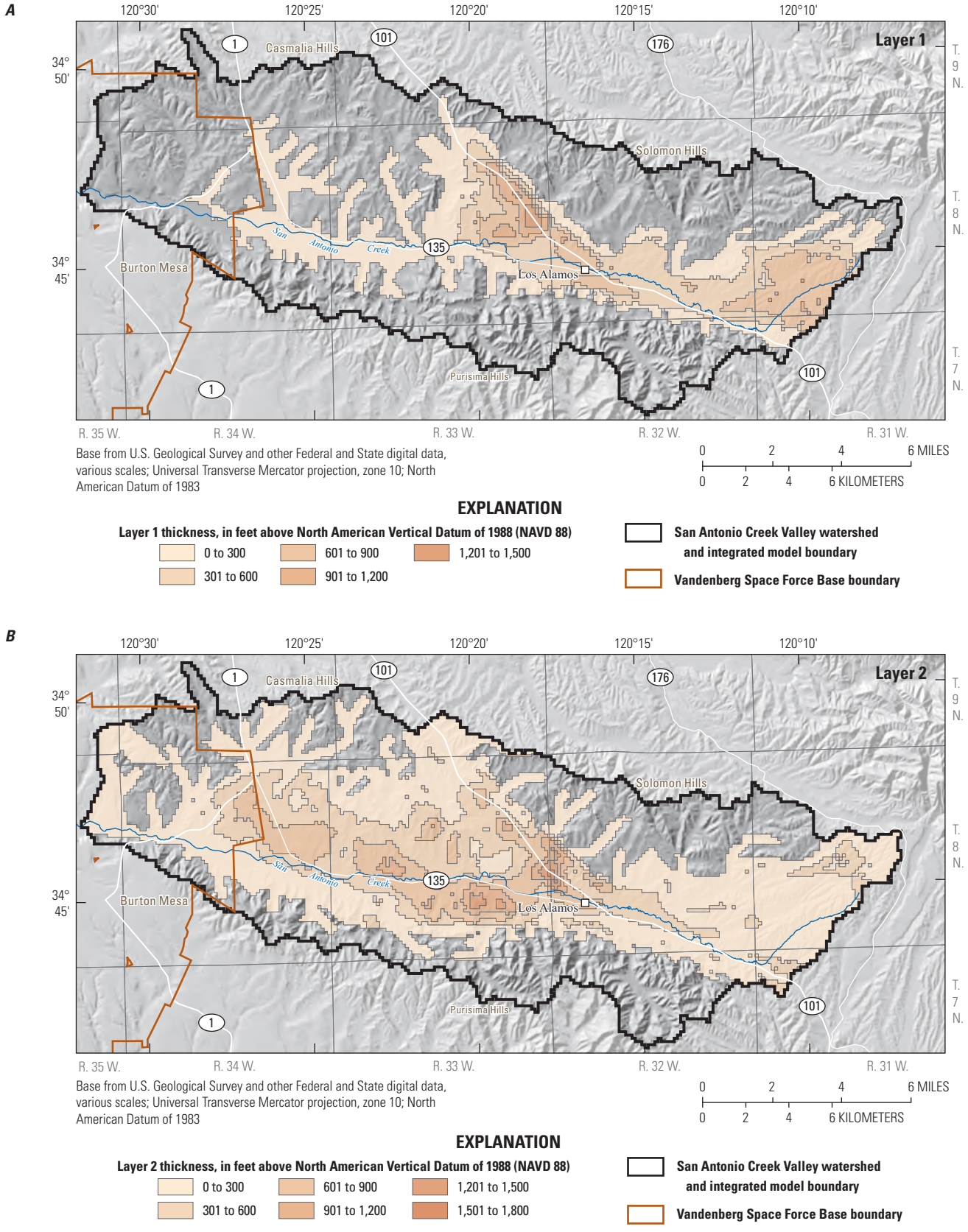

Figure 11. Thickness of model layers *A*, 1, *B*, 2, *C*, 3, and *D*, 4 in the San Antonio Creek Valley integrated model, Santa Barbara County, California.

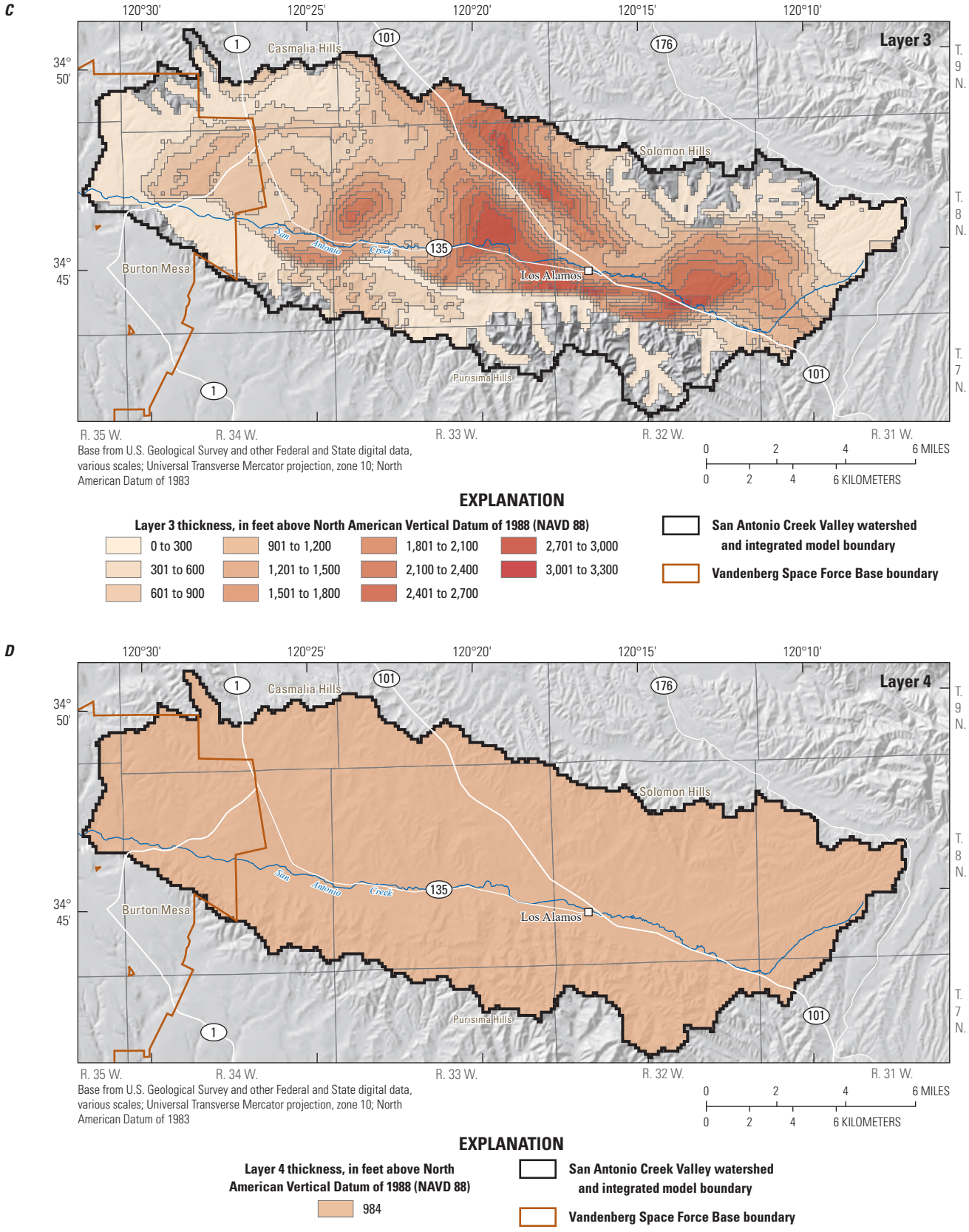

Figure 11.—Continued

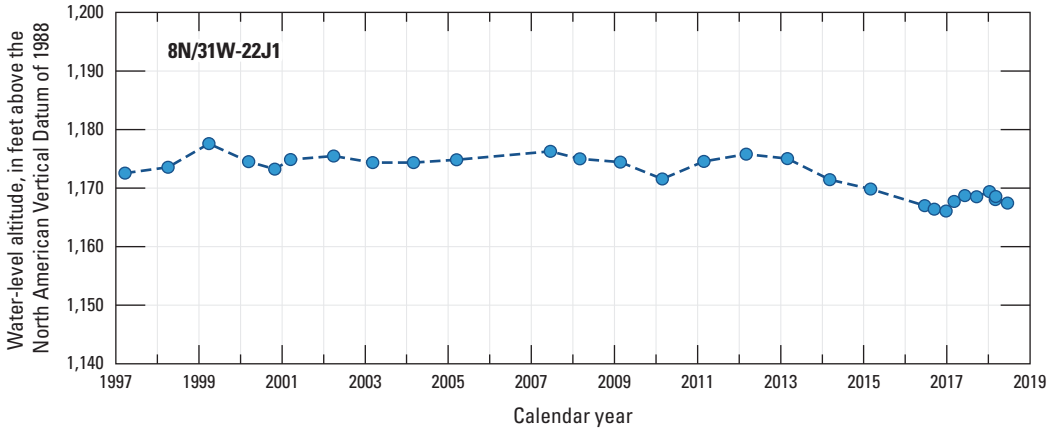

Figure 12. Measured water-level elevations for well 8N/31W-22J1 for calendar years 1997–2018, San Antonio Creek Valley watershed, Santa Barbara County, California.

Hydraulic Properties

Hydraulic properties for the MF-NWT model are horizontal and vertical hydraulic conductivity, specific storage, and specific yield. These properties affect the rate at which water moves through the aquifer and the rate and areal extent of changes in groundwater levels caused by groundwater pumping and recharge. Estimates of average hydraulic properties are assigned to each model cell. All layers are convertible and can switch between confined and unconfined flow. The hydraulic properties were adjusted during model calibration and the final hydraulic values are given in "MODFLOW-NWT Results" section of this report.

Hydraulic Parameter Zonation

Hydraulic parameter zones are the basis for distributing hydraulic properties to model cells. The hydraulic parameter zones in the SACIM initially were based on the hydrogeologic units defined in the 3D HFM (Cromwell and others, 2022). The hydraulic property distributions were input to the UPW package (Niswonger and others, 2011) in GSFLOW. During model calibration, the parameter zonation was refined to better match the simulated hydraulic heads to the measured data. A description of the hydrogeologic units in the refined zonation is given in table 4. The refined zonation included (1) separate zones for the hydrogeologic units in upland and valley areas, (2) the area where the upper and middle Paso Robles Formation were incorporated into model layer 1 in the eastern part of the watershed to account for the reduced horizontal and vertical conductivity where the fine-grained middle unit is present, and (3) separate zones for the different members of the Careaga Sandstone and the consolidated bedrock. The distributions of the final hydraulic parameter zones for model layers 1–4 are shown in figure 14.

Hydraulic Conductivity

A steady-state model was developed as part of the calibration process to provide the initial values of horizontal hydraulic conductivity (HK) for the SACIM. The initial horizontal hydraulic conductivity (HK) distribution for the steady-state model was estimated from reported values (Martin, 1985; Tetra Tech, Inc., 2013) and from aquifer-test results for this study (Cromwell and others, 2022). The HK values were distributed by hydraulic parameter zone. The initial values for the SACIM were adjusted during model calibration. The final HK values are given in the "MODFLOW-NWT Results" section of this report.

Horizontal anisotropy (HANI) indicates a different HK along columns (north-south direction) of the model grid from the HK along rows (east-west direction); HANI is calculated as the ratio of HK along columns to the HK along rows (Harbaugh, 2005). Horizontal anisotropy was included in the model because of the steeply dipping layers in parts of the northern and southern parts of the SACVW, which are likely to have a north-south HK between the horizontal HK and vertical hydraulic conductivity (VK). A constant value of HANI was used for each layer in the SACIM. The initial value of HANI was one for each layer, indicating each layer was isotropic. These values were adjusted during model calibration and the final values are given in the "MODFLOW-NWT Results" section.

The VK for each model layer is computed in the model by dividing the HK values by the vertical anisotropy (VANI), where VANI is defined as the ratio of HK to VK. For example, a VANI of 10 means that the HK is 10 times greater than the VK. The VANI distribution in the SACIM is determined for each hydraulic parameter zone in the model. The initial VANI values were based on reported HK and VK values (Bright and others, 1997; Tetra Tech, Inc., 2013). These values were adjusted by parameter zone during model calibration; the final VANI values are given in the "MODFLOW-NWT Results" section of this report.

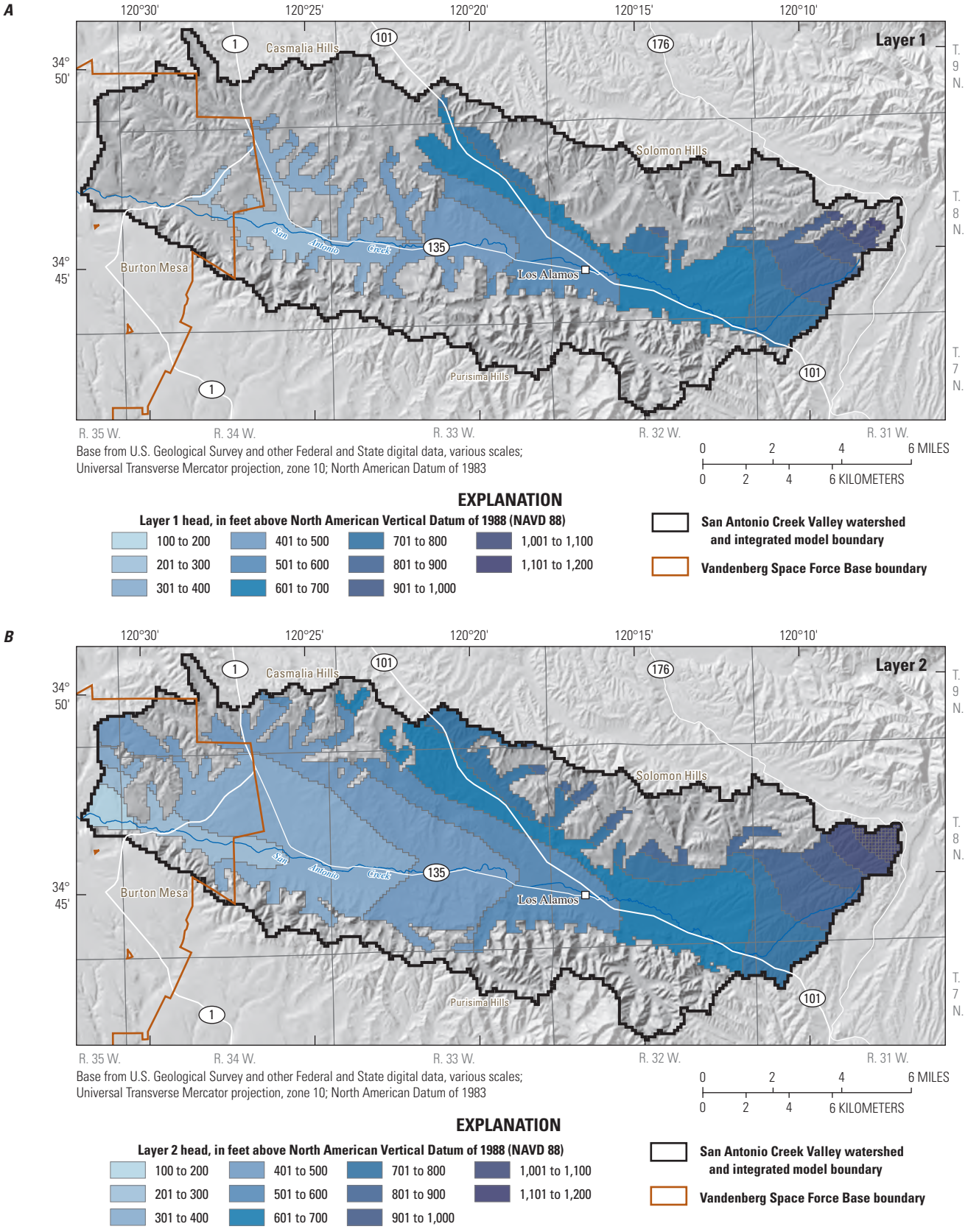

Figure 13. Final distributions of starting hydraulic heads in model layers *A*, 1, *B*, 2, *C*, 3 and *D*, 4 in the San Antonio Creek Valley integrated model, Santa Barbara County, California.

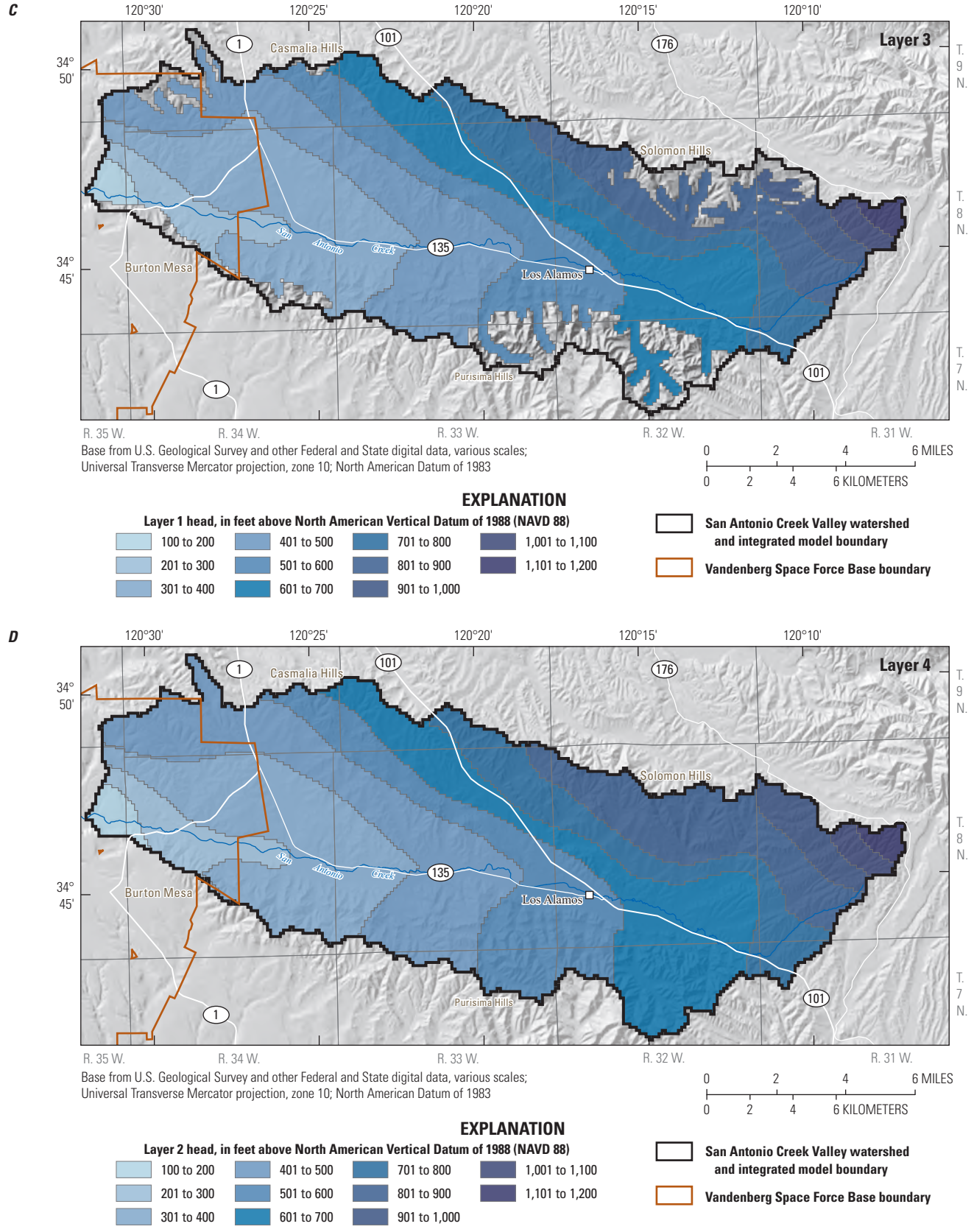

Figure 13.—Continued

Table 4. Description of hydrogeologic units in parameter zones of the San Antonio Creek Valley integrated model, Santa Barbara County, California.

[West valley and uplands refers to area where the middle Paso Robles Formation is absent; east valley and uplands refer to area where the middle Paso Robles Formation is present.]

Zone number	Geologic unit represented
Layer 1	
Valley	
13	Channel Alluvium
135	Channel Alluvium with upper and middle Paso Robles Formation
Uplands	
131	Channel Alluvium
141	Channel Alluvium with upper and middle Paso Robles Formation
151	Upper and middle Paso Robles Formation
161	Upper and lower Paso Robles Formation, middle member absent
Layer 2	
Channel Alluvium	
13	Valley
132	Uplands
134	Uplands
Lower Paso Robles Formation	
Valley	
10	West
11	East
Uplands	
102	West
103	West
104	West
111	East
Layer 3	
133	Channel Alluvium
Careaga Sandstone	
Valley	
91	Cebada member
92	Graciosa member
93	Undifferentiated
Northeast Uplands	
931	Cebada member
932	Graciosa member
933	Undifferentiated
Northwest Uplands	
934	Undiifferentiated
935	Undiifferentiated
Southern Uplands	
9311	Cebada member
9322	Graciosa member
9333	Undifferentiated
Layer 4	
Consolidated Bedrock	
Valley	
81	Foxen Formation
82	Sisquoc Formation, southeast valley
811	Foxen Formation, western valley
Uplands	
841	Foxen Formation
842	Monterey Formation
843	Sisquoc Formation, northern and central uplands
8411	Sisquoc Formation, eastern uplands
8433	Sisquoc Formation, soutwestern uplands
8434	Sisquoc Formation, southeastern uplands

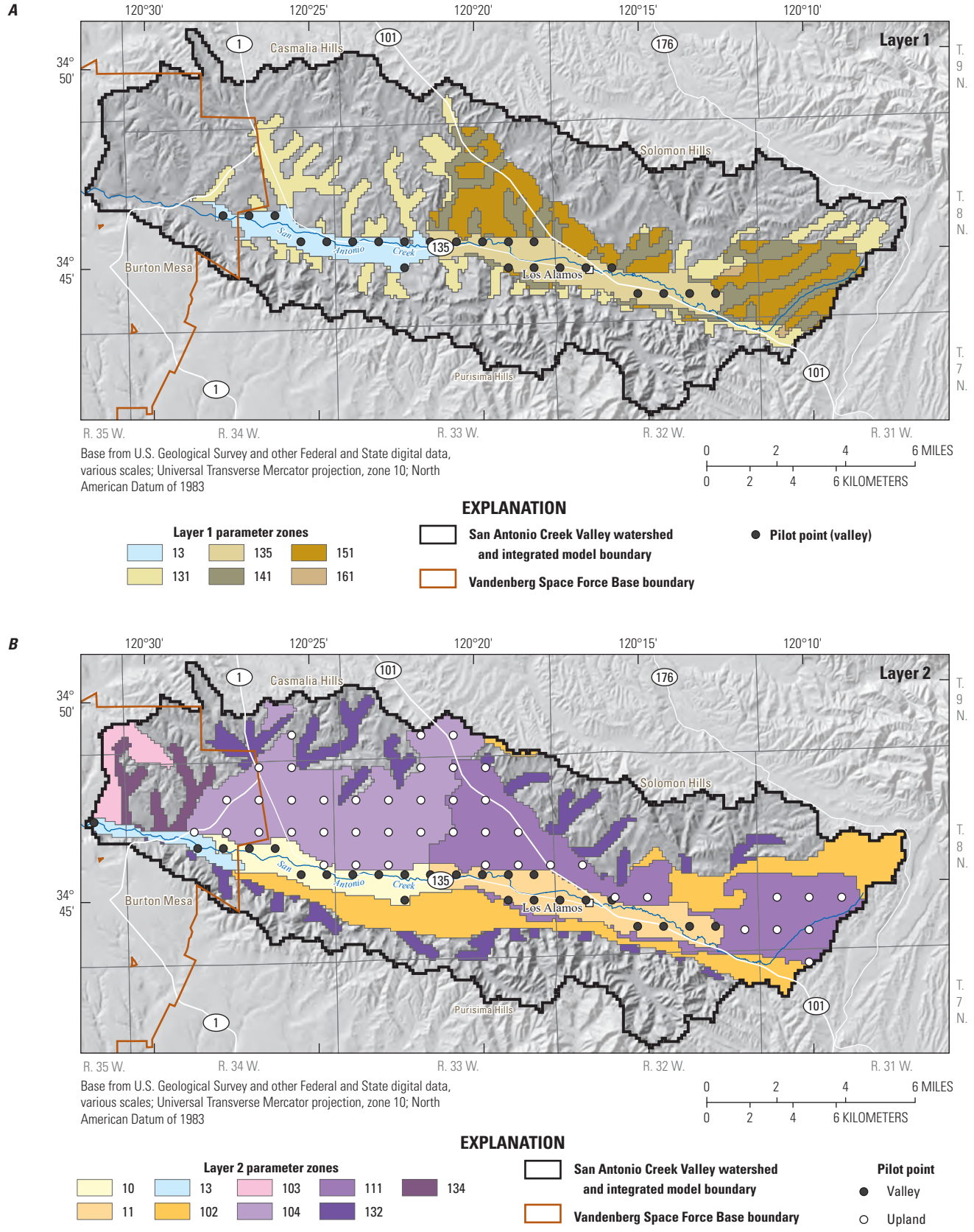

Figure 14. Parameter zones and location of pilot points for model layers *A*, 1, *B*, 2, *C*, 3, and *D*, 4 in the San Antonio Creek Valley integrated model, Santa Barbara County, California.

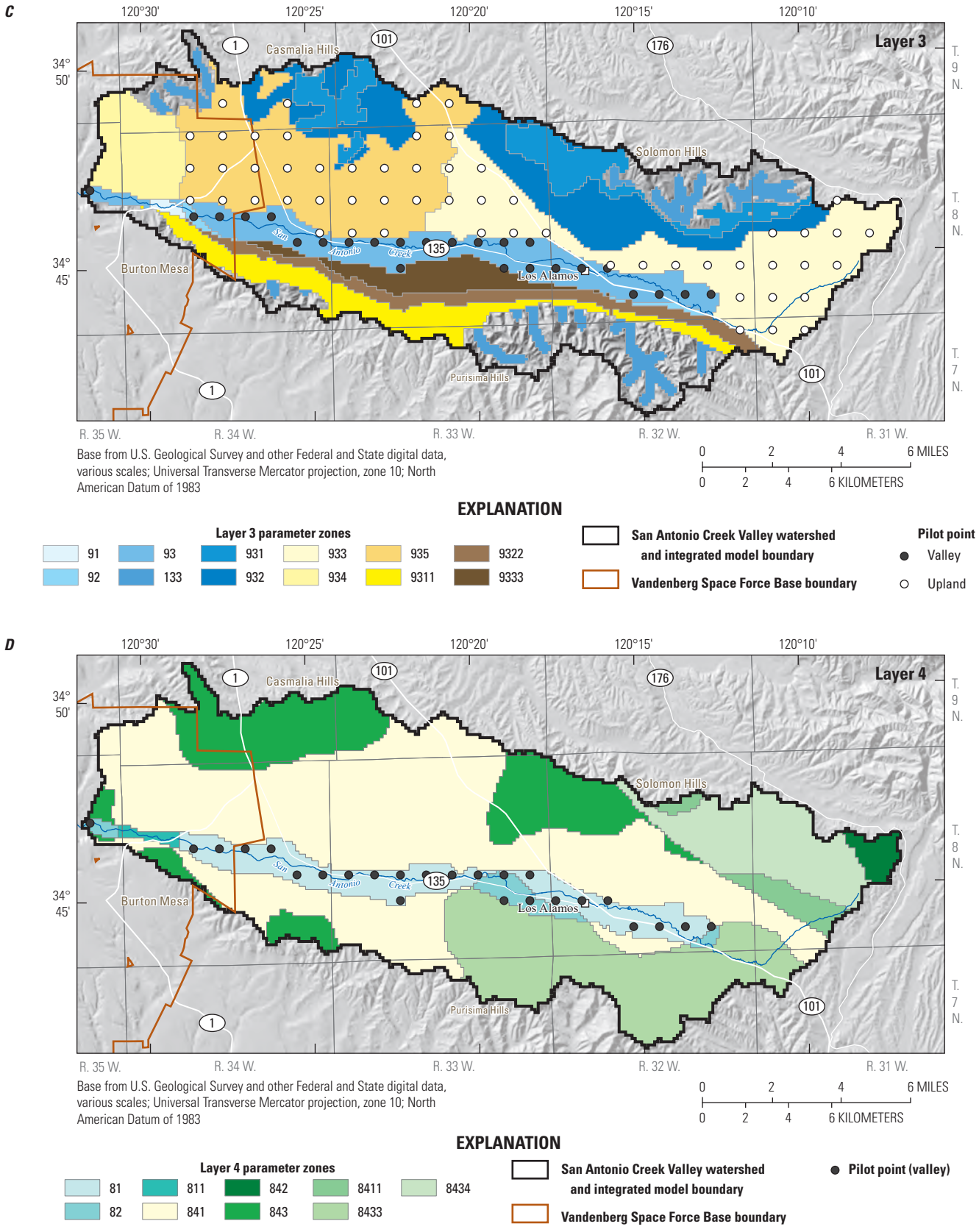

Figure 14.—Continued

Storage Properties

Storage properties (specific yield and specific storage) are defined for each cell in the model domain and are distributed according to parameter zone. Specific yield (SY) is the volume of water that an unconfined aquifer releases from or takes into storage for each unit of surface area of aquifer for each unit of change in hydraulic head in the water table (Freeze and Cherry, 1979). Specific storage (SS) is the volume of water that a unit volume of confined aquifer releases from or takes into storage for each unit of change in hydraulic head in the confined aquifer. The SY and SS values were distributed by parameter zone and were adjusted during model calibration. The final values are given in the "MODFLOW-NWT Results" section of this report.

An initial SY value of 0.15 was assigned to each parameter zone in the SACIM. The value is within the range of reported SY values for the alluvium and Paso Robles Formation (Hutchinson, 1980; Tetra Tech, Inc., 2013). In the UPW package, model layers for the GSFLOW model are defined as convertible. In convertible layers, a confined layer becomes unconfined when the hydraulic head declines below the top of the layer. The SY is used when simulating unconfined or water-table conditions. Because layers in the SACIM are designated as convertible, the SY was defined for all layers but was not necessarily used.

The initial SS value for each parameter zone was 3.28×10^{-5} per foot (1/ft). Prior information about specific storage for the San Antonio Creek Valley groundwater basin was not available; however, the initial value is within the range of model-calibrated specific-storage values for inland groundwater basins near the city of Santa Barbara (Nishikawa, 2018).

Flow Processes

Flow processes in the MF-NWT component of the SACIM include one-dimensional unsaturated vertical flow below the soil zone and three-dimensional saturated flow below the water table. Groundwater flow through the UZ, groundwater recharge, and groundwater discharge to land surface is simulated in GSFLOW using the UZF1 package (Niswonger and others, 2006). Saturated flow is simulated using MF-NWT (Niswonger and others, 2011). Stream-aquifer interactions and streamflow routing along San Antonio Creek and its tributaries are simulated using the SFR2 package (Niswonger and Prudic, 2005).

Unsaturated Zone

Inputs to the UZF1 package are made to each active model cell underlying the corresponding soil-zone HRU in the PRMS model (fig. 5). These inputs include the recharge and potential evapotranspiration rates for the steady-state model that are simulated by the PRMS model, vertical saturated hydraulic conductivity (VKS), the surface hydraulic conductivity (SURFK), the average height of undulations in the land surface (SURFDEP), the saturated water content, the extinction water content, and the Brooks-Corey epsilon used for the transient simulations (Niswonger and others, 2006). SURFK and SURFDEP are used to calculate rejected infiltration and surface leakage (Niswonger and others, 2006).

In the transient SACIM, the residual PET is the unused PET computed by the PRMS model that is available to the UZ and groundwater system (Markstrom and others, 2008). The residual PET rates are the maximum rates of ET from the unsaturated and saturated zones. Parameters in the UZF1 package that are used to determine groundwater ET are the ET extinction depth and the extinction-water content. The ET extinction depth is relative to land surface, and the PET rates and ET extinction depths are defined for each active model cell underlying the soil zone. If the simulated hydraulic head is at or above the UZ, then the residual PET rates are computed by the PRMS model (Markstrom and others, 2008). If the simulated hydraulic head declines below the specified extinction depths, subsurface ET ceases. The distribution of the ET extinction depth is based on the rooting-depth of vegetation present in the SACVW. The ET extinction-depth distribution was adjusted during calibration of the steady-state model using a multiplier; this value was not adjusted during calibration of the transient model. The spatially constant extinction-water content (3.54 ft^3 of water per 35 ft^3 of UZ) was not adjusted during the calibration process.

The VKS influences the rate of groundwater movement through the UZ to the saturated zone with higher VKS values allowing greater infiltration through the UZ. The VKS was discretized by dividing the uppermost active layer in the model into six zones (fig. 15). An index value was assigned to each zone corresponding to the geologic unit present in the uppermost active layer, with the highest value (20 feet per day; ft/d) for the channel alluvium, which is the most permeable unit, and the lowest value (3.3 ft/d) for the consolidated bedrock. The VKS distribution also was used to define the SURFK distribution. The VKS and SURFK distributions were adjusted during model calibration by using a multiplier, which had an initial value of 1.0. The final multipliers were 0.1 and 9.03×10^{-3} for the VKS and SURFK distributions, respectively. SURFDEP is a constant value that was determined during model calibration to be 0.46 ft.

Other hydraulic properties that are used to simulate flow through the UZ were given spatially constant values. These properties include the saturated, residual, and initial moisture contents (10.6, 5.3, and 5.9 ft^3 of water per 35 ft^3 of UZ, respectively), and the Brooks-Corey epsilon (4.0). These values were not adjusted during calibration of the SACIM.

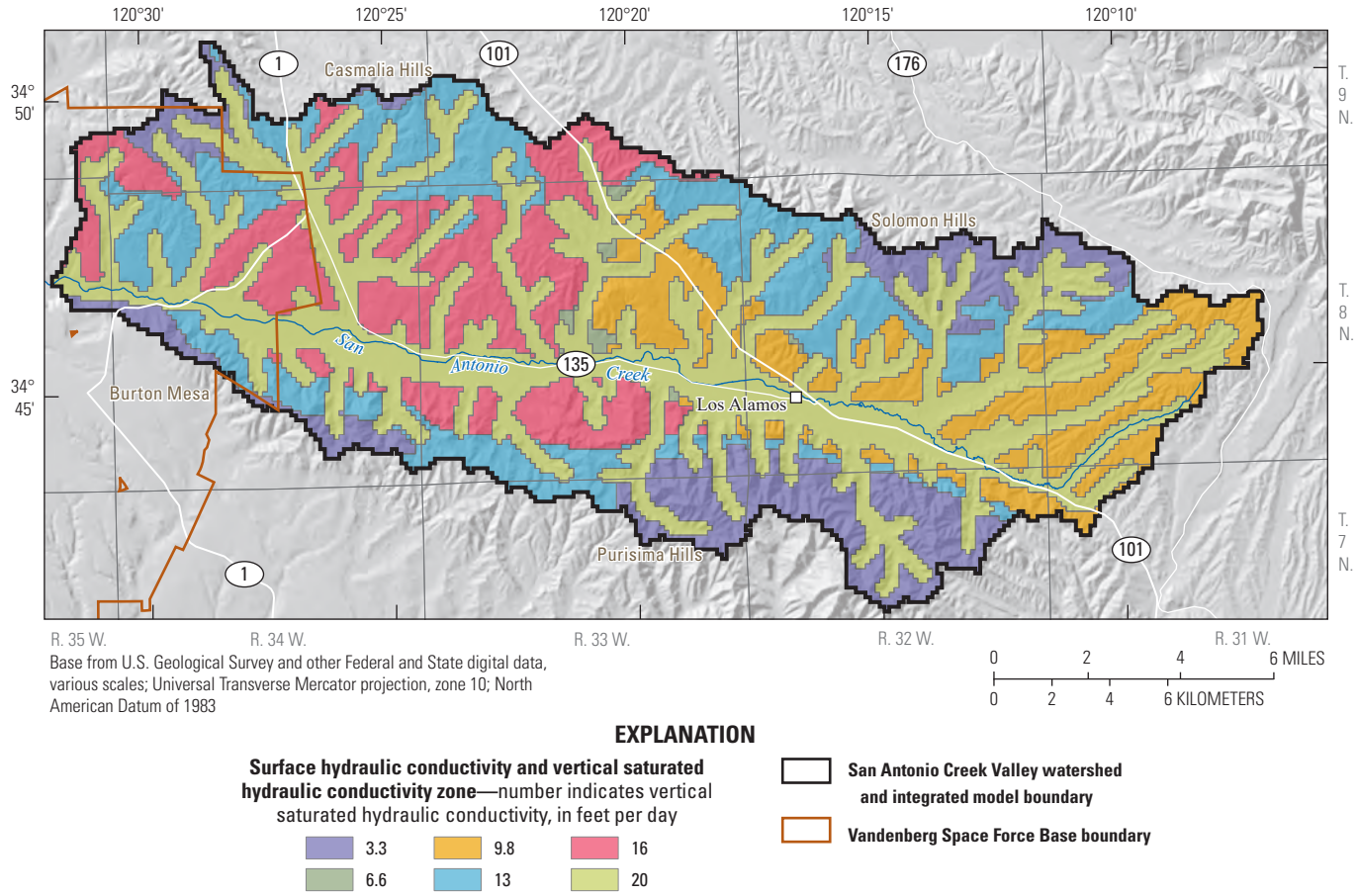

Figure 15. Surface hydraulic conductivity and vertical saturated hydraulic conductivity zones in the MODFLOW-NWT model for the San Antonio Creek Valley integrated model, Santa Barbara County, California.

Streamflow Routing

The SFR2 package simulates the interactions among San Antonio Creek, its tributaries, and the groundwater system and tracks the amount of flow in the streams. This head-dependent boundary condition allows for groundwater discharge to streams (gaining stream reaches) and stream infiltration into the underlying aquifer (losing stream reaches). The main factors that determine whether a stream reach is gaining or losing are the simulated hydraulic heads in the aquifer below the stream, the streambed elevation, and the vertical hydraulic conductivity of the streambed. The length and width of the stream reach and the vertical hydraulic conductivity of the streambed are used to calculate the streambed conductance for the reach. In GSFLOW, streams superimposed on the aquifer system are divided into segments and reaches (Markstrom and others, 2008). A segment begins where streamflow from surface sources, such as overland flow, is added to the stream. A reach is the part of a segment that corresponds to an individual model cell in the finite-difference grid used to simulate groundwater flow in the aquifer system.

There are 203 segments divided into 1,638 reaches in the SACIM. The stream segments route streamflow along San Antonio Creek to one outflow point on the boundary of the SACIM near USGS streamgage San Antonio Creek near Casmalia, Calif. (11136100; fig. 7), herein referred to as “the Casmalia streamgage” (11136100). The streambed elevation in each SFR cell was determined using the mean DEM value that was adjusted by the CRT to fill undeclared swales or circular flow paths (Henson and others, 2013). The initial values for streambed hydraulic conductivity were estimated from reasonable values (Cromwell and others, 2022). The stream segments initially were grouped into six zones. The number of segment zones were increased to 13 (fig. 7) during model calibration; the hydraulic conductivity values for each zone also were adjusted during model calibration.

Inflows

Inflows to the saturated zone include leakage from streams, groundwater-boundary flow, recharge in areas not containing stream channels, and irrigation-return flow. Leakage from streams is a head-dependent boundary simulated by the SFR2 package as explained previously in the "Streamflow Routing" section of this report. Groundwater-boundary flow from an adjacent groundwater basin is simulated as a head-dependent boundary, as explained in the "Boundary Conditions" section of this report. Groundwater recharge is defined for this report as the net quantity of water that moves downward through the UZ. The source of inflow into the saturated UZ is infiltration through the bottom of the soil zone. Irrigation-return flow from pumped wells is the quantity of water applied to irrigated crops that is returned to the groundwater system after ET from crop irrigation. Irrigation-return flow is simulated by the SACIM as described in the "Agricultural Pumpage" section in this report. Other possible sources of recharge include infiltration of effluent irrigation-return flow and leaking water-supply pipes and septic systems. Effluent irrigation is measured, but the quantities are small (55 to 150 acre-ft/yr; Cromwell and others, 2022) compared with other fluxes in the watershed; therefore, effluent irrigation was not included in the model. Leakage from water-supply lines and septic systems was assumed to be negligible.

Outflows

Groundwater outflow from the SACVW is primarily pumpage, stream discharge, and ET. Groundwater is the main source of water for municipal and irrigation and is used to supplement military water supply. Measured data or estimates were available for municipal and military pumpage; however, stream discharge, ET, and pumpage for agricultural irrigation were estimated as part of this study.

Military and Municipal Pumpage

Municipal and military pumpage was simulated using the MNW2 package (Konikow and others, 2009). The MNW2 package simulates wells completed in multiple aquifers and allows vertical groundwater movement through the well bores. The groundwater pumping rates for municipal and military wells were distributed dynamically to model layers on the basis of hydraulic conductivity and the saturated length of the perforated interval in each layer.

Municipal pumpage was assigned to five wells during the simulation period; the wells are located within the Los Alamos Services District boundary area (fig. 16). Prior to 1958, there was no reported municipal pumpage in the SACVW. Annual pumpage was reported for 1958 through 1992 calendar years (Martin, 1985; Cromwell and others, 2022) and monthly pumpage was reported for 1993 through 2018 calendar years (K. Barnard, Los Alamos Community Services District, written commun., 2019). Two of the five wells were active during calendar years 1958–77 (County of Santa Barbara, 2010), and the reported annual pumpage from Martin (1985) and Cromwell and others (2022) was distributed evenly for each month and evenly to each well during this period. The locations of these older wells are not known but are assumed to be near the location of recent active wells. Pumping from these wells was discontinued in the 1970s (County of Santa Barbara, 2010). Three wells became active at different times after 1977 (County of Santa Barbara, 2010), and the location of these wells are known (fig. 16). From 1978 through July 1988, the estimated pumpage was assigned to one well. From July 1988 through 1992, the estimated pumpage was distributed evenly for each month and evenly to two wells, and from 1993 through June 2006, the measured data were assigned to each of these two wells. From July 2006 through September 2018, the measured data were assigned to three wells.

Military pumpage in the SACVW was reported monthly for each active well during the period 1964 through 2018 (K. Domako, Vandenberg Space Force Base, written commun., 2019). The military wells are located only within the bounded area in the western part of the SACVW shown in figure 16.

Agricultural Pumpage

The amount of pumpage for agriculture had not been measured; therefore, pumping rates were estimated by simulating irrigation demand using the Agricultural Water-Use (AG) Package (Niswonger, 2020). Agricultural irrigation demand was reconstructed from areas of irrigated crop types. The compilation and analysis of land-use data used to determine the irrigated areas are described in Cromwell and others (2022). Irrigated areas for seven years with land-use data (land-use year), 1959, 1968, 1977, 1986, 1996, 2006, and 2016, were mapped to model cells. The irrigated model cells for each land-use year were used for the time periods (designated as "land-use period" herein) given in table 5. For example, the irrigated model cells for the 1959 land-use year were used for the water years 1948–63 land-use period (table 5). The number of years in the land-use periods ranged from 6 to 16 (table 5).

The ETDEMAND option in the AG package is used to indicate that irrigation demand is estimated by the model. The simulated irrigation demand is a net value that also accounts for irrigation-return flow. An additional seasonal ramp-down factor was used for crops that are irrigated primarily from April through September. KC values were ramped down from October through December to 10 percent of the specified KC value and ramped back up from 10 to 100 percent during January through March to account for potential irrigation during winter to early spring and frost protection (table 6). Monthly KC values for each land-use subcategory in the SACVW are used in the calculation of irrigation demand (Niswonger, 2020).

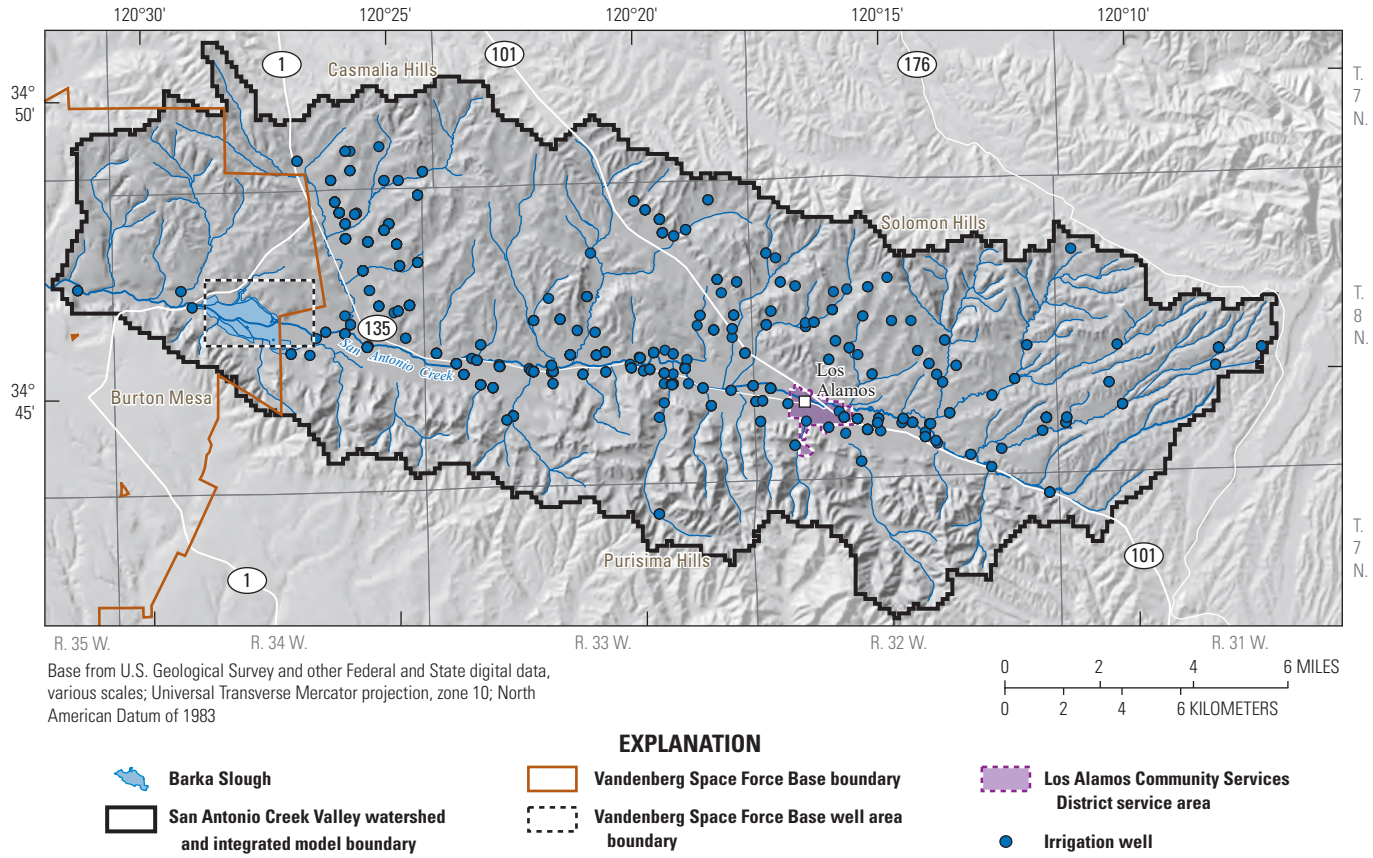

Figure 16. Location of pumping wells in the San Antonio Creek Valley integrated model, Santa Barbara County, California.

Table 5. Land-use period and number of active agricultural wells in the San Antonio Creek Valley integrated model, Santa Barbara County, California.

Land-use year	Land-use period	Number of wells
1959	1948–63	43
1968	1964–73	47
1977	1974–82	59
1986	1983–92	100
1996	1993–2001	103
2006	2002–12	171
2016	2013–18	175

Well location, perforated interval, and maximum pumping rate for each irrigation well are required to integrate groundwater pumpage into the model. Because a complete record of irrigation wells in the SACVW was not available, the existing record of well locations was mapped according to tax assessors' parcels that overlay the polygons representing irrigated areas for each land-use year. In general, one well was assigned to a model cell in each parcel overlying the irrigated polygon; however, if the parcel contained multiple irrigated fields, additional wells were added. If a known irrigation well was not located near an irrigated polygon, a virtual well was created, and construction information for other known wells nearby were used to distribute pumpage to model layers. Simulated irrigation demand was distributed to model layers based on the perforated interval of the well. The perforated interval or depth of the well or borehole were known for most wells; these data are published in NWIS (U.S. Geological Survey, 2021) or in a companion data release (Ely and others, 2022). If only the depth of a well or borehole was known, the length of the perforated interval from a nearby well was used; it was assumed that the bottom of the well or borehole was the bottom of the perforated interval. If construction information was not available, the well depth and perforated interval for a nearby well was used. The number of active wells changed for each land-use period and ranged from 43 for the 1948–63 period to 175 for the 2013–18 period (table 5). The distribution of irrigation wells is shown in figure 16. The irrigation demand was distributed evenly to the model cells representing the irrigated area; the demand is used as pumpage for agricultural well corresponding to the irrigated area.

Maximum irrigation pumping rates are used in the AG package to constrain the amount of water required to meet the irrigation demand (Niswonger, 2020). The daily maximum pumping rates for irrigation wells in the SACIM were calculated by multiplying the area of the irrigated field by an annual crop-water demand of about 6 ft/yr and dividing

Table 6. Ramping factors for crop coefficients in the San Antonio Creek Valley integrated model, Santa Barbara County, California.

[FAO-56, Food and Agriculture Organization (FAO) of the United States Irrigation and Drainage Paper No. 56; VSP, vertical shoot positioned trellis]

Landfire code	Crop type	Jan.	Feb.	Mar.	Apr.	May	June	July	Aug.	Sept.	Oct.	Nov.	Dec.
13980	Avocado (mature FAO-56[1])	1	1	1	1	1	1	1	1	1	1	1	1
13984	Dry Beans (double cropped bare FAO-56)	0.1	0.25	0.5	1	1	1	1	1	1	0.5	0.25	0.1
13981	Vineyard (VSP 8-foot spacing)	0.1	0.25	0.5	1	1	1	1	1	1	0.5	0.25	0.1
13982	Truck and Berry Crops	0.1	0.25	0.5	1	1	1	1	1	0.8	0.5	0.25	0.1

[1]Allen and others, 1998.

by the number of days in a year. The value for crop-water demand was chosen to be higher than the likely actual demand for crops in the SACVW but low enough to constrain irrigation pumpage to reasonable values. If the irrigation well was perforated in more than one layer, the maximum pumpage initially was distributed to each layer based on the percent perforated interval in the layer and HK values of the steady-state model. This distribution was revised using HK values from the transient model during calibration.

PRMS-Only Model Calibration and Model Fit

The first step of model calibration was performed using the PRMS-only mode to ensure the PRMS component in the SACIM was properly simulating the surface-ET processes. The SACIM uses the modified degree-day (**ddsolrad**) module for simulating daily solar radiation and the Jensen-Haise (**potet_jh**) module for simulating ET_0 (Markstrom and others, 2015). In the first step of the PRMS-only calibration process, parameters *dday_intcp* and *dday_slope* were adjusted to calibrate the model to mean monthly values for solar radiation (table 1). In the second step, the monthly parameter *jh_coef* was adjusted to calibrate PRMS to mean monthly values for potential ET (table 1). Data used to calibrate solar radiation are from the Western Regional Climate Center (2017) for Remote Automatic Weather Station (RAWS) Vandenberg (fig. 1) and two locations on the CIMIS 2-km spatial-data grid (California Irrigation Management Information System, 2017b) that were chosen to represent the valley bottom (Los Alamos, fig. 1) and the valley ridge (Camelback; fig. 1). Data from these two locations on the CIMIS 2-km spatial-data grid were used to calibrate ET_0. The selected period calendar years 2003–16 for solar-radiation and potential-ET calibration reflects the availability of published data for these sites. The lack of temporal data is a limitation because the available data do not capture all the climate variations during the water years 1948–2018 simulation period of the SACIM.

The automated method used to estimate *dday_intcp*, *dday_slope*, and monthly values for *jh_coef* is a nonlinear-regression, parameter-estimation software known as PEST++ (Welter and others, 2015; White and others, 2018), which uses a widely used algorithm known as the Gauss-Marquardt-Levenberg method. This method is used to adjust initial parameter values so that the weighted sum of the squared differences between observations and their corresponding model-simulated values (that is, the objective function) is minimized. Comparisons of simulated and observed solar radiation (fig. 17) and ET_0 (fig. 18) data indicate an overall good fit of simulated values to observed data. The PEST++ correlation coefficient for the solar-radiation calibration is 0.98; the correlation coefficient for the ET_0 calibration also is 0.98. However, potential ET is underestimated in the summer and overestimated in the winter at the Los Alamos location, while it is slightly overestimated in the summer and underestimated in the winter at the Camelback location. The calibrated parameters *dday_intcp* and *dday_slope* are fixed throughout the calibration of the coupled SACIM. The monthly values for *jh_coef* from this stage are multiplied by the KC for each HRU (table 3) to produce a new *jh_coef* value for every HRU for every month. These new *jh_coef* values, now with dimension nmonths by nhru, are further calibrated during the SACIM calibration stage.

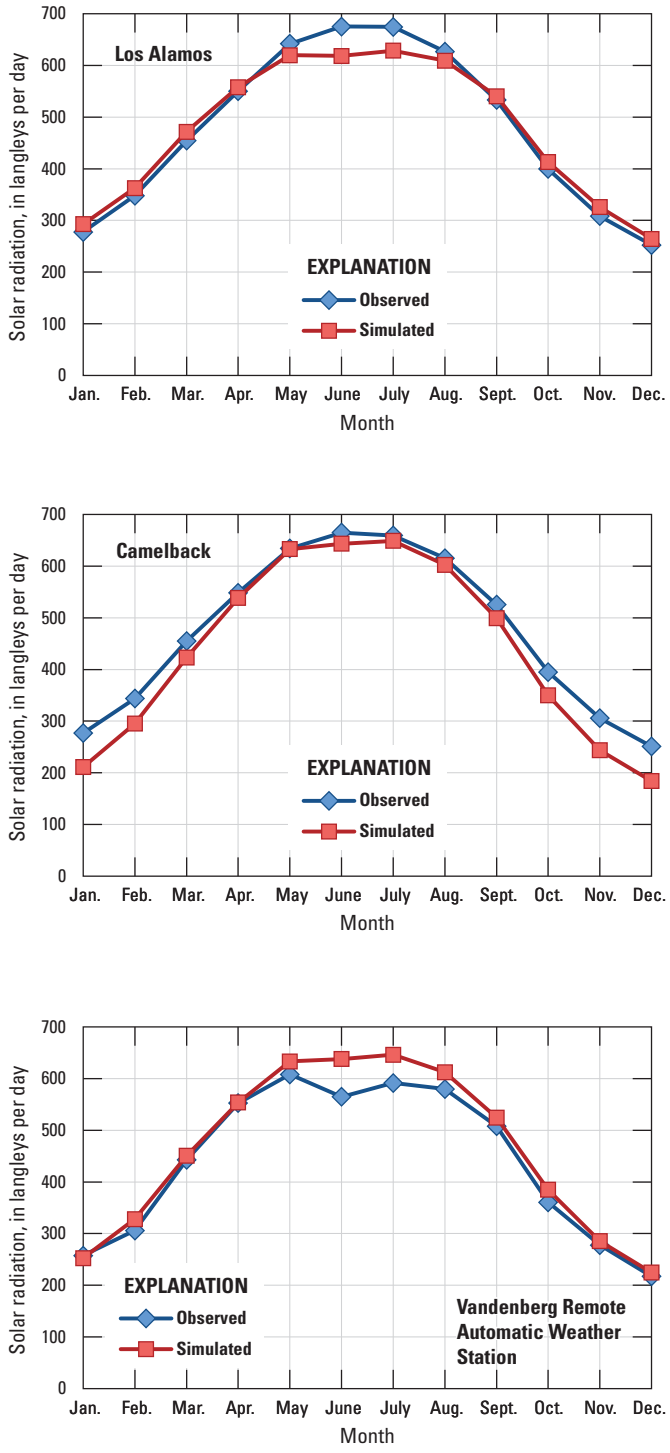

Figure 17. Comparison of Precipitation Runoff Modeling System (PRMS)-simulated and observed (California Irrigation Management Information System, 2017b) mean monthly solar radiation for three locations in the San Antonio Creek Valley watershed, Santa Barbara County, California.

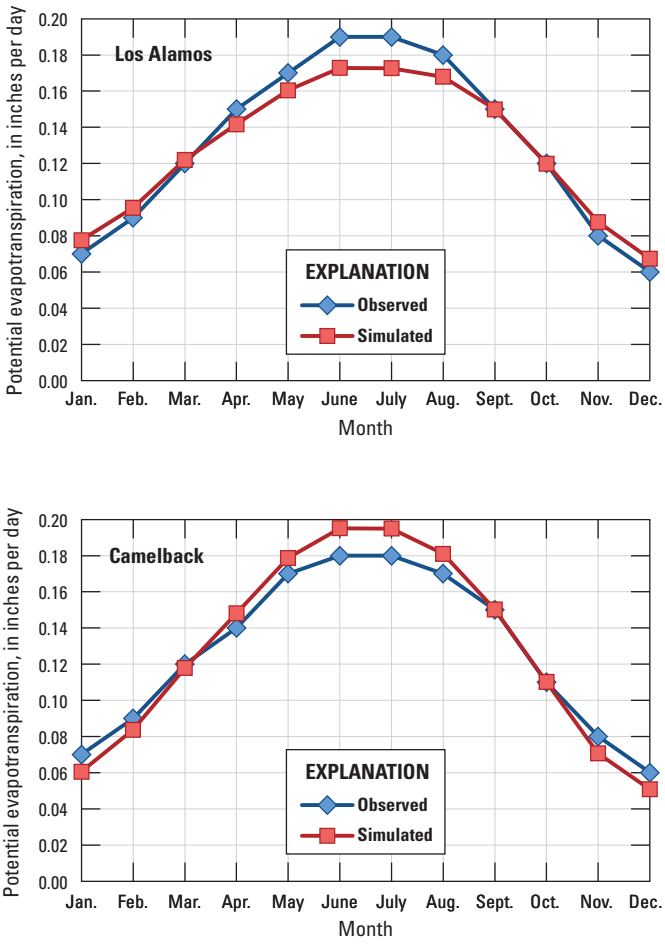

Figure 18. Comparison of Precipitation Runoff Modeling System (PRMS)-simulated and observed (California Irrigation Management Information System, 2017b) mean monthly potential evapotranspiration for two locations in the San Antonio Creek Valley watershed, Santa Barbara County, California.

Integrated Model Calibration

The SACIM was calibrated through a combination of trial-and-error and the automated parameter-estimation method PEST++. Aquifer properties, streambed conductivity, unsaturated-zone parameters, and selected PRMS-model input were modified as part of this process. Each model cell must have values for each physical property (for example hydraulic conductivity in MF-NWT or the *ssr2gw_rate* in PRMS). The large number of parameters in an integrated model can be reduced by using the parameterization technique of parameter zonation. The parameter zonation for the PRMS model is based on land-surface elevation (fig. 19*A*); the parameter zonation for the MF-NWT model is based on the hydrogeologic units present in the SACVW (fig. 14; table 4). In the SACIM, parameter zonation was used in PEST++ to characterize the following properties:

- Horizontal-hydraulic conductivities, vertical anisotropy, specific yield and specific storage for all zones in all layers.
- Streambed conductivity for each stream-segment zone.
- PRMS parameters *ssr2gw_rate*, *slowcoef_sq*, *slowcoef_lin*, *smidx_coef*, *carea_max*, *sat_threshold*, *soil_moist_max*, *soil_rechr_max_frac*, and *pref_flow_den* for all elevation zones.

Pilot points were added during model calibration to provide additional information for characterizing the heterogeneity of the hydraulic conductivity within the parameter zones described in the "Hydraulic Parameter Zonation" section. The pilot point values are spatially interpolated within a zone using kriging; the interpolation does not occur across zone boundaries (Doherty and Hunt, 2010). A total of 198 pilot points were used in the SACIM: 23 valley points in model layer 1, 25 valley points and 44 upland points in model layer 2, 25 valley points and 56 upland points in model layer 3, and 25 valley points in model layer 4 (fig. 14). The pilot points in the valley and uplands had a constant spacing; pilot points in the valley were spaced at 3,936 ft, and pilot points in the uplands were spaced at 4,920 ft. Because the shapes of the MF-NWT parameter zones are not uniform, some pilot points in the valley are close to the pilot points in the uplands in some areas (fig. 14).

Some model inputs were calibrated without using parameter zonation:

- Crop coefficients were calibrated using a crop-coefficient multiplier that increased or decreased the KC for individual crop types.
- The SURFK distribution was calibrated by adjusting a multiplier.
- The SURFDEP parameter was calibrated by adjusting a single variable value.
- Horizontal anisotropy values were adjusted by adjusting a single variable value for each model layer.

PEST Observation Groups and Final Weights

The eleven observation groups defined in PEST++ were (1) initial conditions, (2) hydraulic heads, (3) hydraulic heads in the northern part of the watershed (4) drawdown, (5) drawdown in the northern part of the watershed, (6) streamflow, (7) base flow, (8) agricultural pumpage, (9) hydraulic-head gradients, (10) artesian hydraulic head, and (11) regularization. The locations of observation wells and USGS streamgages are shown in figure 19*B*. Water-level and streamflow data are in the NWIS data repository (U.S. Geological Survey, 2021). Hydraulic-head observations for the initial conditions group consisted of the first water-level measurements for 148 wells. These observations were used in the calculation of drawdown; however, they were given a weight of zero because they also were included in the hydraulic head observation group. The ratio of precipitation to total ET is in the initial conditions observation group and is calculated by dividing precipitation by total ET, which is the sum of canopy, soil-zone, unsaturated-zone and saturated-zone ET. A reported value for San Antonio Creek Valley is between 0.80 and 0.90 (Sanford and Selnick, 2012; Reitz and others, 2017); a value of 0.8 was used for the observed value in PEST++. Transient hydraulic-head observations include 5,477 measurements that represent conditions during periods of groundwater pumping (water years 1948–2018). The 5,329 drawdown observations are based on the transient hydraulic heads and were calculated as the rise or decline in hydraulic head after the first observation.

The hydraulic-head and drawdown observations in the northern part of the SACIM were separate from the observations in the rest of the observations so that higher weights could be used for each group because of the sparse data in that area. The artesian observation group includes five hydraulic-head observations for one well. Streamflow observations include the 1,200 monthly mean streamflow values calculated from daily recorded and measured data for 5 streamgages. Agricultural pumpage observations include annual average pumpage for water years 1948 through 1977 estimated by Muir (1964), Hutchinson (1980), and Martin (1985) and 1978 through 2010 by Tetra Tech, Inc. (2012); for water years 2011 to 2018, the agricultural pumpage was estimated by (Cromwell and others, 2022). Vertical head-gradient observations were included in the hydraulic head-gradient observation group to represent upward and downward gradients between geologic units in the basin; these observations were calculated from water-level data in NWIS (U.S. Geological Survey, 2021) that spanned multiple geologic units. A total of 25 wells at 8 locations in the basin (labeled "Multiple completion hydrograph comparison well" in fig. 19*B*) were used for these observations. Head-gradient observations are the observed vertical gradients at multiple-completion well sites and selected paired wells (fig. 19).

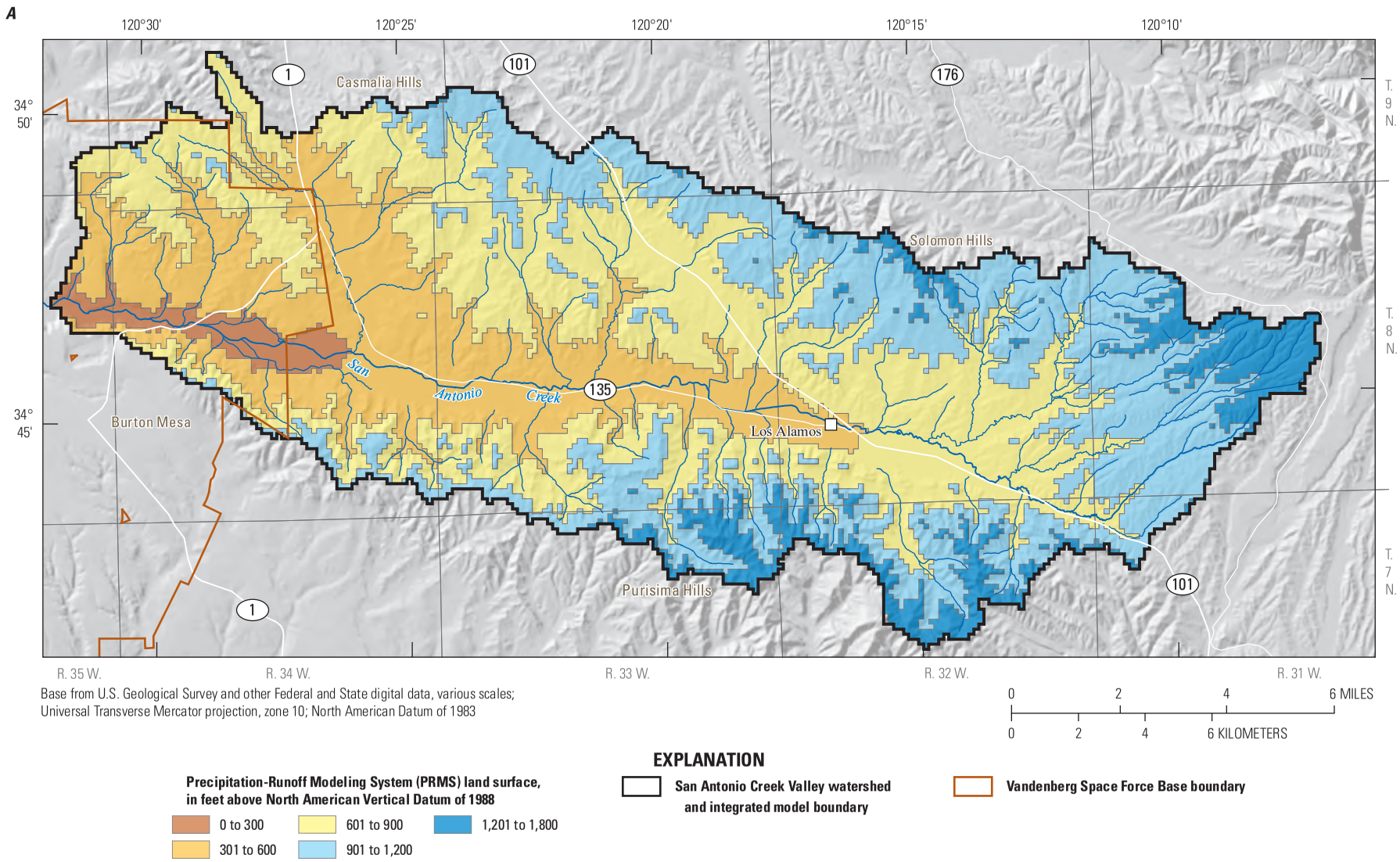

Figure 19. Locations in the San Antonio Creek Valley watershed, Santa Barbara County, California, of *A*, parameter zones for the Precipitation and Runoff Modeling System (PRMS) model; and *B*, hydrograph comparison wells, transient statistics wells and streamgages used for calibration of the San Antonio Creek Valley integrated model. Also shown in figure 19*B* are groundwater subareas used to assess model fit and evaluate simulated groundwater budgets for the San Antonio Creek Valley integrated model. Information for wells and streamgages is presented in U.S. Geological Survey (2021).

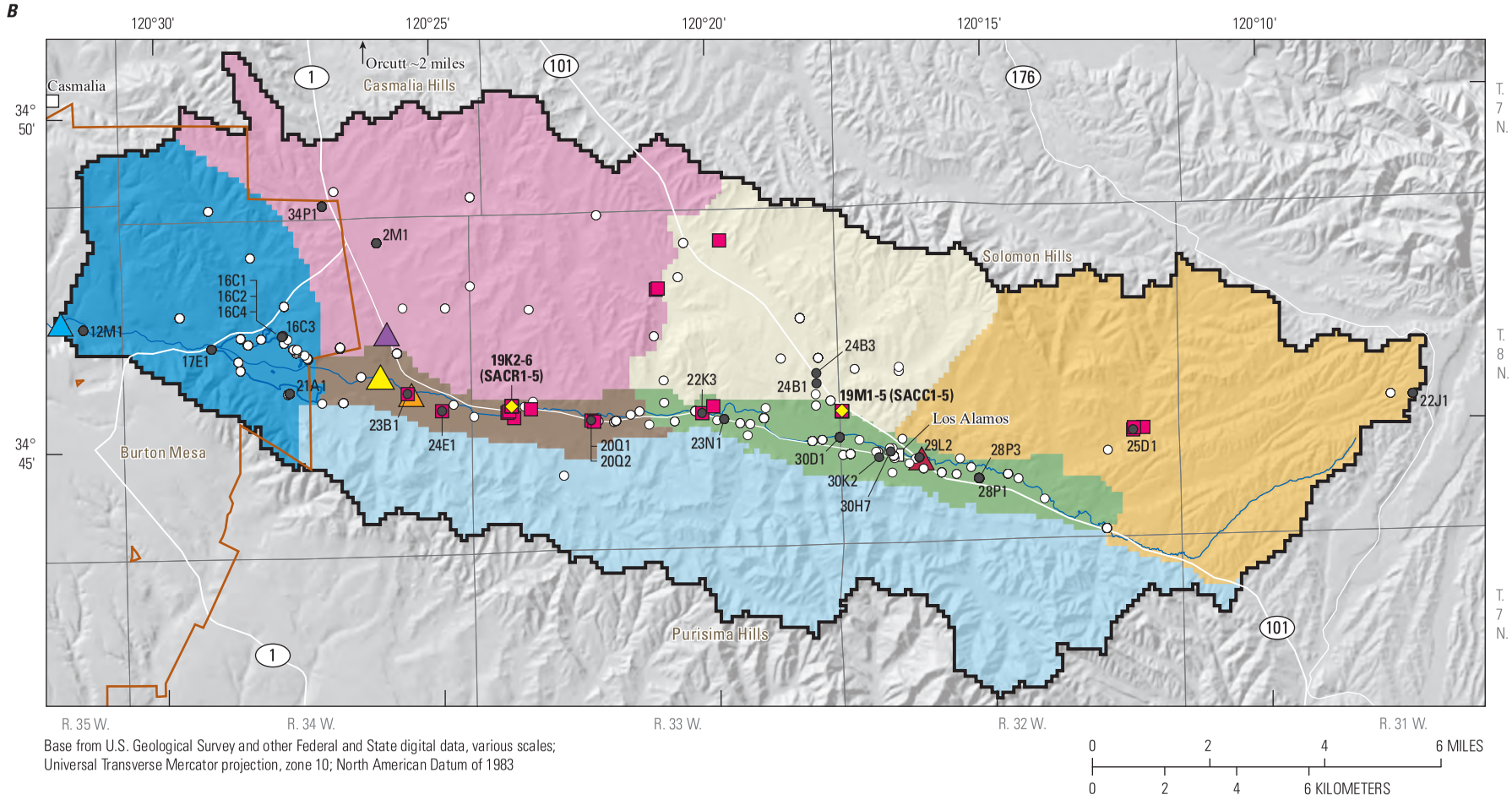

Figure 19.—Continued

The SACIM has more parameters than can be constrained uniquely by the available observations. Available information about what value should be assigned to a parameter (prior information) can be incorporated into the parameter-estimation process (Doherty, 2010), and regularization is used to limit the degree of parameter variability to reasonable values during the calibration process (Tikhonov and Arsenin, 1977; Doherty and Hunt, 2010). The regularization observation group includes information in the form of estimates of parameter values from prior parameter-estimation simulations. These estimates are considered prior knowledge of the hydrologic system and help constrain calibration by providing a penalty to the objective function for changes to the input parameter values. Prior estimates were used for 208 parameters; however, this number changed with individual PEST++ runs because some insensitive parameters were assigned fixed values and were not estimated.

Observation groups are given weights such that any one observation group does not dominate the calibration process. In addition, observations for specific times or locations may be given different weights from the rest of the observations within a group to reduce its influence in the calibration process. Initially, all the observations were given the same weight (0.10). The weights were changed during calibration because different aspects of the model were tested. Higher weights were assigned to observations that were the focus of the test, and lower weights were given to observations that introduced noise in the calibration process. The final weights for each observation group are given in table 7.

Table 7. Observation groups and final weights for the San Antonio Creek Valley integrated model, Santa Barbara County, California.

Observation group	Minimum weight	Maximum weight
Initial conditions		
Heads	0	0
Precipitation to evapotranspiration ratio	1.00E+05	1.00E+05
Heads	0	0.4
Heads in northern part of watershed	1	1
Drawdown	0	0.1
Drawdown in northern part of watershed	1	1
Streamflow	3.00E–06	3.00E–06
Baseflow	3.00E–03	3.00E–03
Agricultural pumpage	0	0
Head gradients	5	5
Artesian head	2	2

The ratio of precipitation to total ET was given a weight of 10 because there is only one value, and a higher weight allows for greater contribution to the calibration process. In the hydraulic heads observation group, wells that are representative of the hydrologic system (labeled "Hydrograph comparison well" in fig. 19*B*) were given an observation weight of 0.40, all other observations were given a weight of 0.10, except hydraulic heads calculated using measured groundwater levels affected by pumping, which are not representative of the hydrologic system; these observations were given a weight of zero. Weights for observations in the drawdown observation group were 0.10, except for drawdown calculated using hydraulic heads affected by pumping which were given a weight of zero. To reduce the influence of uncertainty in the streamflow measurements due to the quality of the data (Cromwell and others, 2022) on the parameter-estimation process, the streamflow observation group (excluding base flow) was given a low weight of 3.0×10^{-6}; the base flow observation group was given a higher weight (3.0×10^{-3}) than the other streamflow observations to increase the influence of the interaction of streamflow with the groundwater system on the calibration process. Reported estimates of agricultural pumpage were used as observations during model calibration; however, once the simulated pumpage reasonably matched the increasing trend of the reported values for the simulation period, the weights were assigned a value of zero so the pumpage observations would not influence the calibration process.

Calibration Results

PRMS Results

PRMS parameters were adjusted during the calibration of the integrated model using one-dimensional multipliers that scale the magnitude of each parameter within the model domain while maintaining the initial relative spatial distribution of the parameter. Final multipliers are given in table 8. The parameter *sat_threshold*, which is important for controlling runoff and interflow generation (fig. 6), had the largest multiplier in every parameter zone and was adjusted upward by about an order of magnitude in each zone. The parameter *smidx_coef*, which is important for controlling runoff generation and infiltration, had the lowest multiplier in each zone and was adjusted downward by about two orders of magnitude in each. The combination of increasing *sat_threshold* and decreasing *smidx_coef* tends to result in more interflow (shallow subsurface flow to streams) and less runoff (surface flow to streams) in the system.

Table 8. Final calibration multipliers for Precipitation Runoff Modeling System (PRMS) parameters in the San Antonio Creek Valley integrated model, Santa Barbara County, California; definitions of parameter names listed in this table can be found in Markstrom and others (2015).

PRMS parameter	Dimension	PRMS calibration zone				
		1	2	3	4	5
pref_flow_den	one	1.19	1.07	0.42	0.73	0.81
smidx_coef	one	0.01	0.01	0.01	0.01	0.01
slowcoef_sq	one	0.97	0.97	1.00	0.96	1.18
carea_max	nhru	0.10	0.10	0.06	0.05	0.10
sat_threshold	nhru	8.61	15.11	10.16	11.59	15.32
slowcoef_lin	nhru	0.35	0.28	0.26	0.17	0.24
slowcoef_sq1	nhru	0.97	0.97	1.00	0.96	1.18
soil_moist_max	nhru	3.93	3.41	4.88	4.87	4.96
soil_rechr_max_frac	nhru	0.68	0.42	0.63	0.47	0.32
ssr2gw_rate	nhru	2.63	2.05	3.51	5.00	2.87

Table 9. Final calibration multipliers for crop coefficients in the San Antonio Creek Valley integrated model, Santa Barbara County, California.

[NA, not applicable]

General land-use subcategory	Multiplier, unirrigated agriculture	Multiplier, irrigated agriculture
Riparian, forrest woodland	0.60	NA
Montane riparian systems	1.37	NA
Orchard	0.93	0.75
Row crop	0.66	1.51
Vineyard	0.90	1.09
Bush fruit and berries	1.23	1.25
Pasture and hayland	1.01	1.32
Fallow/Idle Cropland	1.26	1.0
Wheat	1.21	1.27

Crop-Coefficient Multipliers

Initial monthly KCs for sparsely vegetated, riparian, and agricultural land were adjusted during the calibration of the integrated model using one-dimensional multipliers that scale the magnitude of each monthly KC within each land-use subcategory while maintaining the initial relative temporal distribution of the parameter; the final multiplier values for irrigated and unirrigated land use are given in table 9. An additional seasonal ramp down factor was used for crops that are irrigated primarily from April through September. KC values were ramped down from October through December to 10 percent of the specified KC value and ramped back up from 10 to 100 percent during January to March to account for potential irrigation and frost protection (table 6). The KC multiplier of 1.09 for irrigated vineyards (table 9) likely is indicative of the lack of an explicit accounting for frost protection in the SACIM. Increasing the KC for irrigated vineyards increases simulated pumping and may partially account for actual historical pumping needed to fill frost-protection ponds in the late winter and spring. Another reason for a KC multiplier greater than 1.0 may be a poor accounting of irrigation-method efficiency in the AG package or transmission losses.

MODFLOW-NWT Results

Parameters in the MF-NWT model adjusted during model calibration were aquifer hydraulic properties (hydraulic conductivity, specific yield, specific storage, and vertical anisotropy, and horizontal anisotropy) and streambed hydraulic conductivity. The final values for hydraulic properties for the MF-NWT parameter zones and hydraulic conductivity for pilot points are summarized in tables 10 and 11, respectively.

Hydraulic Properties

The highest HK value is 206 ft/d for parameter zone 133, representing the channel alluvium in model layer 3. The lowest HK value (0.006 ft/d) is for parameter zones 843 and 8434 (table 10), representing the Sisquoc Formation of the consolidated bedrock in the uplands in model layer 4 (table 4; fig. 14). The final HK values for parameter zones in the upland areas, where the channel alluvium is not present, are generally lower than in the parameter zones in the valley, indicating the greater degree of weathering, and at depth, consolidation. A summary of the HK values estimated by pilot points within parameter zones shows the highest mean and median values for HK (183 and 93 ft/d, respectively) are for parameter zone 10 (table 11), representing the lower Paso Robles Formation in the western part of the valley in model layer 2 (table 4; fig. 14). The mean and median values for HK (0.20 and 0.15 ft/d, respectively) are for parameter zone 933 (table 11), representing the undifferentiated Careaga Sandstone in the northeastern uplands in model layer 3 (table 4; fig. 14). The highest and lowest values for horizontal anisotropy were 0.41 in model layer 2 to 0.81 in model layer 3, respectively (table 10).

Table 10. Final hydraulic properties by parameter zone in the San Antonio Creek integrated model, Santa Barbara County, California.

[ft/d, foot per day; NA, unitless]

Parameter identifier	Group	Value	Unit
	Hydraulic properties		
hk1z131	Horizontal hydraulic conductivity of zone 131, layer 1	18	ft/d
hk1z141	Horizontal hydraulic conductivity of zone 141, layer 1	1.6	ft/d
hk1z151	Horizontal hydraulic conductivity of zone 151, layer 1	0.30	ft/d
hk1z161	Horizontal hydraulic conductivity of zone 161, layer 1	40	ft/d
hk2z13	Horizontal hydraulic conductivity of zone 13, layer 2	5.3	ft/d
hk2z102	Horizontal hydraulic conductivity of zone 102, layer 2	0.70	ft/d
hk2z103	Horizontal hydraulic conductivity of zone 103, layer 2	2.0	ft/d
hk2z132	Horizontal hydraulic conductivity of zone 132, layer 2	46	ft/d
hk2z134	Horizontal hydraulic conductivity of zone 134, layer 2	10	ft/d
hk3z931	Horizontal hydraulic conductivity of zone 931, layer 3	1.3	ft/d
hk3z932	Horizontal hydraulic conductivity of zone 932, layer 3	2.0	ft/d
hk3z934	Horizontal hydraulic conductivity of zone 934, layer 3	0.02	ft/d
hk3z9311	Horizontal hydraulic conductivity of zone 9311, layer 3	1.5	ft/d
hk3z9322	Horizontal hydraulic conductivity of zone 9322, layer 3	0.59	ft/d
hk3z9333	Horizontal hydraulic conductivity of zone 9333, layer 3	0.29	ft/d
hk3z133	Horizontal hydraulic conductivity of zone 133, layer 3	206	ft/d
hk4z811	Horizontal hydraulic conductivity of zone 811, layer 3	1.2	ft/d
hk4z841	Horizontal hydraulic conductivity of zone 841, layer 3	0.04	ft/d
hk4z842	Horizontal hydraulic conductivity of zone 842, layer 3	0.01	ft/d
hk4z843	Horizontal hydraulic conductivity of zone 843, layer 3	0.006	ft/d
hk4z8411	Horizontal hydraulic conductivity of zone 8411, layer 3	0.04	ft/d
hk4z8434	Horizontal hydraulic conductivity of zone 8434, layer 3	0.006	ft/d
hk4z8433	Horizontal hydraulic conductivity of zone 8433, layer 3	0.15	ft/d
hani_1	Horizontal anisotropy, layer 1	0.45	NA
hani_2	Horizontal anisotropy, layer 2	0.41	NA
hani_3	Horizontal anisotropy, layer 3	0.81	NA
hani_4	Horizontal anisotropy, layer 4	0.53	NA
vani1z13	Vertical anisotropy of zone 13, layer 1	1,605	NA
vani1z131	Vertical anisotropy of zone 131, layer 1	13	NA
vani1z135	Vertical anisotropy of zone 135, layer 1	2,037	NA
vani1z141	Vertical anisotropy of zone 141, layer 1	2.2	NA
vani1z151	Vertical anisotropy of zone 151, layer 1	2.8	NA
vani1z161	Vertical anisotropy of zone 161, layer 1	27	NA
vani2z10	Vertical anisotropy of zone 10, layer 2	400	NA
vani2z102	Vertical anisotropy of zone 102, layer 2	25	NA
vani2z103	Vertical anisotropy of zone 103, layer 2	56	NA
vani2z104	Vertical anisotropy of zone 104, layer 2	0.32	NA
vani2z11	Vertical anisotropy of zone 11, layer 2	102	NA
vani2z111	Vertical anisotropy of zone 111, layer 2	1.3	NA
vani2z13	Vertical anisotropy of zone 13, layer 2	19	NA

Table 10. Final hydraulic properties by parameter zone in the San Antonio Creek integrated model, Santa Barbara County, California.—Continued

[ft/d, foot per day; NA, unitless]

Parameter identifier	Group	Value	Unit
	Hydraulic properties—Continued		
vani2z132	Vertical anisotropy of zone 132, layer 2	0.27	NA
vani2z134	Vertical anisotropy of zone 134, layer 2	1.1	NA
vani3z91	Vertical anisotropy of zone 91, layer 3	1.0	NA
vani3z92	Vertical anisotropy of zone 92, layer 3	6.9	NA
vani3z93	Vertical anisotropy of zone 93, layer 3	101	NA
vani3z931	Vertical anisotropy of zone 931, layer 3	1.1	NA
vani3z932	Vertical anisotropy of zone 932, layer 3	1.7	NA
vani3z933	Vertical anisotropy of zone 933, layer 3	3.3	NA
vani3z934	Vertical anisotropy of zone 934, layer 3	1.0	NA
vani3z935	Vertical anisotropy of zone 935, layer 3	6	NA
vani3z9311	Vertical anisotropy of zone 9311, layer 3	8.8	NA
vani3z9322	Vertical anisotropy of zone 9322, layer 3	6.8	NA
vani3z9333	Vertical anisotropy of zone 9333, layer 3	22	NA
vani3z133	Vertical anisotropy of zone 133, layer 3	165	NA
vani4z81	Vertical anisotropy of zone 81, layer 4	31	NA
vani4z811	Vertical anisotropy of zone 811, layer 4	29	NA
vani4z82	Vertical anisotropy of zone 82, layer 4	0.1	NA
vani4z841	Vertical anisotropy of zone 841, layer 4	14.5	NA
vani4z842	Vertical anisotropy of zone 842, layer 4	5.9	NA
vani4z843	Vertical anisotropy of zone 843, layer 4	1.6	NA
vani4z8411	Vertical anisotropy of zone 8411, layer 4	0.9	NA
vani4z8434	Vertical anisotropy of zone 8434, layer 4	1.9	NA
vani4z8433	Vertical anisotropy of zone 8433, layer 4	12.8	NA
	Storage properties		
sy1z13	Specific yield for zone 13, layer 1	0.17	NA
sy1z131	Specific yield for zone 131, layer 1	0.20	NA
sy1z135	Specific yield for zone 135, layer 1	0.16	NA
sy1z141	Specific yield for zone 141, layer 1	0.16	NA
sy1z151	Specific yield for zone 151, layer 1	0.17	NA
sy1z161	Specific yield for zone 161, layer 1	0.12	NA
sy2z10	Specific yield for zone 10, layer 2	0.10	NA
sy2z11	Specific yield for zone 11, layer 2	0.13	NA
sy2z102	Specific yield for zone 102, layer 2	0.10	NA
sy2z103	Specific yield for zone 103, layer 2	0.09	NA
sy2z104	Specific yield for zone 104, layer 2	0.17	NA
sy2z111	Specific yield for zone 111, layer 2	0.19	NA
sy2z13	Specific yield for zone 13, layer 2	0.17	NA
sy2z132	Specific yield for zone 132, layer 2	0.09	NA
sy2z134	Specific yield for zone 134, layer 2	0.18	NA
sy3z91	Specific yield for zone 91, layer 3	0.19	NA

Table 10. Final hydraulic properties by parameter zone in the San Antonio Creek integrated model, Santa Barbara County, California.—Continued

[ft/d, foot per day; NA, unitless]

Parameter identifier	Group	Value	Unit
	Storage properties—Continued		
sy3z92	Specific yield for zone 92, layer 3	0.17	NA
sy3z93	Specific yield for zone 93, layer 3	0.21	NA
sy3z931	Specific yield for zone 931, layer 3	0.13	NA
sy3z932	Specific yield for zone 932, layer 3	0.15	NA
sy3z933	Specific yield for zone 933, layer 3	0.14	NA
sy3z934	Specific yield for zone 934, layer 3	0.19	NA
sy3z935	Specific yield for zone 935, layer 3	0.15	NA
sy3z9311	Specific yield for zone 9311, layer 3	0.15	NA
sy3z9322	Specific yield for zone 9322, layer 3	0.15	NA
sy3z9333	Specific yield for zone 9333, layer 3	0.06	NA
sy3z133	Specific yield for zone 133, layer 3	0.10	NA
sy4z81	Specific yield for zone 81, layer 4	0.20	NA
sy4z811	Specific yield for zone 811, layer 4	0.18	NA
sy4z82	Specific yield for zone 82, layer 4	0.18	NA
sy4z841	Specific yield for zone 841, layer 4	0.22	NA
sy4z842	Specific yield for zone 842, layer 4	0.14	NA
sy4z843	Specific yield for zone 843, layer 4	0.16	NA
sy4z8411	Specific yield for zone 8411, layer 4	0.15	NA
sy4z8434	Specific yield for zone 8434, layer 4	0.21	NA
sy4z8433	Specific yield for zone 8433, layer 4	0.21	NA
ss1z13	Specific storage for zone 13, layer 1	2.73E–06	per foot
ss1z131	Specific storage for zone 131, layer 1	2.12E–06	per foot
ss1z135	Specific storage for zone 135, layer 1	2.31E–06	per foot
ss1z141	Specific storage for zone 141, layer 1	5.38E–06	per foot
ss1z151	Specific storage for zone 151, layer 1	5.81E–06	per foot
ss1z161	Specific storage for zone 161, layer 1	1.11E–06	per foot
ss2z10	Specific storage for zone 10, layer 2	5.54E–06	per foot
ss2z11	Specific storage for zone 11, layer 2	3.20E–06	per foot
ss2z102	Specific storage for zone 102, layer 2	2.32E–06	per foot
ss2z103	Specific storage for zone 103, layer 2	3.52E–06	per foot
ss2z104	Specific storage for zone 104, layer 2	3.35E–06	per foot
ss2z111	Specific storage for zone 111, layer 2	3.92E–06	per foot
ss2z13	Specific storage for zone 13, layer 2	2.22E–06	per foot
ss2z132	Specific storage for zone 132, layer 2	3.20E–06	per foot
ss2z134	Specific storage for zone 134, layer 2	3.64E–06	per foot
ss3z91	Specific storage for zone 91, layer 3	3.00E–06	per foot
ss3z92	Specific storage for zone 92, layer 3	5.41E–06	per foot
ss3z93	Specific storage for zone 93, layer 3	3.67E–06	per foot
ss3z931	Specific storage for zone 931, layer 3	4.08E–06	per foot
ss3z932	Specific storage for zone 932, layer 3	5.84E–06	per foot

Table 10. Final hydraulic properties by parameter zone in the San Antonio Creek integrated model, Santa Barbara County, California.—Continued

[ft/d, foot per day; NA, unitless]

Parameter identifier	Group	Value	Unit
	Storage properties—Continued		
ss3z933	Specific storage for zone 933, layer 3	3.13E–06	per foot
ss3z934	Specific storage for zone 934, layer 3	2.02E–06	per foot
ss3z935	Specific storage for zone 935, layer 3	3.10E–06	per foot
ss3z9311	Specific storage for zone 9311, layer 3	2.31E–06	per foot
ss3z9322	Specific storage for zone 9322, layer 3	3.31E–06	per foot
ss3z9333	Specific storage for zone 9333, layer 3	1.74E–06	per foot
ss3z133	Specific storage for zone 133, layer 3	3.37E–06	per foot
ss4z81	Specific storage for zone 81, layer 4	1.68E–06	per foot
ss4z811	Specific storage for zone 811, layer 4	1.68E–06	per foot
ss4z82	Specific storage for zone 82, layer 4	7.06E–06	per foot
ss4z841	Specific storage for zone 841, layer 4	4.90E–06	per foot
ss4z842	Specific storage for zone 842, layer 4	5.01E–06	per foot
ss4z843	Specific storage for zone 843, layer 4	3.87E–06	per foot
ss4z8411	Specific storage for zone 8411, layer 4	3.83E–06	per foot
ss4z8434	Specific storage for zone 8434, layer 4	4.36E–06	per foot
ss4z8433	Specific storage for zone 8433, layer 4	4.78E–06	per foot
	Stream-channel properties		
sfr_k1, zone 1	Vertical hydraulic conductivity of streambed in zone 1	0.04	ft/d
sfr_k2, zone 2	Vertical hydraulic conductivity of streambed in zone 2	0.03	ft/d
sfr_k3, zone 3	Vertical hydraulic conductivity of streambed in zone 3	0.03	ft/d
sfr_k4, zone4	Vertical hydraulic conductivity of streambed in zone 4	0.05	ft/d
sfr_k5, zone 5	Vertical hydraulic conductivity of streambed in zone 5	0.08	ft/d
sfr_k6, zone 6	Vertical hydraulic conductivity of streambed in zone 6	0.18	ft/d
sfr_k7, zone 7	Vertical hydraulic conductivity of streambed in zone 7	0.07	ft/d
sfr_k8, zone 8	Vertical hydraulic conductivity of streambed in zone 8	0.04	ft/d
sfr_k9, zone 9	Vertical hydraulic conductivity of streambed in zone 9	0.05	ft/d
sfr_k10, zone 10	Vertical hydraulic conductivity of streambed in zone 10	0.05	ft/d
sfr_k11, zone 11	Vertical hydraulic conductivity of streambed in zone 11	0.18	ft/d
sfr_k12, zone 12	Vertical hydraulic conductivity of streambed in zone 12	0.11	ft/d
sfr_k13, zone 13	Vertical hydraulic conductivity of streambed in zone 13	0.007	ft/d

Table 11. Final horizontal hydraulic conductivity statistics for pilot points by parameter zone in the San Antonio Creek integrated model, Santa Barbara County, California.

[Horizontal hydraulic conductivity statistics in feet per day. **Abbreviation**: NA, not applicable]

Parameter zone number	Model layer	Minimum	Maximum	Average	Median
13	1	6.2	216	27	21
135	1	2.1	30	11	7.7
10	2	2.2	763	183	93
11	2	1.3	25	7.9	5.4
13	2	23	23	NA	NA
104	2	0.004	4.8	0.86	0.18
111	2	0.003	4.8	0.57	0.05
92	3	3.07	3.07	NA	NA
93	3	0.12	7.9	2.0	1.4
935	3	0.005	5.8	0.95	0.18
933	3	0.005	0.82	0.20	0.15
81	4	0.05	1.3	0.46	0.37
82	4	0.52	0.32	0.43	0.45

The vertical hydraulic conductivity (VK) is computed in the SACIM by dividing the HK by the VANI. Computed values of VK vary in the same manner as the HK values estimated by parameter zone. The VANI values were adjusted by parameter zone to better approximate the vertical gradients observed in wells close to each other but were perforated at different depths. The smallest VANI value at the completion of model calibration (0.1) is for parameter zone 82 (table 10) in model layer 4 representing the Sisquoc Formation of the consolidated bedrock in the valley (table 4; fig. 14). The highest VANI value (2,037) for parameter zone 135 (table 10) represents the channel alluvium and upper and middle Paso Robles Formation in the valley in model layer 1 (tables 4; fig. 14).

The SY distributions are assigned to model layers as described in the "Storage Properties" section of this report. The SY values were adjusted by parameter zone during calibration; however, the model was sensitive only to changes in parameter zones 10 and 102 in model layer 2 and parameter zones 843 and 8433 in model layer 4 (table 10; fig. 14). The final SY values ranged from 0.06 in parameter zone 9333 in model layer 3 to 0.22 in parameter zone parameter zone 841 in model layer 4. The highest values of SY are in the eastern part of the SACVW and represent the Paso Robles Formation in model layer 1 and the Careaga Sandstone in model layer 3 (table 10; fig. 14).

The SS distributions were assigned to model layers as described in the "Storage Properties" section in this report. The SS values were adjusted by parameter zone during calibration; however, the model was fairly insensitive to the SS values. The SS values ranged from 1.11×10^{-06} to 7.06×10^{-06} per ft in layers 1 and 4, respectively (table 10).

Streambed Hydraulic Conductivity

The streambed hydraulic conductivities were adjusted by zonation as described in the "Streamflow Routing" section in this report. The calibrated values of streambed hydraulic conductivity ranged from 0.007 ft/d in zone 13 to 0.185 ft/d in zone 11 (table 10; fig. 7). The highest value was for tributaries in the eastern upland and valley areas of the SACVW, and the lowest value was in the downstream section of San Antonio Creek from Barka Slough to the outflow point at the Casmalia streamgage (11136100; fig. 7).

Sensitivity Analysis

Sensitivity analysis is used to assess the effects of different parameter values on observation data, including measured groundwater levels and streamflow, reported agricultural pumpage, and prior information. The analysis involved keeping all input parameters constant except the one being analyzed and varying that parameter through a range of values. Parameters are considered sensitive when varying the parameter by a small amount causes a large change in the simulation results; parameters are considered insensitive when varying the parameter by a small or large amount causes a small change in the simulation results. Model sensitivity was evaluated using PEST++ (Welter and others, 2015; White and others, 2018).

The sensitivity process in PEST++ identifies the sensitivity of computed values at observation locations to changes in model parameters. PEST++ was used to identify which parameters to include in the parameter estimation process (Hill and others, 2000) and to adjust the parameter values during calibrations. Figure 20 shows the composite sensitivities by parameter group for the most sensitive 25 of the 414 parameters included in the sensitivity analysis. Results of the sensitivity analysis indicate that the model was most sensitive to two parameters related to recharge processes (sfr_k7 and sfr_k1), vertical anisotropy in parameter zones 8433 and 9322, five parameters related to PRMS processes (pref_flow_d2, soil_moist_3, soil_moist_2, pref_flow_d4, and pref_flow_d3), and the horizontal hydraulic conductivity in parameter zone 133. The most sensitive parameters in the SACIM are the streambed conductivity in zone 7 (sfr_k7) and the vertical anisotropy in zone 8433 of model layer 4 (vani4z8433; fig. 20). Other sensitive parameters were related to soil moisture, soil-zone and groundwater storage properties, horizontal anisotropy, and streambed hydraulic conductivity.

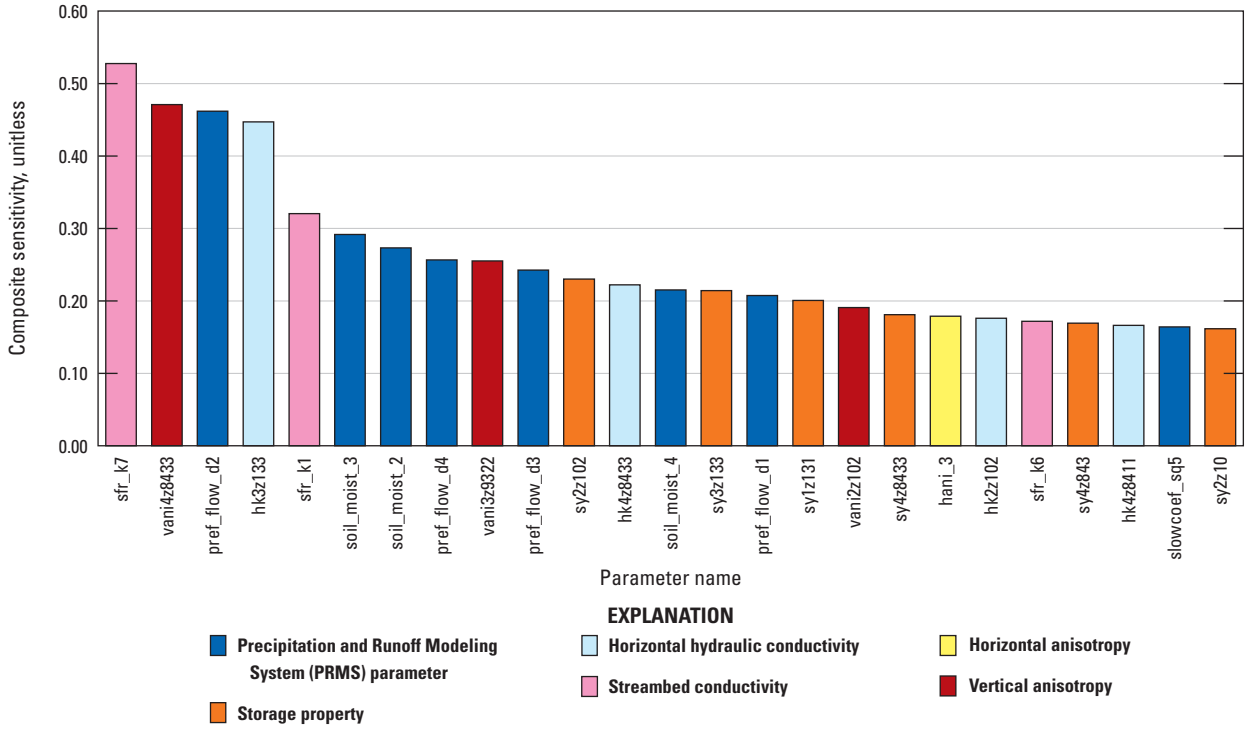

Figure 20. Composite sensitivities for the 25 most sensitive parameters of the San Antonio Creek Valley integrated model, Santa Barbara County, California. Descriptions of parameter names are given in table 10.

Assessment of Integrated Model Fit

Comparisons of simulated and measured streamflow and groundwater levels indicate how well the SACIM replicates the flow system. The methods of analysis described in the "Integrated Model Calibration" section of this report help to assess how accurately the SACIM simulates groundwater levels, the direction of groundwater flow in the SACVW hydrologic system, and the quantity of streamflow. Model fit to the flow system is considered with respect to individual groundwater observation wells and streamgages (fig. 19*B*), broader valley and upland areas (fig. 14), and more specific groundwater subareas (fig. 19*B*). Groundwater subareas within the SACVW were broadly defined based on the extent of hydrogeologic units and surface-water (topographic) divides (fig. 19*B*; Cromwell and others, 2022); groundwater subareas are used to evaluate model fit and groundwater budget components.

Measures of Model Fit

Measures of model fit include the following:

- Model-fit statistics for residuals (simulated hydraulic heads minus measured groundwater levels), including the mean, median, minimum, maximum, root mean square error (RMSE), and normalized RMSE (NMRSE).
- Model fit statistics for streamflow, including mean, minimum, maximum, percent-average-estimation error (PAEE), absolute average estimation error (AAEE), and Nash-Sutcliffe efficiency (NSE) and normalized Nash-Sutcliffe efficiency (NNSE).
- Plots comparing measured groundwater levels and streamflow to simulated hydraulic heads and streamflow, respectively, and plots comparing residuals to hydraulic heads.

For the SACIM calibration to measured groundwater levels, simulated hydraulic heads were compared with measured groundwater levels from 148 wells for model-fit statistics; the hydrographs shown for 22 of these wells (the locations of which are shown in fig. 19*B*) were considered to be representative of the system spatially and temporally.

Comparison of Measured Groundwater Levels to Simulated Hydraulic Heads

Simulated hydraulic heads were compared directly with measured groundwater levels if the wells were perforated in a single model layer. For wells perforated across multiple model layers, MF-NWT calculated a composite, simulated-equivalent hydraulic head by using the head-observation package (HOB; Hill and others, 2000), which is a function of the simulated hydraulic heads and the hydraulic properties of the perforated model layers. Measures of model fit for the MF-NWT model presented herein are (1) model-fit statistics for residuals; (2) plots of measured groundwater levels against simulated hydraulic heads and residuals against simulated hydraulic heads; and (3) spatial distribution of average residuals for each well.

The NMRSE is calculated by dividing the RMSE of the residuals by the total range of measured groundwater levels in the groundwater system (Anderson and Woessner, 1992). The value is expressed as a percentage, and previous studies indicate that this should be less than 10 percent to be acceptable (Drost and others, 1999; Ely and Kahle, 2012).

The NRMSE for the SACIM was calculated using all 5,482 groundwater-level observations used for calibration, and the NRMSE of 2.6 percent (table 12) indicated an overall acceptable model fit to observed data. The RMSE and NMRSE for the central uplands subarea were the greatest; however, the central uplands subarea also had the fewest observations which could account for the poorer model fit. The RMSE and NMRSE were smallest for the eastern uplands, even though there were comparatively few (141) observations for this subarea. The range in residuals and median residual for this subarea also were the smallest. The RMSE and NMRSE for the other subareas were less than or equal to 10 percent, which is considered acceptable (table 12).

When plotting simulated hydraulic heads versus measured groundwater levels, all the points would plot on the 1:1 correlation line if the SACIM results matched the measured data perfectly. The composite simulated hydraulic heads plotted against the measured groundwater levels in figure 21*A* show the relation between measured groundwater levels and simulated hydraulic heads followed the 1:1 correlation line; however, the SACIM generally underestimated measured groundwater levels (fig 21*A*). About 40 percent of the simulated heads are within 10 ft of measured groundwater levels and bout 76 percent of the simulated heads are within 25 ft of the measured data.

Residuals randomly distributed around zero indicate a lack of bias in the simulated values (Hill, 1998). Comparisons of SACIM residuals and simulated hydraulic heads plotted in figure 21*B* show the residuals distributed around zero; however, the greater number of negative residuals compared with positive residuals indicated the overall tendency of the SACIM to underestimate measured groundwater levels. The residuals for the simulation period showed that 72 percent of the simulated heads were less than measured groundwater levels, with a median residual value of about –15 ft. More than 50 percent of residuals for the eastern, central, and southern upland subareas were positive and showed that simulated hydraulic heads were higher than measured water levels. Residuals for the other subareas showed that as much as 80 percent of simulated heads underestimate measured groundwater levels. Underestimated groundwater levels in these subareas may be caused by uncertainty in the distribution of agricultural pumpage in the model and local variations in hydraulic properties not captured in the model, resulting in a large number of negative residuals.

Table 12. Summary of model-fit statistics for groundwater subareas in the San Antonio Creek Valley integrated model, Santa Barbara County, California.

[Residual is calculated by subtracting the measured water level from the simulated head]

Subarea	Mean residual (feet)	Median residual (feet)	Minimum negative residual (feet)	Maximum positive residual (feet)	Root mean square error (RMSE) (feet)	Normalized root mean square error (NRMSE) (percent)	Range of measured groundwater levels (feet)	Number of observations
East valley	–0.97	–3.7	–146	192	38	10	368	964
West valley	–12	–14	–77	56	22	7.5	292	1,347
Eastern uplands	6.9	0.81	–52	90	18	3.1	581	141
Central uplands	0.10	28	–145	94	58	17	341	88
Western uplands	–10	–15	–97	103	24	6.1	398	448
Barka slough	–13	–9.5	–117	60	24	6.8	354	2,492
San Antonio Creek Valley watershed								
SACIM	–9.9	–8.6	–146	192	27	2.6	1,058	5,482

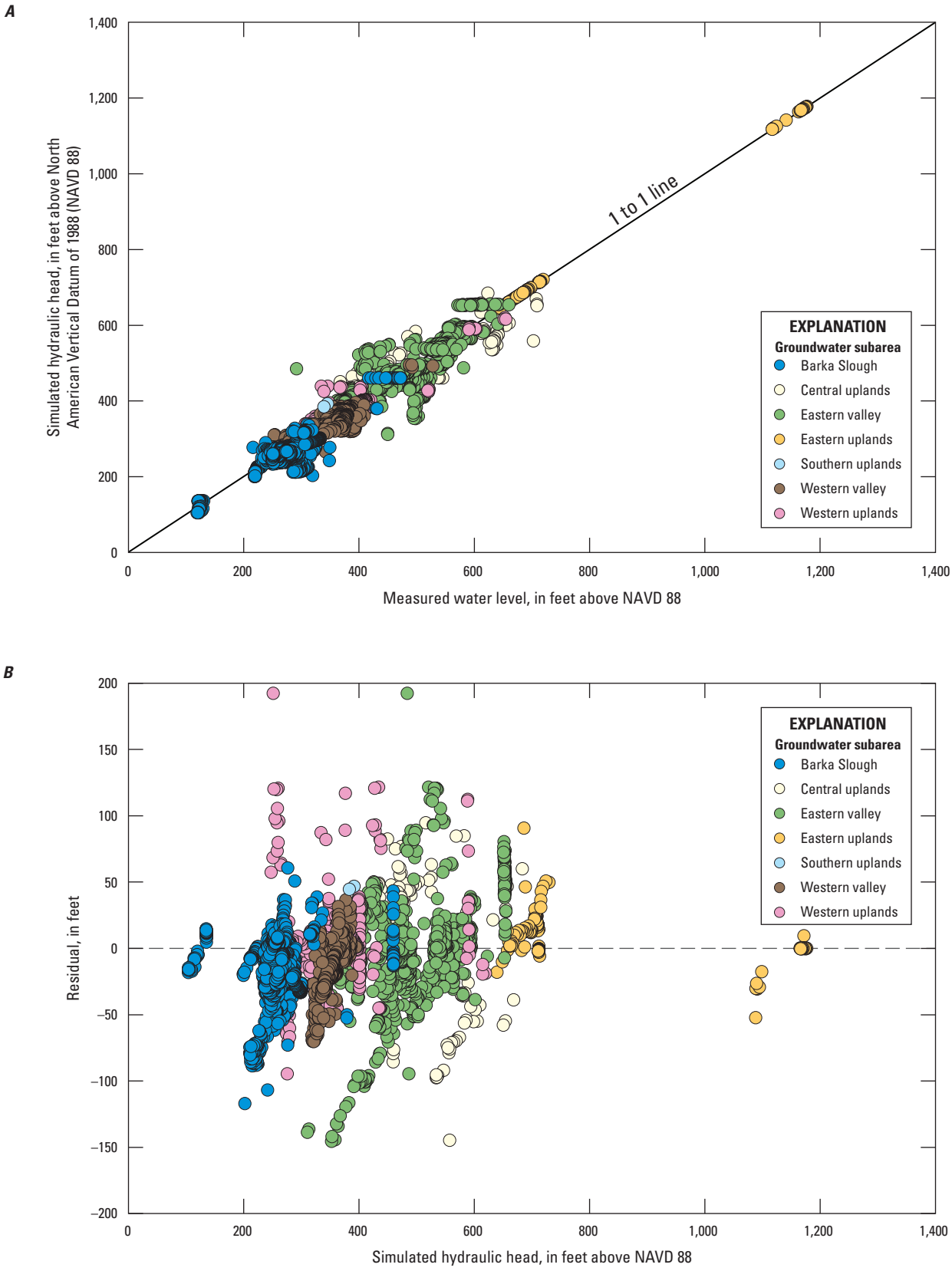

Figure 21. Composite simulated equivalent groundwater levels from the San Antonio Creek Valley integrated model, Santa Barbara County, California, compared with *A*, measured groundwater levels; and *B*, differences between measured and simulated hydraulic heads (residuals).

The distributions of average residuals for simulated hydraulic heads and measured groundwater levels indicate a general spatial bias of the SACIM results (fig. 22). The SACIM predominantly underestimates the measured data in the uplands and valley. The smallest magnitudes of the residuals generally are in the valley for all model layers. For the uplands as a whole, the model underestimates the measured data but the overestimations that do occur generally are largest in the uplands.

Simulated Hydrographs

Long-term groundwater-level data from 25 wells document patterns in the groundwater levels throughout the valley and were used to evaluate the long-term effects of pumping and climate. The wells were selected to represent areal and vertical coverages and temporal variations and seasonal fluctuations that extend through the entire model period. Water-level data from six wells near each other that have similar construction and hydrogeologic setting were combined to represent variability in water levels over the longest possible period. Simulated and measured groundwater levels for selected wells are shown in figure 23.

Although the SACIM reasonably simulated measured water levels, simulated hydraulic heads generally underestimated measured groundwater levels during the simulation period. Mismatches between simulated heads and measured water levels can be attributed, at least in part, to the uncertainty in the spatial and vertical distribution of agricultural wells, uncertainty in the parameters in the SACIM used to estimate agricultural pumpage, and local variability in hydraulic properties within the parameter zones that are not reflected in the model. The simulated hydrographs will be discussed for each subarea shown in figure 19*B*.

Eastern Uplands

Measured water levels in wells in the eastern part of the uplands in the Solomon Hills (fig. 19*B*) are influenced by natural recharge and, in some areas, groundwater pumping. The data from well 8N/31W-22J1, which is perforated in model layer 4, show steady groundwater levels over the period of record; the simulated hydraulic heads generally agree with the measured data. The well is adjacent to a general-head boundary, and simulated heads likely were influenced by inflow from the neighboring groundwater basin (fig. 23*A*). In contrast, measured groundwater levels in well 8N/32W-25D1 show pronounced variations (fig. 23*B*). Prior to 1993, simulated hydraulic heads showed a steady decline, but the measured data show an abrupt decline around 1980 that is not represented by the simulated values. Furthermore, simulated values overestimate the steady decline in measured groundwater levels from about 1980 to 1993. After 1993, variations in the simulated values indicate increased pumping and periods of above-average recharge, and the fluctuations in simulated values are fairly evenly distributed above and below measured data points. However, water levels generally are measured when the well is not pumped, hence, the highest simulated heads overestimate the measured data. The simulated hydraulic heads match the decline in the measured groundwater levels after 2000 (fig. 23*B*).

Central Uplands

Wells 8N/33W-24B1 and 8N/33W-24B3 are perforated in model layer 1 in adjacent model cells and together show a greater rate of groundwater-level decline (fig. 23*C*) than wells in the eastern uplands (fig. 23*A, B*). The simulated hydraulic heads generally matched the measured groundwater-level decline during the simulation period but were higher than the measured data after about water year 1978. The measured data for wells 8N/33W-24B1 and 8N/33W-24B3 showed a declining trend for the period of record from water years 1955 through 2015 (fig. 23*C*). The available groundwater-level data for the period of record were limited. Simulated hydraulic heads were lower than the measured data between 1955 and 1960 and higher than the measured data between 1975 and 1980; however, the simulated hydraulic heads generally approximated the decline in measured groundwater levels for 2003–15 but were about 10 to 50 ft higher than the measured data (fig. 23*C*).

Eastern Valley

Wells 8N/32W-28P1 and 8N/32W-28P3 are both perforated in model layer 1 (fig. 23*D*). Measured groundwater levels in these wells and nearby well 8N/32W-29L2 (fig. 23*E*), which also is perforated in model layer 1, show declines from about 1983 to 1990 that are associated with expanded development and increased groundwater pumping over that period (Cromwell and others, 2022; fig. 23). The increase in water levels between 1990 and 1999 is associated with 7 years with greater-than-average precipitation (15 in/yr) during the period (Cromwell and others, 2022). Measured water levels showed an overall declining trend after 1999. Although the SACIM generally simulated the declining trend after 1999, the simulated hydraulic heads were lower than the measured data for all three wells (fig. 23*D, E*). Wells 8N/32W-30K2 and 8N/32W-30H7 are located about 1.5 mi west of 8N/32W-28P1 and 8N/32W-28P3 (fig. 19*B*) and are perforated in model layer 1 (fig. 23*F*). Groundwater levels in wells 8N/32W-30K2 and 8N/32W-30H7 showed a steady decline from 1958 to 1972, although the rate of decline was less pronounced after 1961 (fig. 23*F*). Simulated hydraulic heads approximate the measured groundwater levels and reasonably match the declining trend of the measured data (fig. 23*F*).

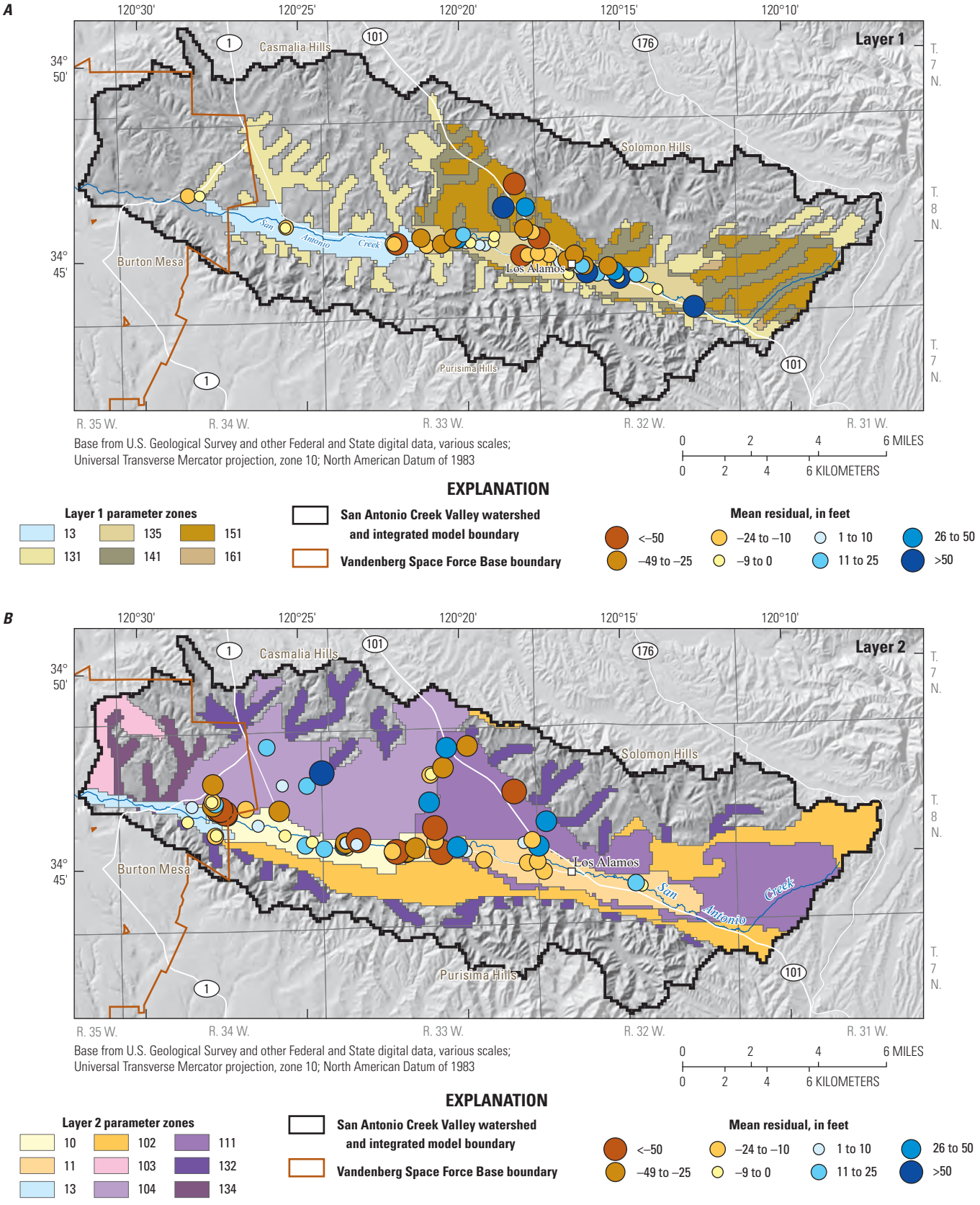

Figure 22. Distribution of average residuals for model layers *A*, 1, *B*, 2, *C*, 3, and *D*, 4 for the San Antonio Creek Valley integrated model, Santa Barbara County, California.

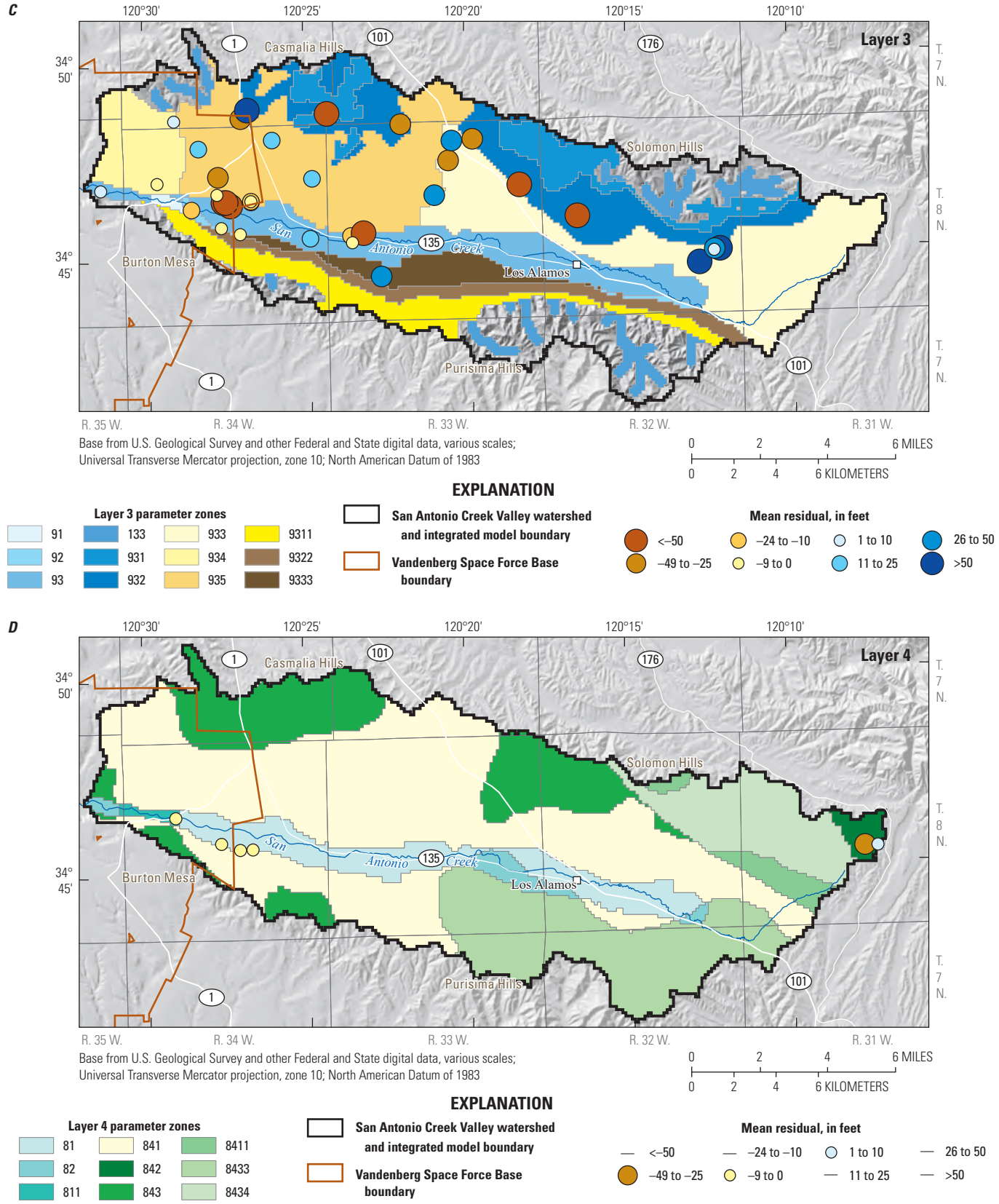

Figure 22.—Continued

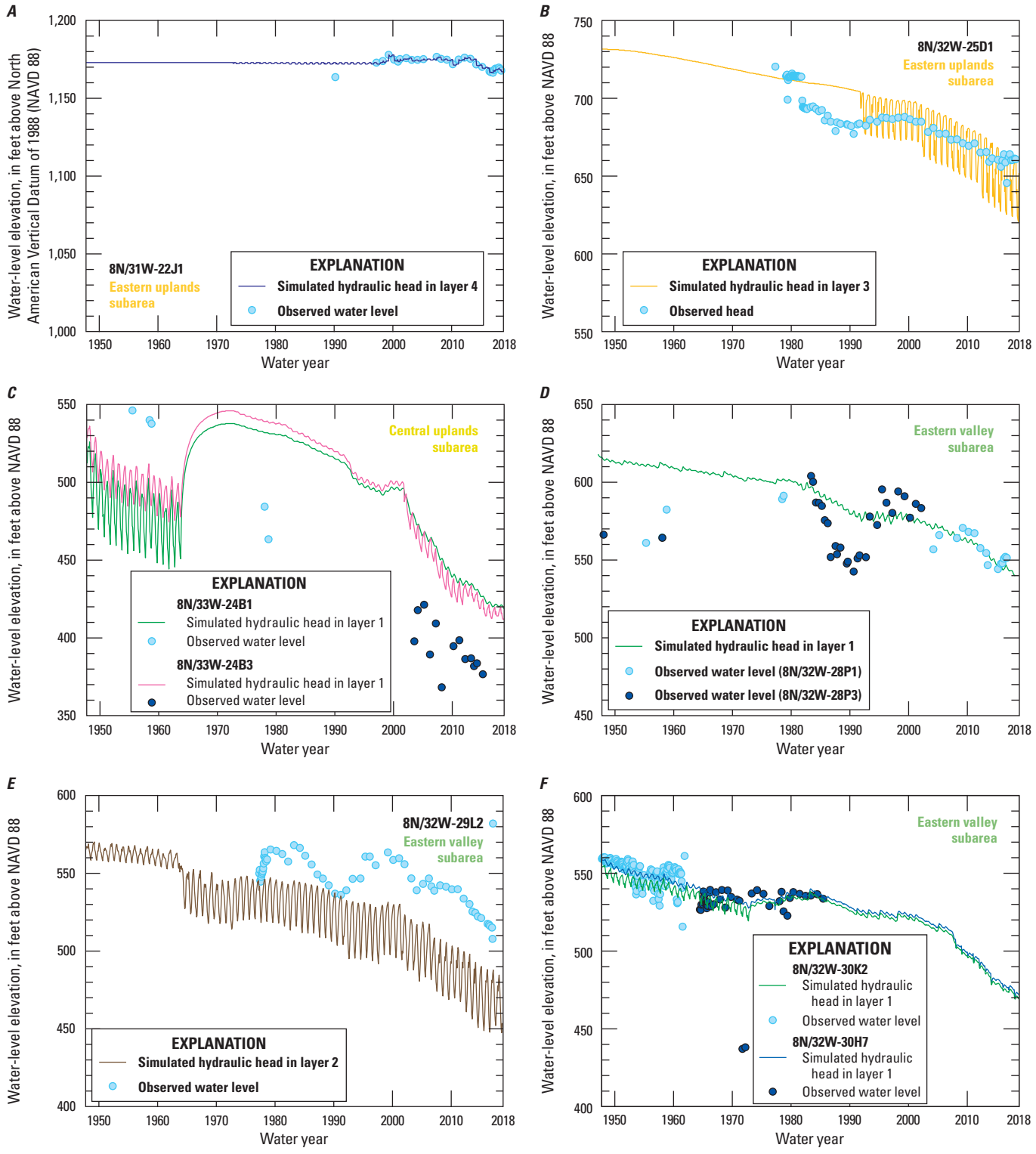

Figure 23. Measured and simulated hydraulic heads for selected wells in the San Antonio Creek Valley integrated model, Santa Barbara County California: eastern uplands subarea *A*, 8N/31W-22J1; *B*, 8N/32W-25D1; central uplands subarea: *C*, 8N/33W-24B1 and 8N/33W-24B3; eastern valley subarea: *D*, 8N/32W-28P1 and 8N/32W-28P3; *E*, 8N/32W-29L2; *F*, 8N/32W-30K2 and 8N/32W-30H7; *G*, 8N/32W-30D1; *H*, 8N/33W-22K3; western valley subarea: *I*, 8N/33W-20Q1; *J*, 8N/33W-20Q2; *K*, 8N/34W-23B1; *L*, 8N/34W-24E1; western uplands subarea: *M*, 8N/34W-2M1; *N*, 9N/34W-34P1; Barka Slough subarea: *O*, 8N/34W-24A1; *P*, 8N/34W-16C1; *Q*, 8N/34W-16C4; *R*, 8N/34W-17E1; *S*, 8N/35W-12M1.

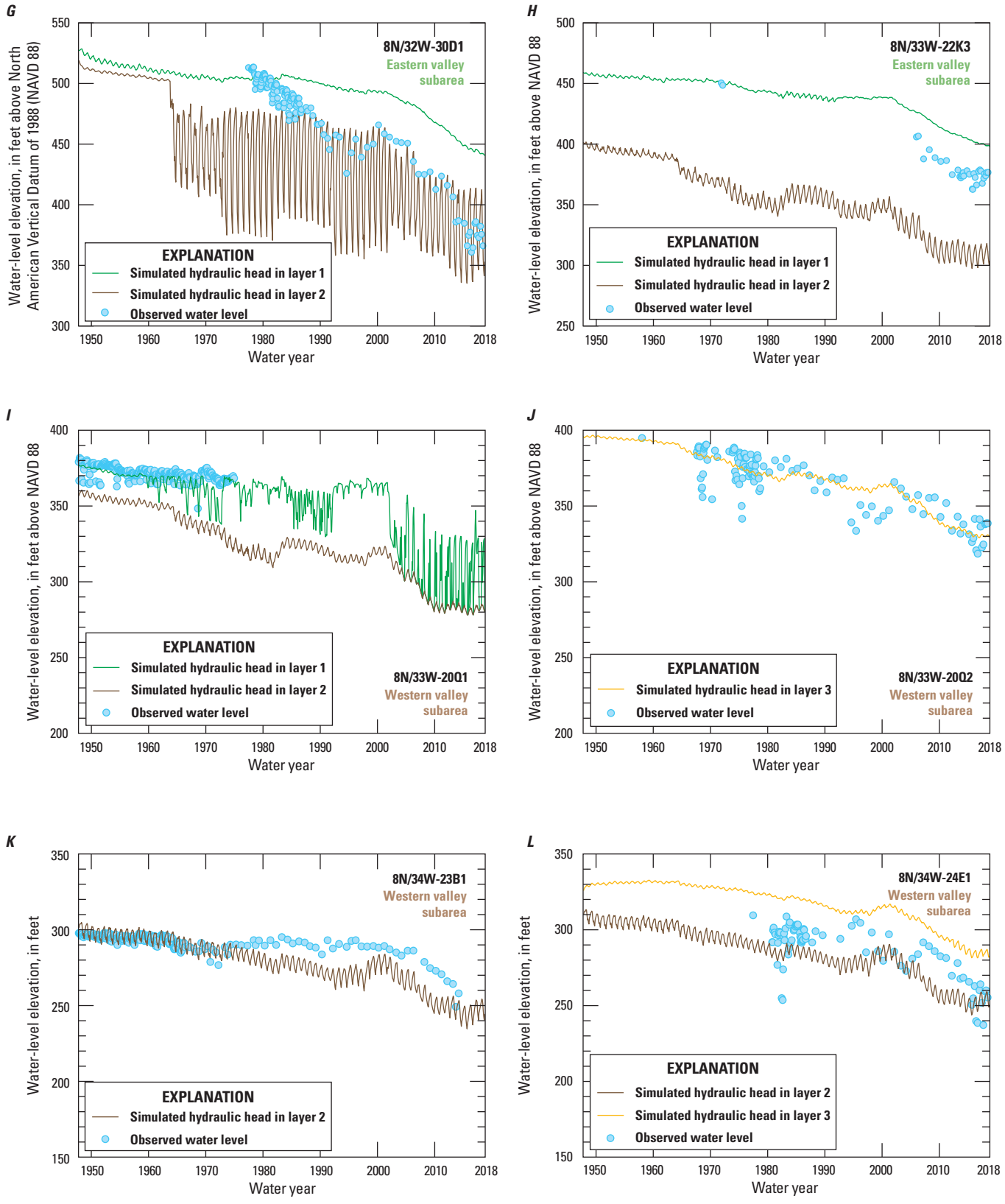

Figure 23.—Continued

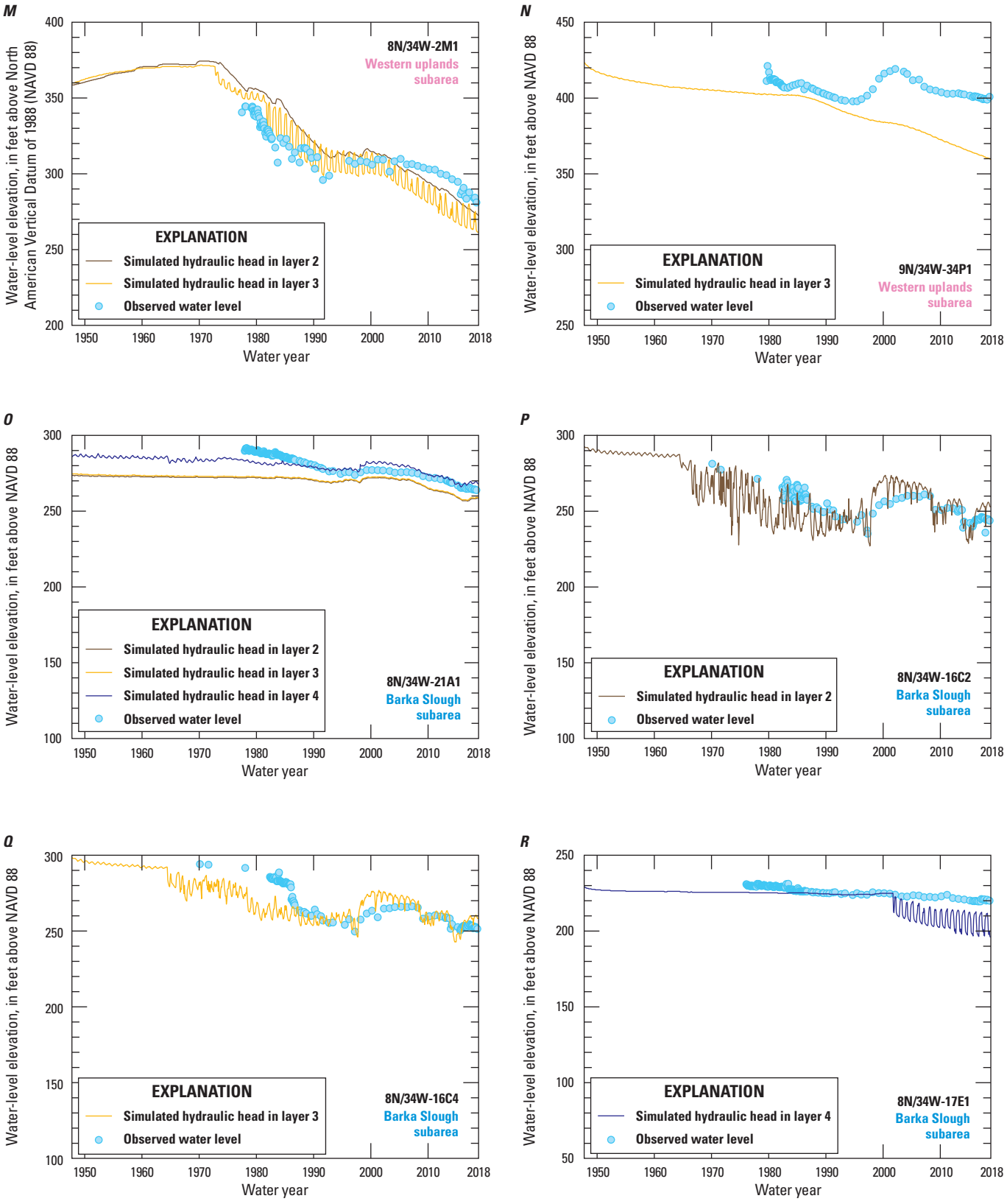

Figure 23.—Continued

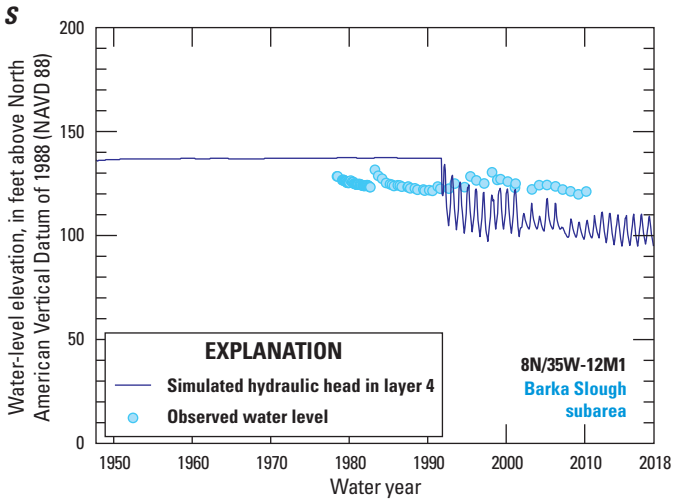

Figure 23.—Continued

Wells 8N/32W-30D1 (fig. 23*G*) and 8N/33W-22K3 (fig. 23*H*) are perforated in model layers 1 and 2 and showed greater rates of groundwater-level decline than those perforated only in model layer 1 discussed previously (fig. 23*C, D, F*). The rates of groundwater-level decline in wells 8N/32W-30D1 (fig. 23*G*) and 8N/33W-22K3 (fig. 23*H*) were similar to rates of decline in wells 8N/33W-24B1 and 8N/33W-24B3 in the central uplands (fig. 23*C*). Measured data for wells 8N/32W-30D1 and 8N/33W-22K3 show a decline in groundwater levels from about water years 1980 to 2018. The simulated hydraulic heads generally matched the measured groundwater-level decline in both wells during this period. The SACIM simulated seasonal fluctuations in model layer 2 for both wells; however, the simulated fluctuations in well 8N/32W-30D1 were much larger than the measured data (fig. 23*G*). Measured data for well 8N/33W-22K3 are limited for the period of record (fig. 23*H*). The simulated hydraulic heads in model layer 1 matched the early data in 1971 and 1972. Groundwater-level measurements from 2005 to 2017 show a steep decline until about 2011; after 2011, the decline becomes more gradual. The SACIM simulates the declining hydraulic heads in model layers 1 and 2 between 2005 and 2018; however, the simulated heads in model layer 1 are about 25 ft higher and in model layer 2 are about 75 ft lower than the measured data (fig. 23*H*).

Data from the USGS multiple-well monitoring site SACC1-5 (San Antonio Creek – Cat Canyon; SACC1 [8N/32W-19M1], SACC2 [8N/32W-19M2], SACC3 [8N/32W-19M3], SACC4 [8N/32W-19M4], SACC5 [8N/32W-19M5]; U.S. Geological Survey, 2021) show a downward gradient in groundwater levels between the shallow (SACC4 and SACC5) and deep wells (SACC1, SACC2, and SACC3; fig. 24*A*; Cromwell and others, 2022). Wells SACC5 and SACC4 are perforated in model layer 1; well SACC3 is perforated in model layers 1 and 2; and wells SACC1 and SACC2 are perforated in model layer 3. There are downward gradients between well SACC5 and SACC4; and between SACC4 and the three deepest wells (fig. 24*A*). These downward gradients may be caused by localized recharge from wastewater effluent spray field adjacent to the well site (Cromwell and others, 2022) that is not simulated in the model. Although the simulated hydraulic heads reasonably match the measured data, the seasonal fluctuations are more pronounced in model layer 2 than observed in the measured data for wells SACC1, SACC2, and SACC3. The downward gradient was reasonably matched between well SACC4 and wells SACC1, SACC2, and SACC3 (fig. 24*A*).

Western Valley

Well 8N/33W-20Q1 is perforated in model layers 1 and 2 (fig. 23*I*), and well 8N/33W-20Q2 is perforated in model layer 3 (fig. 23*J*). Measured groundwater levels in both wells showed a gradual but consistent decline prior to 1974; the SACIM generally simulated this gradual decline. Simulated heads in model layer 1 matched the measured water levels in well 8N/33W-20Q1 (fig. 23*I*), indicating that groundwater originates from channel deposits that are represented by model layer 1 at this location. Simulated hydraulic heads for well 8N/33W-20Q2 were within the range of monthly fluctuations of the measured groundwater levels and generally matched the increased decline in the measured data after 1974 (fig. 23*J*).

Well 8N/34W-23B1 is perforated in model layer 2 (fig. 23*K*). Measured groundwater levels in 8N/34W-23B1 were relatively stable until about 2002 when they began to decline. The simulated hydraulic heads generally matched measured stable groundwater levels and seasonal fluctuations from 1948 to 1974; however, after about 1974, simulated heads began to decline even though measured groundwater levels remained relatively steady (fig. 23*K*). After about 2002, simulated hydraulic heads reasonably matched the rate of decline in measured groundwater levels; however, simulated hydraulic heads were lower than measured groundwater levels by about 20 ft. Seasonal fluctuations in the simulated hydraulic heads after 1974 were similar to measured seasonal fluctuations in water levels (fig. 23*K*).

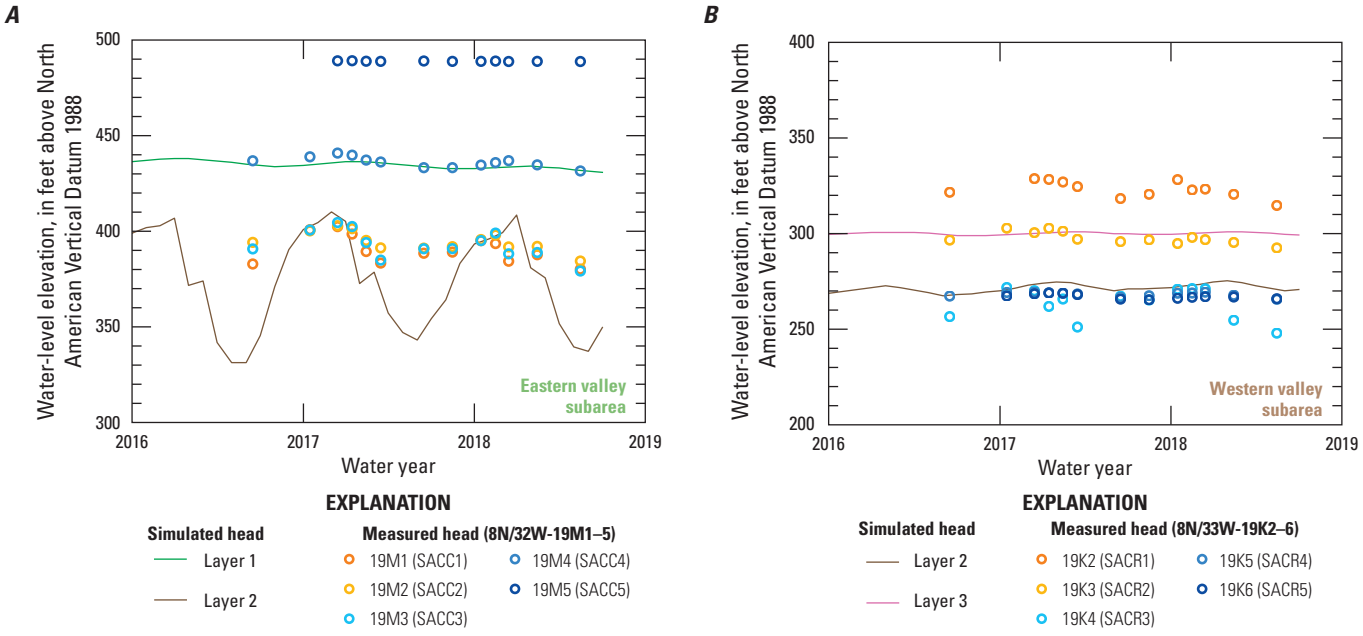

Figure 24. Measured and simulated hydraulic heads for U.S. Geological Survey multiple-completion wells *A*, 8N/32W-19M1–5 (SACC1–5) and *B*, 8N/33W-19K2–6 (SACR1–5), San Antonio Creek Valley integrated model, Santa Barbara County California; information for these wells can be found in U.S. Geological Survey (2021).

Well 8N/34W-24E1 is perforated in model layers 2 and 3 (fig. 23*L*). Measured groundwater levels in well 8N/34W-24E1 showed seasonal fluctuations from 1977 to 1997 that varied about a groundwater-level elevation of 295 ft. Groundwater levels began a gradual decline between 1998 and 2007; after 2007, the rate of decline in increased (fig. 23*L*). The simulated heads in model layers 2 and 3 generally matched patterns in the measured groundwater levels and seasonal fluctuations of the measured data; however, simulated hydraulic heads for model layer 3 were higher than the measured groundwater levels and simulated hydraulic heads for model layer 2 were lower than measured groundwater levels (fig. 23*L*).

The western valley subarea receives recharge from depth as groundwater flows from the eastern valley subarea and moves upward as indicated by an upward gradient at USGS multiple-well monitoring site SACR1-5 (San Antonio Creek – Old Careaga Road; SACR1 [8N/33W-19K2], SACR2 [8N/33W-19K3], SACR3 [8N/33W-19K4], SACR4 [8N/33W-19K5], SACR5 [8N/33W-19K6]; fig. 24*B*). Additional site information about these wells are in U.S. Geological Survey (2021). Wells SACR5, SACR4, and SACR3 are perforated in model layer 2 (fig. 10). Groundwater-level elevations in these wells are similar, but groundwater levels in SACR-3 respond more to nearby pumping. Well SACR2 also is perforated in model layer 2, but measured groundwater-levels are about 30 ft higher than the three shallower wells. Well SACR1 is perforated in model layer 3, and measured groundwater-levels are about 20–30 ft higher than well SACR2. The SACIM reasonably simulates the magnitude of the upward gradient between well (SACR2) and wells SACR3 SACR4), and SACR5 (fig. 24*B*). The simulated hydraulic heads in model layer 2 are similar to the highest measured groundwater levels in SACR3, and the simulated heads in model layer 2 are similar to the measured groundwater levels in SACR2 (fig. 24*B*).

Western Uplands

Well 8N/34W-2M1 is located in Harris Canyon (fig. 2) and is perforated in model layers 2 and 3 (fig. 23*M*). The simulated hydraulic heads generally matched the declines in the measured groundwater-levels from about 1980 to about 1991, relatively stable measured groundwater levels from 1992 to about 2005, and declining measured groundwater levels from 2006 to 2018 (fig. 23*M*). Simulated hydraulic heads generally were higher than measured groundwater levels during 1980–91 and lower than measured groundwater levels during 2006–18 (fig. 23*M*). Declines in simulated hydraulic heads and measured groundwater levels from 1980 to about 1991 and from 2006 to 2018 likely were due to overall dry periods. Relatively stable measured groundwater levels and simulated hydraulic heads from 1992 to about 2005 correspond to a period with 8 of 14 years with greater-than-average precipitation (see fig. 3 in Cromwell and others, 2022).

Well 8N/34W-34P1 is located adjacent to the VSFB boundary northwest of well 8N/34W-2M1 (fig. 19*B*) and is perforated in model layer 3 (fig. 23*N*). Simulated hydraulic heads in model layer 3 generally matched the decline in the measured groundwater levels from 1979 through 1994. Measured groundwater levels increased from about 1995 through 2002 and then declined from about 2003 through 2018; the rate of decline in groundwater levels decreased after about 2007 (fig. 23*N*). Simulated heads show a steady and pronounced decline in groundwater levels after about 1994. Simulated hydraulic heads are lower than the measured data for the period of record (fig. 23*N*). Observed mismatches may be due to local variation in aquifer properties that are not simulated in the model and uncertainty associated with agricultural pumpage simulated by the SACIM from nearby wells.

Barka Slough

Variations in groundwater levels and base flow at Barka Slough indicate changing groundwater stresses and inputs in the upgradient and upstream areas of the SACVW (Cromwell and others, 2022). Wells 8N/34W-21A1, 8N/34W-16C2 and 8N/34W-16C4, and 8N/34W-12M1 are located adjacent to or downstream of Barka Slough (fig. 19*B*). Well 8N/34W-21A1 is perforated in model layers 2–4 (fig. 23*O*). The measured data show relatively muted groundwater-level variations likely because the well is primarily perforated in consolidated bedrock and has a limited hydraulic connection to the groundwater system (Cromwell and others, 2022). Simulated hydraulic heads in model layers 2-4 generally match the magnitudes and seasonal fluctuations of the measured data; however, simulated hydraulic heads were lower than the measured data prior to 1985 and more closely match the measured data after 2000 (fig. 23*O*).

Similar to the western valley subarea, Barka Slough receives recharge from depth as groundwater flows from the eastern parts of the SACVW and moves upward as indicated by an upward gradient between wells 8N/34W-16C2 (fig. 23*P*) and 8N/34W-16C4 (fig. 23*Q*; Cromwell and others, 2022). These wells are part of a multiple-monitoring well site adjacent to Barka Slough and are perforated in model layers 2 and 3, respectively. Simulated hydraulic heads reasonably match the magnitude of the upward gradient from model layer 3 to model layer 2 and the decreasing vertical gradient in the measured data for the period of record (fig. 23*P*, 23*Q*). Magnitudes and seasonal fluctuations of simulated hydraulic heads reasonably match the measured data for 8N/34W-16C2; however, simulated heads were slightly higher than the measured groundwater levels during 1998–2004 (fig. 23*P*). Magnitudes and seasonal fluctuations of simulated hydraulic heads reasonably match the measured data for 8N/34W-16C4; however, simulated hydraulic heads were lower than measured data prior to about 1986 and higher than the measured data during 1998–2004 (fig. 23*Q*). Because reported military pumping in the vicinity of wells 8N/34W-16C2 and 8N/34W-16C4 is measured (see "Military and Municipal Pumpage" section of this report) and, therefore, less uncertain than if estimated, the mismatches between the measured groundwater levels and simulated hydraulic heads for these wells likely are due to local variation in aquifer properties that are not simulated in the model.

Well 8N/34W-17E1 is located along San Antonio Creek, downstream of Barka Slough (fig. 19*B*). Well 8N/34W-17E1 is perforated in model layer 4 (fig. 23*R*), which represents consolidated bedrock. The measured groundwater levels were generally stable from about 1976 through 2001; after 2001, a gradual decline in measured groundwater levels was observed. Magnitudes and seasonal fluctuations of simulated hydraulic heads reasonably match the measured data prior to 2001. After 2001, simulated seasonal fluctuations and declines in groundwater levels are more pronounced compared with measured groundwater level data (fig. 23*R*).

Well 18N/34W-12M1 is located along San Antonio Creek, just upstream of the Casmalia streamgage (11136100; fig. 19*B*) and is perforated in model layer 3 (fig. 23*S*). Measured groundwater levels and seasonal fluctuations were generally stable for the period of record. Prior to 1992, simulated hydraulic heads were stable but higher than measured groundwater levels; after 1992, simulated hydraulic heads showed a gradual decline from 1991 through 1997 that is not indicated by the measured data. After 1997, simulated hydraulic heads were relatively stable but were lower than measured groundwater levels. After 1992, simulated seasonal fluctuations were more pronounced compared to measured groundwater levels.

Calibration to Streamflow

The SACIM was calibrated to monthly mean streamflow at four USGS streamgages (fig. 19*B*). The calibration results presented in this section include simulated and measured monthly mean streamflow for streamgages with the longest periods of record, San Antonio Creek at Los Alamos, Calif. (11135800; herein referred to as "the Los Alamos streamgage"; fig. 25*A*), and the Casmalia streamgage (11136100; fig. 25*B*), including goodness-of-fit statistics (PAEE, AAEE, NSE, and NNSE). The perfect model, where the simulated values are identical to the observed data, results in PAEE and AAEE values of zero, an NSE value of 1.0, and an NNSE value of zero. The PAEE and AAEE statistics are measures of model bias but are not definitive measures of goodness-of-fit because the sample mean has values of zero for both statistics. For the NSE, a value greater than zero indicates an improved fit relative to the mean. The NNSE is used to scale the NSE between values of zero and one. A NNSE value greater than 0.5 indicates that the model simulates streamflow better than the mean of the measured data.

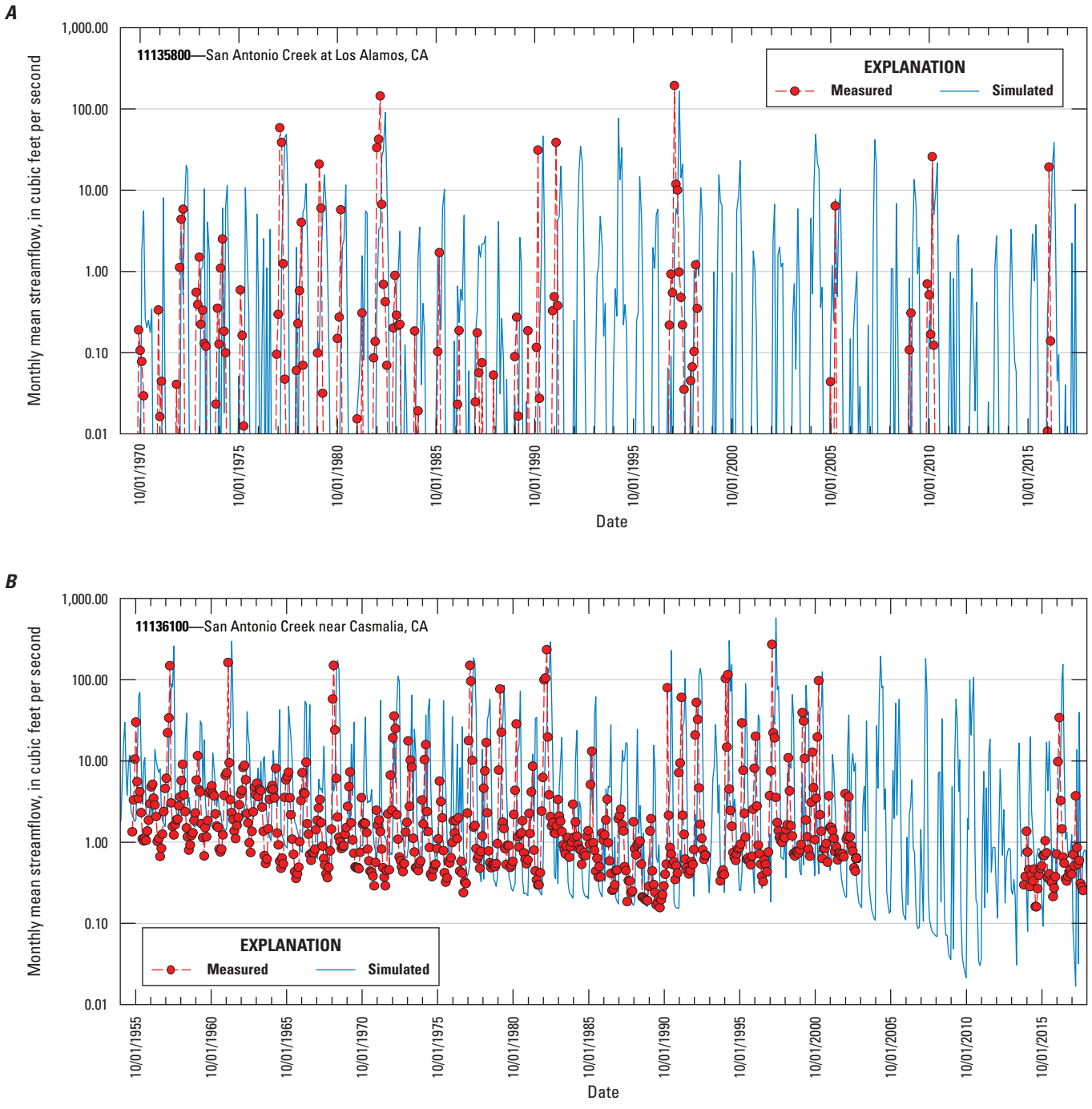

Figure 25. Comparison of simulated and measured monthly mean streamflow at the *A*, San Antonio Creek at Los Alamos, Calif. (11135800); and *B*, San Antonio Creek near Casmalia, Calif. (11136100) streamgages, San Antonio Creek Valley integrated model, Santa Barbara County California.

The PAEE and AAEE values for calibration of the SACIM to measured streamflow at the Casmalia streamgage (11136100) indicate an overall positive bias (simulated streamflow greater than the measured streamflow) with a relatively large error; however, because the NSE value is greater than zero and the NNSE is greater than 0.5 (table 13), the model adds information to the calibration compared with the mean of the measured data. For calibration of the SACIM to measured streamflow at the Los Alamos streamgage (11135800), the NSE and NNSE values less than zero and 0.5, respectively (table 13), indicating the model does not simulate streamflow better than the mean of measured data; however, the PAEE and AAEE values were the lowest relative to the values for the other streamgages. The Los Alamos streamgage (11135800) was active from water years 1971 through 2018 but had periods of inactivity or poor data quality from water years 1993 to 2016 (Cromwell and others, 2022), which likely contributed to the poor model fit at this location.

Simulated streamflows generally matched measured streamflows well at the Los Alamos and Casmalia streamgages (fig. 25*A* and fig. 25*B*, respectively). The monthly hydrographs for these streamgages indicated that the SACIM generally performed well in terms of matching the timing and frequency of the peak streamflows. Base flow at the Los Alamos streamgage (11135800; fig. 25*A*) is largely non-existent, and streamflow consists almost entirely of direct runoff (Cromwell and others, 2022). Simulated peak flows generally match measured peak flows at the Los Alamos streamgage (11135800) and reasonably match the magnitudes of the monthly fluctuations in the measured data (fig. 25*A*); however, simulated streamflows were substantially higher than measured streamflows less than about 10 cubic feet per second (ft^3/s; fig. 26*A*). Overall, simulated peak flows are higher than measured peak flows at the Casmalia streamgage (11136100), but simulated magnitudes of the monthly fluctuations generally match the fluctuations of the measured data (fig. 25*B*). Simulated streamflows reasonably matched measured flows between 1.0 and 10 ft^3/s (fig. 26*B*).

Comparison of Simulated and Reported Agricultural Pumpage

Agricultural pumpage for water years 1948–2018 simulated by the SACIM was compared with reported pumpage (fig. 27). Simulated agricultural pumpage generally was higher than reported agricultural pumpage from Muir (1964), Hutchinson (1980), and Martin (1985) from 1948 to the mid-1970s, and simulated agricultural pumpage generally was lower than reported agricultural pumpage from Tetra Tech, Inc. (2012; water years 1948–2010), and Cromwell and others (2022; water years 2011–18; fig. 27*A*). The relation between reported and simulated agricultural pumpage was linear and generally followed the 1:1 correlation line. Simulated values were generally lower than the reported values (fig. 27*B*); about 56 percent of the points plot below the 1:1 correlation line. Most of the values above the 1:1 line were for simulated pumpage of about 10,000 acre-ft or less. The mean simulated agricultural pumpage for water years 1948–2018 was about 14,400 acre-ft/yr compared with a mean reported agricultural pumpage of about 15,600 acre-ft/yr. The simulated mean pumpage for water years 2002–18, a period with a sharp increase in agricultural pumpage, was about 27,000 acre-ft/yr compared with a mean reported agricultural pumpage of about 28,800 acre-ft/yr.

Table 13. Summary of model-fit statistics for streamflow data from streamgages used to calibrate the San Antonio Creek Valley integrated model, Santa Barbara County, California.

[NA, not applicable]

Stream gaging station	Simulated mean (cubic feet per second)	Simulated maximum (cubic feet per second)	Simulated minimum (cubic feet per second)	Observed mean (cubic feet per second)	Observed maximum (cubic feet per second)	Observed minimum (cubic feet per second)	Nash-Sutcliffe efficiency	Normalized Nash-Sutcliffe efficiency	Percent average estimation error (percent)	Absolute average estimation error (percent)
San Antonio Creek near Casmalia (11136100)	0.45	19	0	0.20	9.0	0.01	0.25	0.57	138	138
San Antonio Creek at Barka Slough (11136050)	0.31	16	0	0	0.01	0	NA	NA	979	979
San Antonio Creek at Los Alamos (11135800)	0.09	5.5	0	0.06	6.4	0	–0.24	0.45	44	44
Harris Canyon near Orcutt (11136040)	0.04	1.4	0	131	1,311	0	NA	NA	–100	100
San Antonio Creek at Harris Canyon (11136000)	0.26	15	0	0.03	1.7	0	NA	NA	420	420

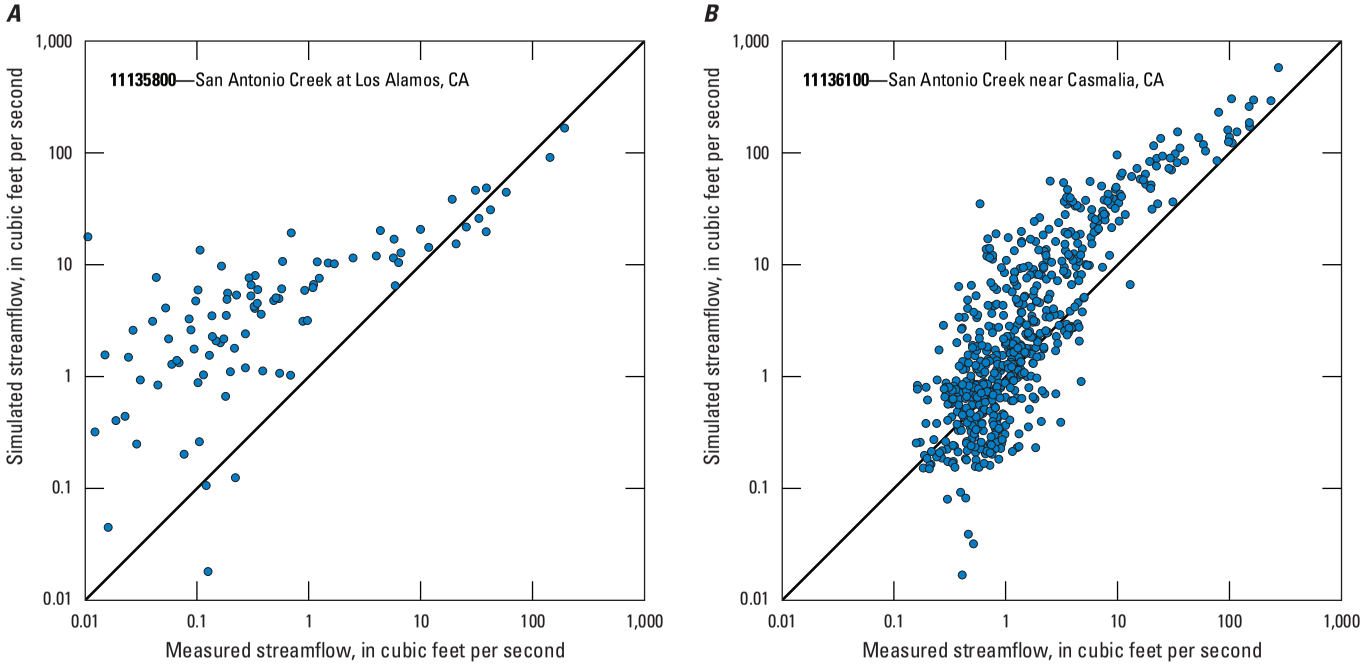

Figure 26. Simulated streamflow from the San Antonio Creek Valley integrated model compared to measured streamflows at U.S. Geological Survey streamgages: *A*, San Antonio Creek at Los Alamos, California (U.S. Geological Survey station 11135800), and *B*, San Antonio Creek near Casmalia, California (U.S. Geological Survey station 11136100), Santa Barbara County, California.

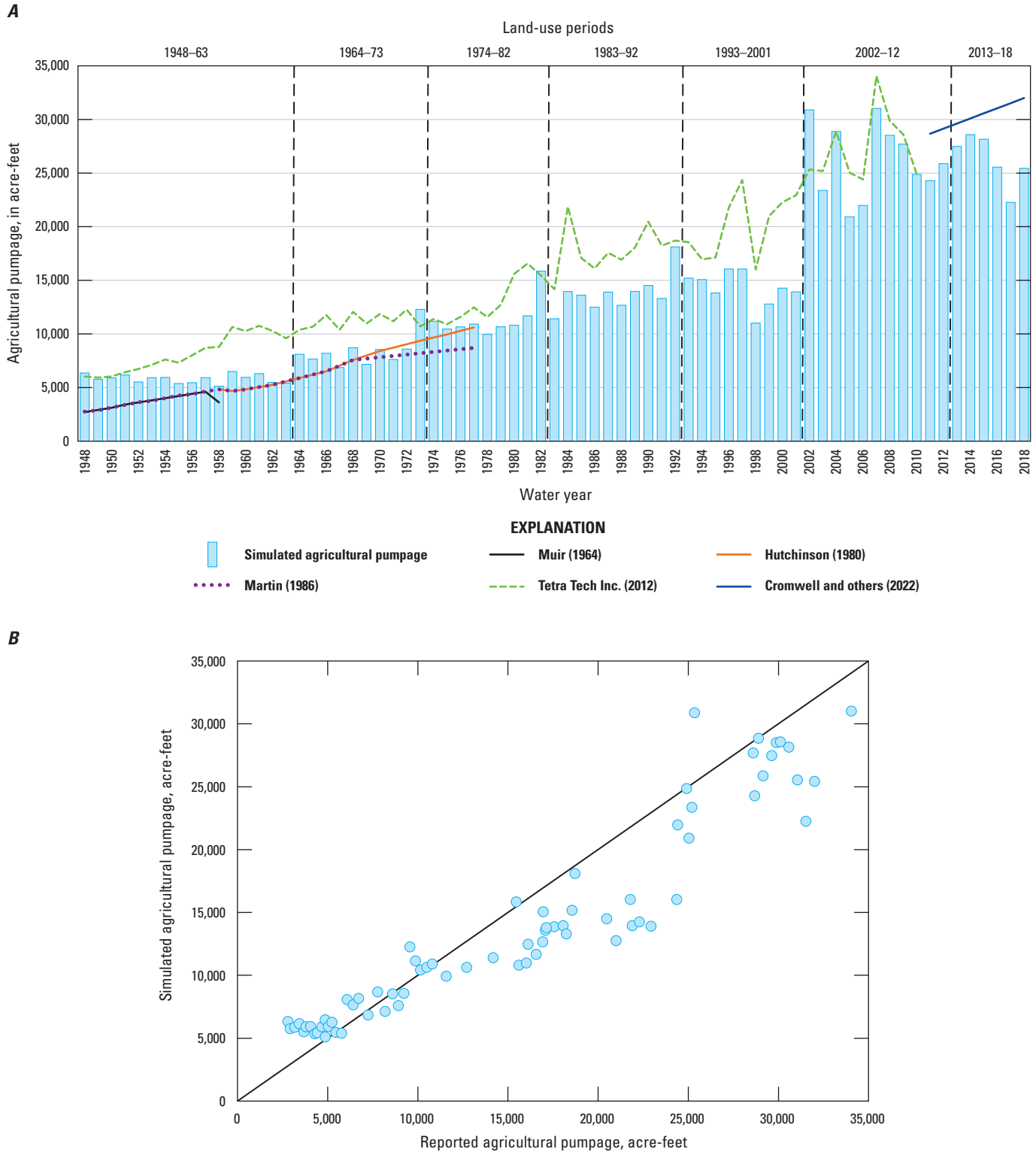

Figure 27. Comparisons of reported agricultural pumpage and agricultural pumpage simulated using the San Antonio Creek Valley integrated model, Santa Barbara County, California: *A*, plots of reported and simulated annual agricultural pumpage, and *B*, relations between reported and simulated agricultural pumpage compared with a 1:1 correlation line.

Simulated Groundwater Budget

The components of the groundwater budget for the 71-year simulation period (waters years 1948–2018) for the SACVW are shown in figure 28. Positive values are inflows to the groundwater system, and negative values are outflows from the groundwater system; for the "storage" component (fig. 28), groundwater from storage is depicted as a positive value, while groundwater to storage is depicted as a negative value. The cumulative storage curve in figure 28 is depicted in conventional sense, where negative values represent groundwater from storage to the groundwater-flow system exceeding groundwater from the groundwater-flow system to storage (storage depletion). During the water year 1948–2018 simulation period, groundwater ET and surface leakage decreased steadily with increased agricultural pumpage. Cumulative storage decreased during the simulation period; the rate of decrease in cumulative storage increased sharply after 2001 with a concurrent large increase in agricultural pumping.

During water years 1948–2018, 924,700 acre-ft of water was added to the groundwater system in the SACVW as boundary flows, stream leakage, and recharge; 1,378,000 acre-ft of groundwater was removed from the SACVW as groundwater ET, surface leakage, municipal and military pumping, and agricultural pumping (table 14). Summing groundwater inflows and outflows resulted in storage depletion of 453,300 acre-ft (table 14). Groundwater from storage accounted for about 33 percent of the water entering the groundwater-flow system; stream leakage and recharge from the unsaturated zone accounted for about 29 and 37 percent, respectively. Boundary flows were small in comparison with the other sources of groundwater inflow, accounting for about one percent of total groundwater inflow. Agricultural pumpage was the largest groundwater outflow (1,020,000 acre-ft) and accounted for about 74 percent of total groundwater outflow during water years 1948–2018 (table 14). Average storage depletion for the water year 2002–12 and 2013–18 land-use periods were 16 percent and 37 percent, respectively, greater than average total inflow for the same periods.

Simulated Agricultural Pumpage

Agricultural pumpage for all groundwater subareas (subareas shown on fig. 19*B*) increased throughout the simulation period, with the most substantial increases occurring in the western, central, and eastern upland subareas (fig. 29*A*). The western and eastern valley subareas were irrigated for the duration of the simulation period, with combined pumpage for the two subareas ranging from about 4,000 to about 13,000 acre-ft/yr. The western, central, and eastern upland subareas had limited agricultural pumpage from 1948 to 1972, totaling less than 1,500 acre-ft/yr during this period; irrigation increased in the western upland subarea beginning in about 1973, and increased in the central and eastern upland subareas beginning in about 2002 (fig. 29*A*). From 1973 to 2001, total agricultural pumpage for the western, central, and eastern upland subareas ranged from about 2,300 to about 7,000 acre-ft/yr; from 2002 to 2018, total agricultural pumpage for these three upland subareas ranged from about 11,900 to more than 16,900 acre-ft/yr. Agricultural pumpage in the southern upland subarea was minimal throughout the simulation period and never exceeded 600 acre-ft/yr (fig. 29*A*).

Agricultural pumpage is distributed primarily in model layers 1 and 2 (fig. 29*B*) throughout the simulation period. From 1948 to 1972, agricultural pumpage in layers 1 and 2 accounted for more than 97 percent of total agricultural pumpage in the SACVW. Agricultural pumpage increased in layers 3 and 4 beginning in 1973 (fig. 29*B*), but from 1973 to 2001, agricultural pumpage in layers 3 and 4 never accounted for more than about 19 percent of the total. During 2002–18, agricultural pumpage increased substantially in layer 3 (fig. 29*B*), primarily in the western and central upland subareas (fig. 29*A*) and accounted for more than 30 percent of total agricultural pumpage. Combined agricultural pumpage in layers 1 and 2 also increased during 2002–18 (fig. 29*B*) and accounted for about 66 percent of total agricultural pumpage. The increase in pumpage in layer 3 is consistent with expansion of vineyards in the eastern, central, and western upland subareas where the Careaga Sandstone (represented by layer 3 in the model) is the uppermost hydrogeologic unit or occurs at shallow depths (Cromwell and others, 2022).

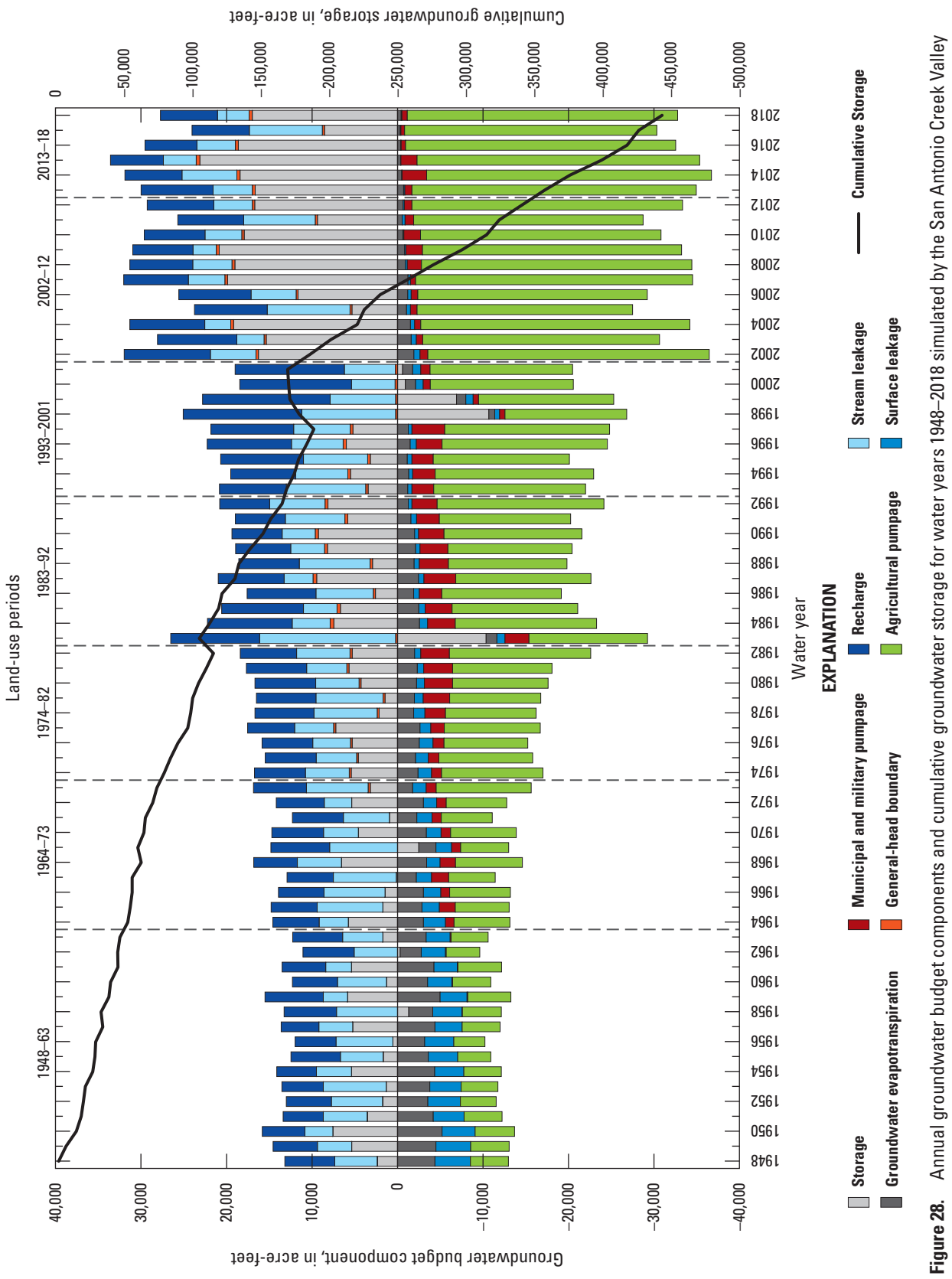

Figure 28. Annual groundwater budget components and cumulative groundwater storage for water years 1948–2018 simulated by the San Antonio Creek Valley integrated model, Santa Barbara County, California.

Table 14. Simulated total and average groundwater budgets for water years 1948–2018 and land-use periods for the San Antonio Creek Valley integrated model, Santa Barbara, California.

[Total groundwater budget components in acre-feet; average groundwater budget components in acre-feet per year; surface leakage is groundwater discharge to the surface and soil zone]

Budgets	Total for simulation period 1948–2018	Average for simulation period 1948–2018	Averages for land-use periods						
			1948–63	1964–73	1974–82	1983–92	1993–2001	2002–12	2013–18
Inflows									
Boundary flows	13,700	193	4	29	222	345	283	295	349
Stream leakage	403,538	5,684	4,934	5,859	5,570	6,385	7,246	5,022	5,262
Recharge	507,246	7,144	5,350	5,730	6,441	7,675	11,028	8,145	6,797
Total inflow	**924,484**	**13,021**	**10,288**	**11,618**	**12,234**	**14,405**	**18,558**	**13,462**	**12,408**
Outflows									
Groundwater evapotranspiration	154,989	2,183	3,913	2,707	2,245	1,965	1,179	1,105	449
Surface leakage	100,506	1,416	3,400	1,847	1,180	660	655	363	87
Municipal and military pumping[1]	102,210	1,440	36	1,326	2,311	3,082	1,966	1,082	1,191
Agricultural pumping	1,019,833	14,364	5,875	8,435	11,401	14,112	15,462	26,557	27,744
Total outflow	**1,377,538**	**19,402**	**13,224**	**14,315**	**17,138**	**19,820**	**19,262**	**29,107**	**29,470**
Net storage[2]	–453,054	–6,381	–2,937	–2,697	–4,904	–5,415	–704	–15,645	–17,062

[1]Average municipal and military pumping for the 1948–63 land-use period is calculated only for 1958–63 because there was no pumping from those sources prior to 1958.

[2]Net storage is total inflow minus total outflow; negative values indicate groundwater from storage recharging the groundwater-flow system (storage depletion).

Groundwater Storage

During the simulation period, groundwater from storage almost always exceeded groundwater to storage each year, resulting in depletion of groundwater storage (fig. 28). The average annual groundwater-storage depletion during water years 1948–2018 was 6,430 acre-ft/yr (table 14), Groundwater-storage depletion generally increased over time (fig. 28) and was correlated primarily to changes in land use and increasing agricultural pumpage (fig. 28). Cumulative groundwater storage increased most notably when there was an accretion in annual groundwater storage in water years 1958, 1962, 1969, 1983, and during water years 1998–2001 (fig. 28). These years had higher than average precipitation (fig. 30*A*), resulting in larger amounts of recharge and stream leakage (fig. 28). For the land-use periods during 1948–92, the average annual groundwater-storage depletion ranged from 3,002 to 5,400 acre-ft/yr (table 14). During the 1993–2001 land-use period, average annual groundwater-storage depletion was 780 acre-ft/yr (table 14); precipitation during this period generally was higher than average (fig. 30*A*) with a corresponding decrease in agricultural pumping (fig. 30*B*), resulting in storage accretion (groundwater from the groundwater-flow system to storage exceeding groundwater from storage to the groundwater-flow system) during 1998–2001 (fig. 28). Average groundwater-storage depletions during the 2002–12 and 2013–18 land-use periods were 15,680 and 17,017 acre-ft/yr, respectively; the large increases in groundwater-storage depletion starting in 2002 (fig. 30*B*) correspond to a sharp increase in agricultural pumping (fig. 29).

Net annual groundwater storage varied among groundwater subareas (fig. 30*B*). From 1948 to 1973, groundwater storage primarily accreted in the western and southern upland subareas, while groundwater storage was depleted in most other subareas. The western and southern upland subareas had negligible amounts of agricultural pumping during water years 1948–73 (fig. 29*A*). After 1974, agricultural pumpage in the western upland subareas increased (fig. 29*A*), with an overall increase in storage depletion in this subarea (fig. 30*B*); agricultural pumpage in the southern upland subarea was relatively small during this period, and storage accretion was simulated in 52 out of 59 years through 2006. Storage was depleted during 1948–2018 simulation period (fig. 30*B*), except during 1998–2001 (fig. 30*A*), when there was greater-than-average precipitation and pumpage declined, resulting in storage accretion or slight storage depletion in all subareas (fig. 30*B*). The increase in agricultural pumpage after 2001 resulted in annual storage depletion in almost every subarea during this period; however, small amounts of storage were accreted in Barka Slough (5 of 17 years), western valley (3 of 17 years, including unidentifiable black lines in 2005 and 2016), and southern uplands (5 of 17 years, including unidentifiable black lines

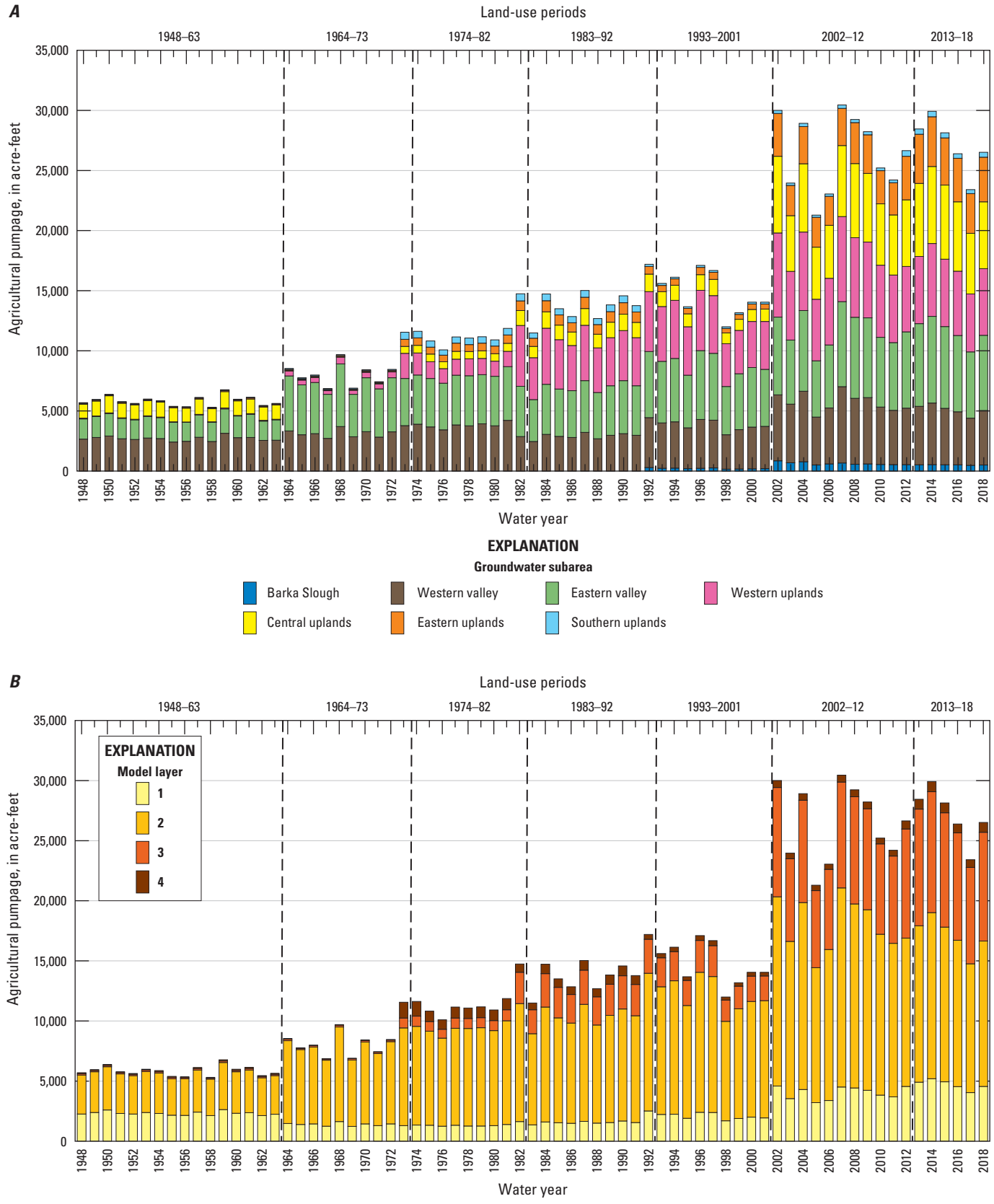

Figure 29. Annual agricultural pumpage for water years 1948–2018 estimated by the San Antonio Creek Valley integrated model, Santa Barbara County, California, for *A*, groundwater subareas and *B*, model layers.

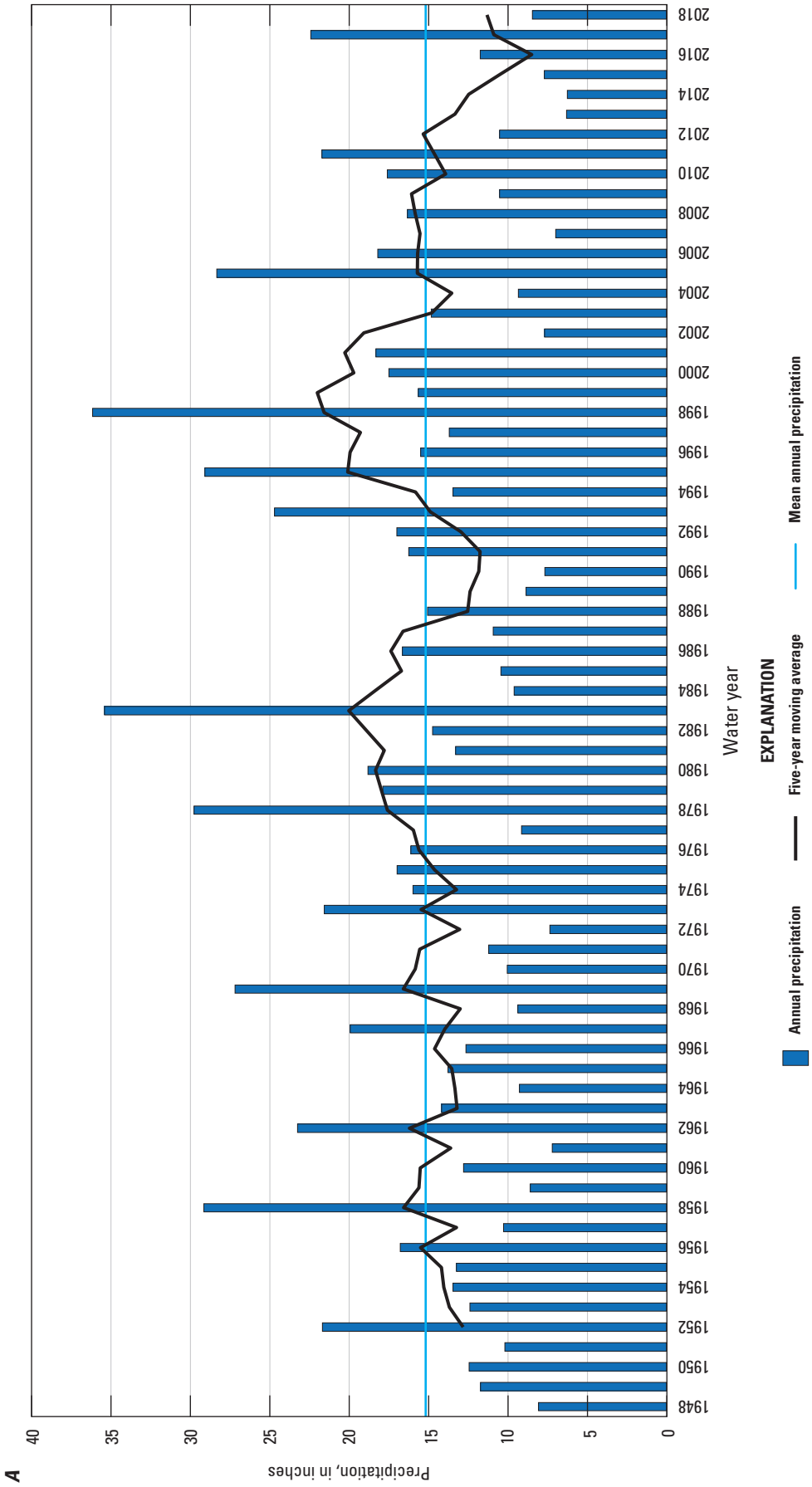

Figure 30. Summaries of *A*, average annual precipitation, and *B*, simulated annual groundwater storage for groundwater subareas and annual pumpage, for the San Antonio Creek integrated model, Santa Barbara County, California.

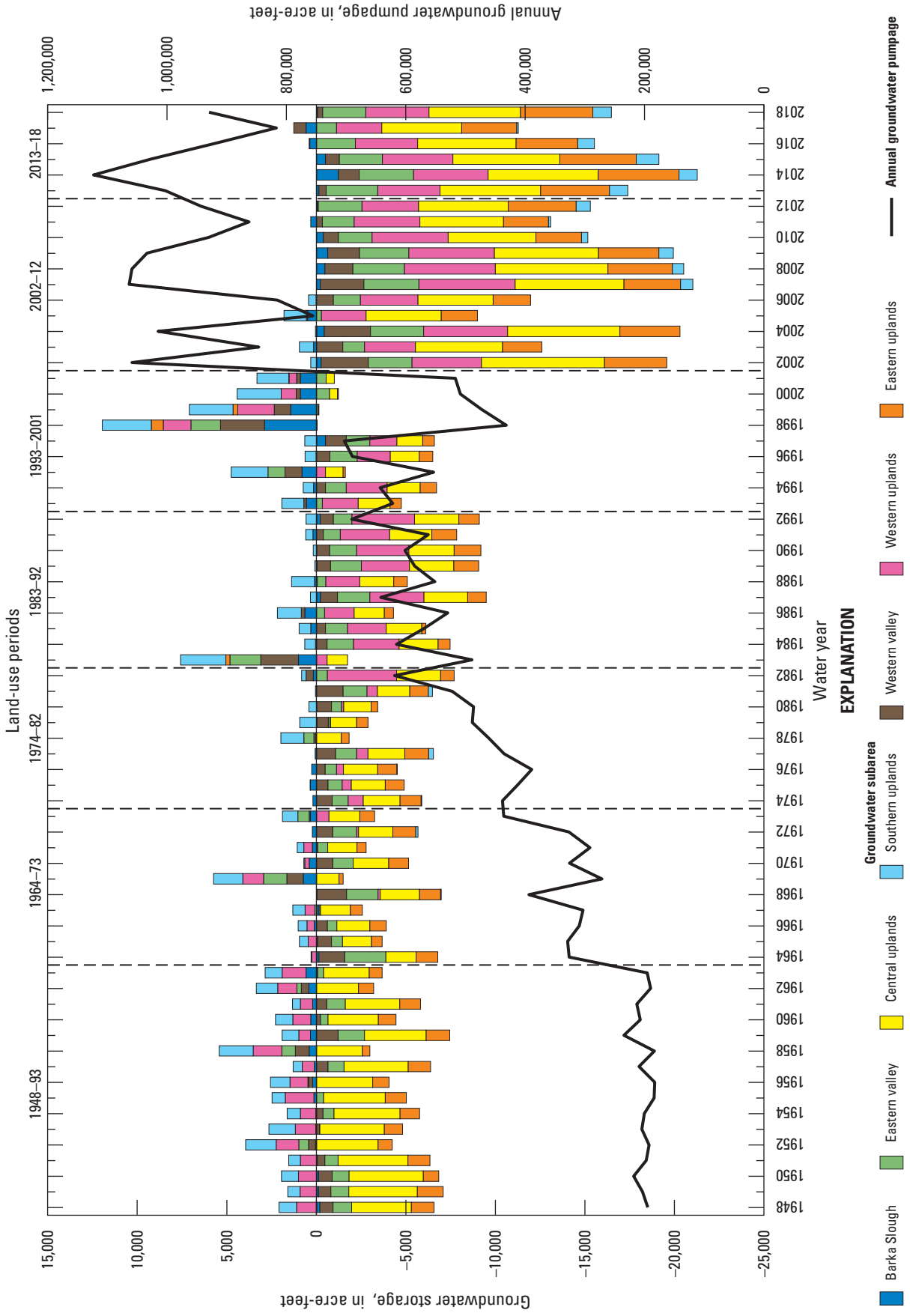

Figure 30.—Continued

in 2004) subareas (fig. 30*B*). The largest increases in storage depletion were in the eastern, central, and western upland subareas; this corresponds with the expansion of vineyards into the uplands areas during this period (Cromwell and others, 2022) and precipitation at or below the average annual precipitation of 15 in/yr for the simulation period (fig. 30*A*).

Groundwater Evapotranspiration

Increasing groundwater pumpage in the SACIM during the simulation period (water years 1948–2018) resulted in a relatively steady decline in annual groundwater ET in the SACVW (fig. 31). Annual groundwater ET for the Barka Slough subarea was fairly stable throughout the simulation period, ranging between about 90 to about 600 acre-ft/yr. Annual groundwater ET generally declined in all other subareas during the simulation period, particularly in the eastern and western valley subareas (fig. 31) that surround the main stem of San Antonio Creek. From 1948 to 1963, annual groundwater ET ranged from about 600 to about 1,700 acre-feet in the eastern valley subarea and from about 800 to about 1,400 acre-ft in the western valley subarea (fig. 31). Annual groundwater ET in the eastern valley subarea was reduced to zero acre-ft/yr by 2008; annual groundwater ET in the western valley subarea was reduced to less than 100 acre-ft/yr by 2010 (fig. 31). The western valley subarea receives a greater volume of surface flow from the surrounding uplands compared to the eastern valley subarea. The western valley subarea also is closer to Barka Slough, where uplifted consolidated bedrock causes groundwater to discharge to land surface (Cromwell and others, 2022).

Hydrologic Budget for Barka Slough

The potential effects of groundwater pumping in the SACVW on Barka Slough are concerning because Barka Slough is an important habitat for several endangered species. The water budgets presented in this section are for the Barka Slough area shown in figure 5. The average inputs and outputs for water years 1981–2018, a period of increasing agricultural irrigation, for the surface and soil zone and the unsaturated and saturated zones of Barka Slough are presented in figure 32. The surface and soil zone are linked to the saturated zone through the interaction of flows through the unsaturated zone and streams. On average for the 1981–2018 period, the dominant stresses for the Barka Slough flow system are precipitation and total ET (the sum of surface evaporation and soil-zone ET, unsaturated-zone ET, and saturated-zone ET; fig. 32).

The surface and soil-zone budget includes inputs from precipitation, lateral inflow from areas outside Barka Slough, and inflow from the saturated zone underlying Barka Slough, and outputs of surface evaporation and soil-zone ET, surface runoff to streams, shallow subsurface discharge to streams, and infiltration to the unsaturated zone. Inflow from the saturated zone to the surface and soil zone is the same as surface leakage, a component of outflow from the saturated zone (table 15). Infiltration from the surface and soil zone to the unsaturated zone is 88 acre-ft/yr, about 6 percent of the total inflow from precipitation, lateral inflow to the surface and soil zone, and inflow from the saturated zone. Groundwater recharge from the unsaturated zone is 60 acre-ft/yr, about 68 percent of the infiltration from the surface and soil zone to the unsaturated zone. The presence of surface leakage (fig. 32) indicates upward flow of groundwater to Barka Slough on average for this period.

The surface and soil-zone and saturated-zone water-budget components vary similarly from year to year during 1948–2018; inflows and outflows for both water budgets generally declined in response to increasing pumpage throughout the SACVW (fig. 33*A*, 33*B*). Although surface evaporation and soil-zone ET and subsurface ET were relatively stable during the 1948–2018 simulation period, there was an overall decline in total ET as indicated by the cumulative total ET curve in figure 33*A*. For the surface and soil-zone budgets prior to 1981, the main inflows were precipitation, inflow from the saturated zone, and lateral inflow. For the 1981–2018 period, inflow from precipitation and lateral flow were similar for the 1981–2018 period; however, inflow from the saturated zone decreased substantially (fig. 33*B*). Precipitation and lateral inflow increased by 17 and 18 percent, respectively, from the 1948–80 period to the 1981–2018 period (table 15). The relative contributions from precipitation to total inflow increased from 28 to 55 percent for precipitation; the relative contribution of lateral inflow to total inflow increased 15 to 30 percent from the earlier period to the later period. In contrast, inflow from the saturated zone decreased 84 percent from the 1948–80 period to 1981–2018 period (table 15). The relative contribution of inflow from the saturated zone to total inflow decreased from 57 to 15 percent from the earlier period to the later period.

The main outflows from the surface and soil zone were surface evaporation and soil-zone ET, shallow subsurface discharge to streams, and surface runoff (fig. 33*A*). Surface evaporation and soil-zone ET was relatively steady for the simulation period (fig. 33*A*); the total surface evaporation and soil-zone ET for 1981–2018 was only 11 percent less than the total for 1948–80 (table 15). The relative contribution of surface evaporation and soil-zone ET to total outflow increased from 42 to 58 percent from the earlier period to the later period. In contrast, shallow subsurface discharge to streams declined substantially; the total shallow subsurface discharge for 1981–2018 was 64 percent less than the total for 1948–80 (table 15). The relative contribution of shallow subsurface discharge to streams to total outflow decreased from 46 to 26 percent from the earlier period to the later period.

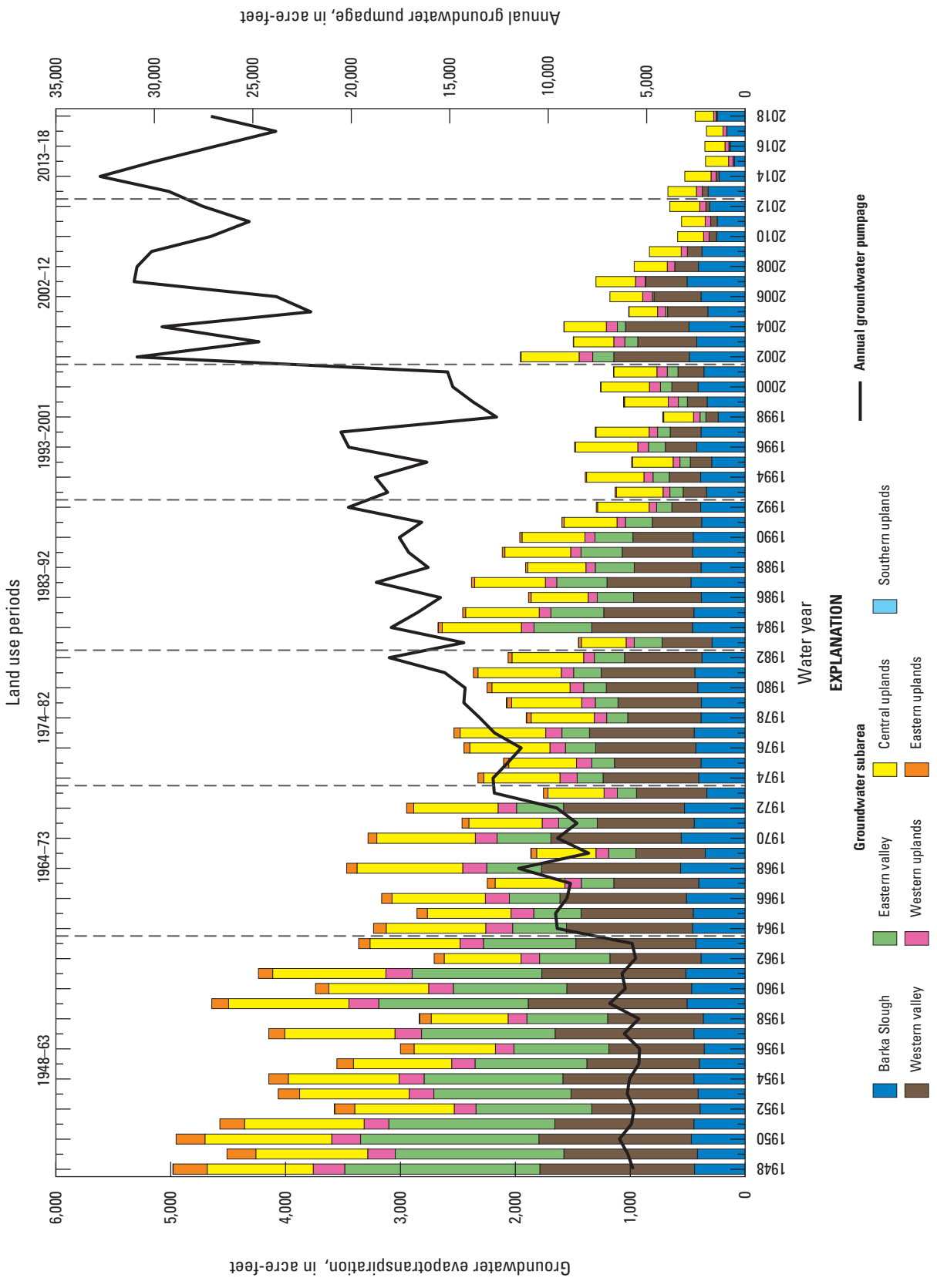

Figure 31. Annual groundwater evapotranspiration for groundwater subareas and annual groundwater pumpage simulated using the San Antonio Creek Valley integrated model, Santa Barbara County, California.

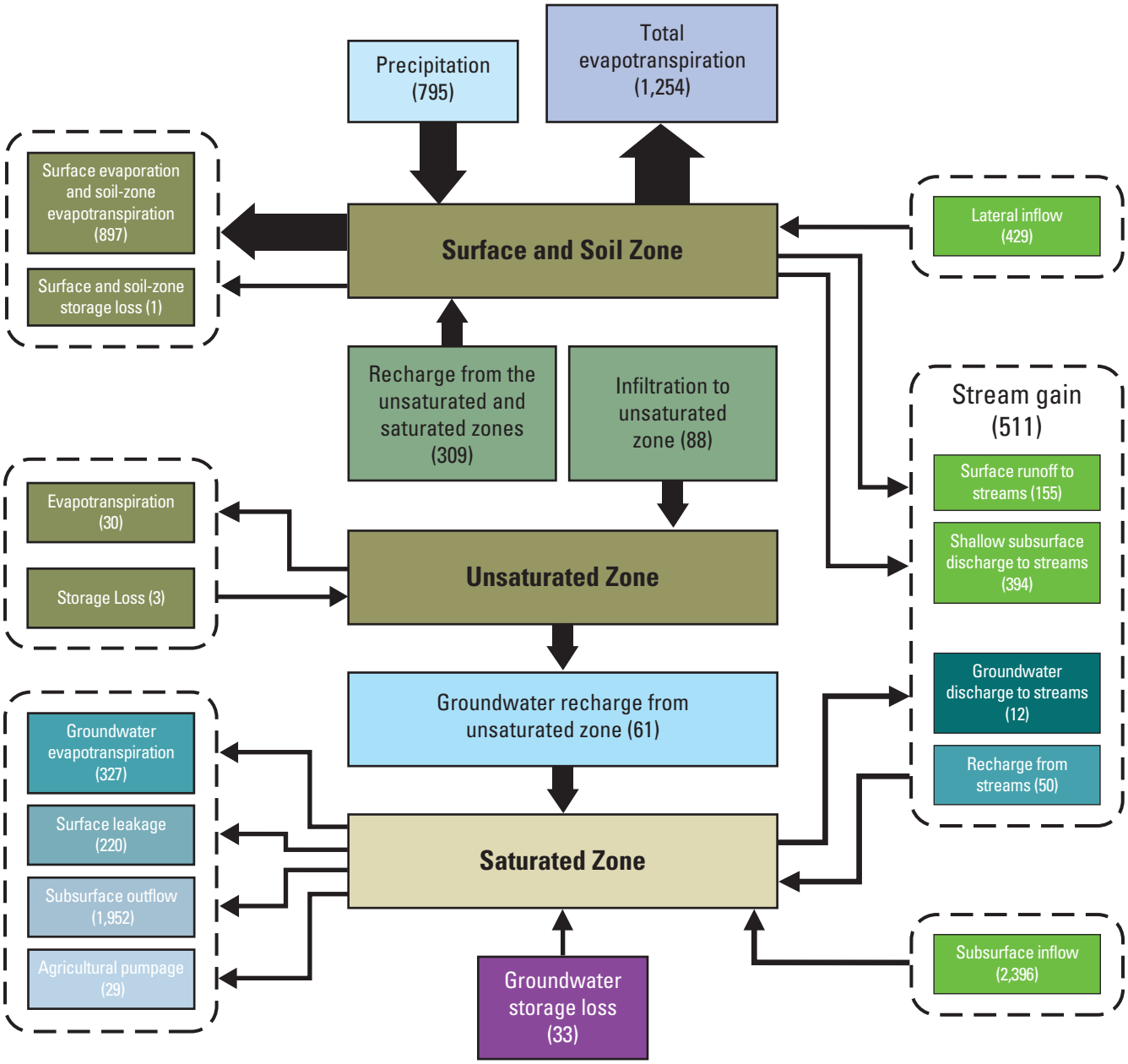

Values in acre-feet per year for water years 1981–2018. Lateral inflow to the surface and soil zone is flow through the shallow subsurface. Surface leakage is a component of outflow from the saturated zone that discharges to the surface and soil zone. Subsurface inflow and outflow is groundwater flow to and from Barka Slough, respectively.

Figure 32. Simulated average hydrologic budget components for water years 1981–2018, San Antonio Creek integrated model, Santa Barbara County, California.

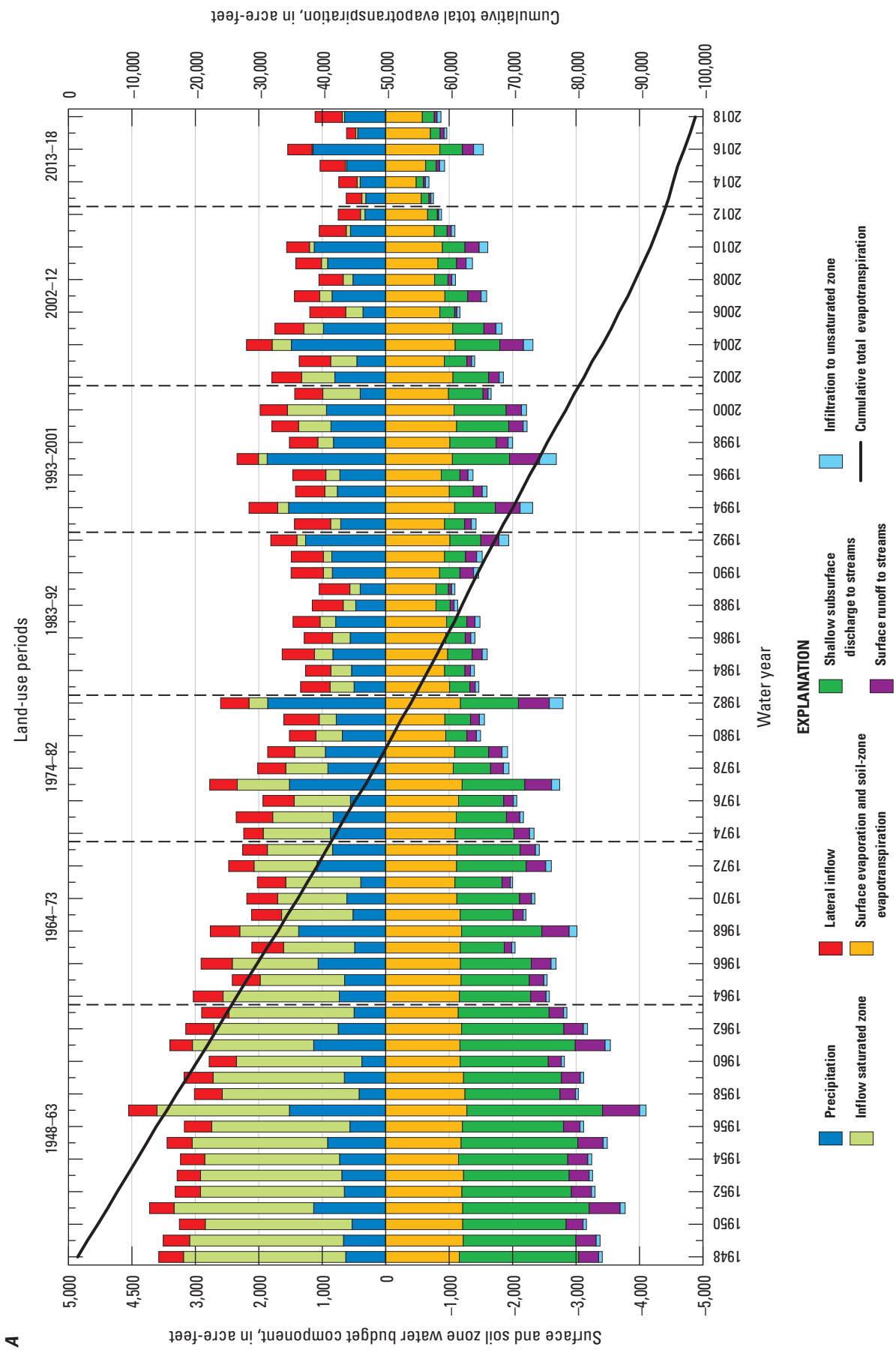

Figure 33. Simulated *A*, water-budget components for the surface and soil zone and cumulative total evapotranspiration; and *B*, water-budget components for the saturated zone for Barka Slough, and annual pumpage in the San Antonio Creek Valley integrated model, Santa Barbara County, California.

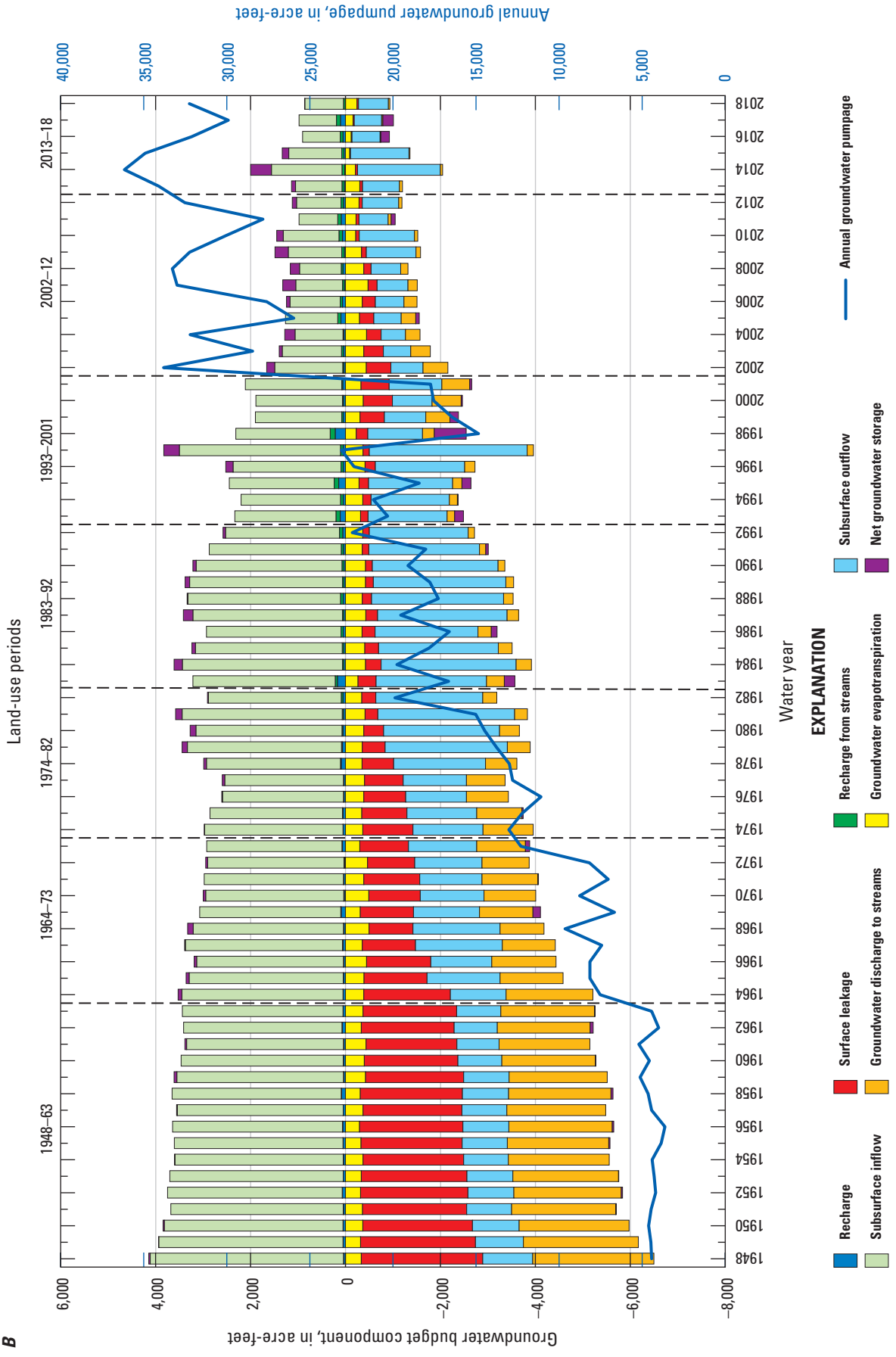

Figure 33.—Continued

Table 15. Hydrologic budget components for Barka Slough simulated using the San Antonio Creek Valley integrated model, Santa Barbara County, California.

[Groundwater budget components are total values for 1948–80 and 1981–2018 in acre-feet; surface leakage is groundwater outflow from the saturated zone that discharges to the surface and soil zone]

Hydraulic budget component	1948–80	1981–2018	Percent change
Surface and soil-zone water budget			
Inflows			
Precipitation	25,892	30,194	–17
Net recharge from the unsaturated zone	49,491	8,411	83
Lateral inflow	13,825	16,312	–18
Outflows			
Surface evaporation and soil-zone evapotranspiration	38,407	34,104	11
Surface runoff	9,293	5,905	36
Shallow subsurface discharge to streams	42,017	14,973	64
Saturated-zone water budget			
Inflows			
Net subsurface inflow	65,636	15,827	76
Recharge from unsaturated zone	1,690	2,294	–36
Net stream leakage	–3,828	1,455	138
Outflows			
Groundwater evapotranspiration	12,200	12,429	–2
Surface leakage	51,768	8,364	84

For the saturated zone, subsurface inflow was the main inflow during the 1948–80 and 1981–2018 periods. Subsurface inflow declined 32 percent from the earlier period to the later period (table 15). The relative contribution of subsurface inflow to total inflow decreased from 98 to 95 percent from the earlier to the later period. The main outflows for the 1948–80 period were surface leakage (groundwater discharge to the surface and soil zone), groundwater discharge to streams, and subsurface outflow; the main outflow for the 1981-2018 period was subsurface outflow (fig. 33*B*). Groundwater flow from Barka Slough to other parts of the SACVW increased with increasing pumpage, resulting a decrease in surface leakage and groundwater discharge to streams by 84 and 89 percent, respectively, and increased subsurface outflow by 37 percent from earlier period to the later period (table 15). The relative contribution of surface leakage to total outflow decreased from 47 to 11 percent from the earlier to the later period. In contrast, the relative contribution of subsurface outflow to total outflow increased from 38 to 73 percent from the earlier to the later period.

Pumping, particularly for irrigation, in other parts of the SACVW has resulted in declining groundwater levels and reduced flow to Barka Slough, which reduces upward flow from the saturated zone to the soil zone. While lateral inflow into the surface and soil zone was relatively stable, possibly sustained by an increase in irrigation return flow from agricultural pumping, subsurface inflow to the saturated zone underlying Barka Slough declined during the simulation period. Reductions in subsurface inflow to the saturated zone and groundwater flow from the saturated zone to the surface and soil zone with increasing groundwater pumpage in the SACVW (fig. 33*B*) indicate that perennial groundwater discharge to Barka Slough may cease in the future if current climate conditions and land-use practices continue; however, increases in shallow-subsurface flow from increased irrigation-return flow may partially mitigate losses in perennial groundwater discharge to Barka Slough.

Model Limitations

A model is an idealized approximation of the actual system that is based on average and estimated conditions. The capability of the SACIM to reliably reproduce hydrologic responses is related to the accuracy of the input data and conceptual model and is inversely related to the magnitude of the changes in the hydrologic stress being applied to the model and the length of the simulation period. Data limitations affected the estimates of pumpage used in the model. Measured data were available only for municipal and military pumping; agricultural pumpage was not measured and, therefore, was estimated as irrigation demand calculated by the AG package in MF-NWT and compared with reported estimates (Muir, 1964; Hutchinson, 1980; Martin, 1986, Tetra Tech, Inc., 2012; Cromwell and others, 2022). The lack of information on the location and construction of agricultural wells also added uncertainty to the distribution of pumpage, possibly resulting in excess or insufficient pumpage in some locations. The limitations associated with estimating agricultural pumpage likely contribute to the mismatch between the simulated heads and the measured groundwater levels for some observation wells.

The complexity of the groundwater-flow system was represented by a hydrogeologic-framework model developed based on lithologic information from drillers' logs for wells in the SACVW. Available borehole-geophysical data were limited; a larger and more robust dataset would likely provide better estimates that better represent the spatial variability of hydraulic properties.

The SACIM was calibrated to streamflow and groundwater-level data. Although streamflow data were available for various periods of record for the five streamgages, additional continuous long-term records would help to calibrate the PRMS model MF-NWT models more accurately in the SACIM. Long-term groundwater-level data with increased spatial coverage in the uplands and additional depth-dependent groundwater-level data also would help to more accurately calibrate the SACIM.

The SACIM synthesizes current data and understanding of the SACVW. The overall fit of the SACIM to measured groundwater levels and streamflow was reasonable based on the mean, median, minimum, and maximum residuals and RMSE, and NMRSE for comparing simulated hydraulic head and measured groundwater levels, and the mean, minimum, and maximum residuals and NSE, NNSE, PAEE, and AAEE for comparing simulated streamflow to measured streamflow. When applied carefully, the model can provide insight to the hydrology of the SACVW and responses to various changes in stresses to the groundwater and surface-water systems. Potential changes in stresses can be assessed by comparing simulated results from specific management scenarios with the simulated results from the calibrated SACIM. However, caution should be used when evaluating simulated results (1) in areas with sparse calibration data, (2) in areas where simulated results do not fit the measured data well, or (3) generated from climatic or pumping conditions that are substantially different from conditions used to calibrate the SACIM. Additional information on the spatial and temporal distribution of agricultural pumpage and spatial distributions of lithologic and well construction data, and collection of additional streamflow and groundwater-level data, could improve the accuracy of simulated results and reduce uncertainty in simulated future water-resource management scenarios.

Summary and Conclusions

Water managers in the San Antonio Creek Valley must deal with the challenges of maintaining sustainable groundwater supplies while trying to meet increased groundwater demand. To address these challenges, Santa Barbara County Water Agency, Vandenberg Space Force base, and the U.S. Geological Survey (USGS), began a cooperative study to characterize the integrated hydrologic system of the San Antonio Creek Valley watershed (SACVW) and develop tools to better understand and manage the groundwater system. The San Antonio Creek Valley integrated model (SACIM) was developed to better understand the hydrology of the SACVW. This report documented the development of the SACIM and presented simulated hydrologic and groundwater budgets. This report included detailed descriptions of the watershed- and groundwater-component models of the SACIM, calibration of the SACIM, and simulation results.

The SACIM used the coupled groundwater and surface-water flow model (GSFLOW), which consisted of two integrated model components: (1) a watershed component developed using the Precipitation Runoff Modeling System (PRMS) and (2) a groundwater-component model developed using the Newton formulation of the Modular Groundwater Flow model MODFLOW-NWT (MF-NWT). The PRMS model was used to simulate hydrology of the land surface, vegetation, and soil zone. The MF-NWT model was used to simulate the properties and processes of the unsaturated and saturated zones, streams, and the interaction between groundwater and surface water.

The watershed component of the model had 15,484 hydrologic response units (HRUs); each HRU was a grid-based cell with dimensions of 492 ft on each side. The HRUs were connected using a network of cascades and stream segments. Surface-water runoff and interflow were routed by cascades to the stream segments; the stream segments routed streamflow to one outflow point on the boundary of the watershed.

PRMS parameters that described land-surface characteristics were topography, soil properties, percent developed impervious area, and land-use representing the years 1959, 1968, 1977, 1986, 1996, 2006, and 2016. Climate input to PRMS was distributed to each HRU and consisted of daily values of precipitation and minimum and maximum temperature (T_{min} and T_{max}, respectively) for the model simulation period, water years 1948–2018. Potential evapotranspiration (PET) in PRMS was directly proportional to the Jensen-Haise coefficient (*jh_coef*). Monthly values for jh_coef were calibrated to observed Penman-Montieth ET_0; the calibrated jh_coef values were multiplied by the crop coefficient (KC) to produce a new jh_coef value for each HRU for every month. Monthly KCs were assigned to sparse land use, riparian, and agricultural subcategories in the model and took into account the growth cycle of crops and provided an index of the integrated effect of vegetation characteristics (reflectance, roughness, and plant physiology) on PET. Calibrations of KCs for these land-use subcategories were important to the SACVW water budget, specifically agricultural pumping and ET.

The MF-NWT model consisted of 4 layers on a grid of 124 rows, 269 columns, and uniform model cells with a length of 492 feet per side. All layers were convertible and could switch between confined and unconfined flow. Hydraulic properties (hydraulic conductivity, vertical anisotropy, specific storage, and specific yield) were spatially distributed by hydrogeologic units that were defined by hydrostratigraphic units to each cell in the model grid. Lateral boundary conditions that controlled the interactions between the SACVW and adjacent areas included no-flow and head-dependent boundaries. The model was divided into subareas for assessment of model fit and evaluation of water budgets.

Sources of inflow to the groundwater system included recharge in areas not containing stream channels, recharge from streams, irrigation-return flow, and subsurface inflow from an adjacent basin. Groundwater outflow from the SACVW included pumping, evapotranspiration, groundwater discharge to streams, and groundwater discharge to the soil zone or land surface. Reported municipal and military pumpage was used in the SACIM. Agricultural pumpage was estimated by using the Agricultural Water Use (AG) package in MF-NWT to simulate irrigation demand. Simulated agricultural pumpage over the model period is consistent with reported estimated values. Streams superimposed on the SACVW aquifer system were divided into segments and reaches. There were 203 segments divided into 1,638 reaches in the SACIM. Recharge to the groundwater system was influenced by the vertical saturated hydraulic conductivity (VKS) of the unsaturated zone; surface hydraulic conductivity (SURFK) and the average height of undulations of the land surface (SURFDEP) were used to calculate rejected recharge and surface leakage (groundwater flow to the surface and soil zone minus the infiltration to the unsaturated zone from the surface and soil zone).

The first step of model calibration was performed using the PRMS-only mode for water years 2003–16 to ensure the PRMS component in the SACIM was properly simulating the surface-ET processes. Comparisons of simulated and observed solar radiation and reference evapotranspiration (ET_0) data indicated an overall good fit of simulated values to observed data. However, potential ET was slightly overestimated in the summer and underestimated in the winter at the Camelback location. Potential ET also was underestimated in the summer and overestimated in the winter at the Los Alamos location.

Calibration of the SACIM for transient conditions during water years 1948–2018 was completed using trial-and-error and automated methods. Model parameters were adjusted to achieve reasonable fits between (1) simulated and measured streamflow and (2) simulated hydraulic heads and measured groundwater levels. Observations within each of the 11 observation groups were given weights such that any one observation group did not dominate the calibration process. The calibration process of the SACIM consisted of adjusting the initial estimates of the properties for the land-surface, soil-zone, unsaturated zone, stream-channels, and aquifer system. The SACIM was calibrated using monthly streamflow records from 5 streamgages, groundwater levels at 148 wells, and prior estimates of agricultural pumpage as observations. In addition, the reported value for the ratio of precipitation to total evapotranspiration (ET) was used to constrain the simulated ET. Regularization was used to help constrain the degree of parameter variability to reasonable values during the calibration process.

PRMS parameters were adjusted during the calibration of the SACIM using one-dimensional multipliers that scaled the magnitude of each parameter within the model domain while maintaining the initial relative spatial distribution of the parameter. Initial monthly KCs for sparse, riparian, and agricultural land were adjusted during the calibration of the integrated model using one-dimensional multipliers that scaled the magnitude of each monthly KC within each land-use subcategory while maintaining the initial relative temporal distribution of the parameter. An additional seasonal ramp down factor was used for crops that are irrigated primarily from April through September.

Parameters in the MF-NWT model adjusted during model calibration consisted of hydraulic properties (hydraulic conductivity, specific yield, specific storage, and vertical and horizontal anisotropy), streambed hydraulic conductivity, and the VKS, SURFK, and SURFDEP of the unsaturated zone. The hydraulic properties were calibrated using parameter zonation and pilot points. Pilot points were added in all layers during model calibration to provide additional information for characterizing the heterogeneity of the hydraulic conductivity within the parameter zones. The stream segments were grouped into 13 zones during model calibration; each zone was assigned a value of streambed conductivity. The VKS, SURFK, and SURFDEP were calibrated using one-dimensional multipliers.

Sensitivity analysis was used to assess the effects of different parameter values on observation data, including measured groundwater levels and streamflow, reported estimates of agricultural pumpage, and prior information. The most sensitive parameters in the SACIM were the streambed hydraulic conductivity in zone 7 (sfr_k7) and the vertical anisotropy in parameter zone 8433 in model layer 4 (vani4z8433). Other sensitive parameters were related to soil moisture, soil-zone and groundwater storage properties, horizontal anisotropy, and streambed hydraulic conductivity.

The normalized root mean square error (NMRSE) for the match between simulated heads and measured groundwater levels was 10 percent or less for most subareas; the only subarea with an NMRSE greater than 10 percent had the smallest number of observations; therefore, the overall fit of the SACIM to measured data was considered reasonable. The Nash-Sutcliffe efficiency (NSE) and normalized NSE statistics for streamflow indicated that the calibration at streamgage San Antonio Creek near Casmalia, California (USGS station 11136100) indicated an improved model fit relative to the mean of the measured data. The SACIM reasonably simulated observed declines in measured groundwater levels during the simulation period (water years 1948–2018); however, simulated hydraulic heads generally underestimated the measured data. Mismatches between simulated heads and measured water levels were attributed in part to the uncertainties in the spatial and vertical distributions of agricultural wells, uncertainties in the parameters in the SACIM used to estimate agricultural pumpage, and local variability in hydraulic properties within the parameter zones that were not represented in the model.

Comparisons of simulated and measured monthly mean streamflow for the streamgages San Antonio Creek at Los Alamos, California (USGS station 11135800), and San Antonio Creek near Casmalia, California (USGS station 11136100), showed that streamflows simulated using the SACIM reasonably matched the timing and frequencies of peak streamflows and the magnitudes of monthly fluctuations in the measured streamflow data. Measured base flow at San Antonio Creek near Casmalia, California (USGS station 11136100), also was simulated reasonably well using the SACIM; however, simulated streamflows generally overestimated peak streamflows at this streamgage.

Results of calibrated model simulations indicated that simulated groundwater pumpage exceeded recharge in most years, resulting in an estimated cumulative depletion of groundwater storage during the 71-year simulation period. Between October 1947 and September 2018, 924,700 acre-ft of water was recharged into the SACVW, and 1,020,000 acre-ft of groundwater was withdrawn from the basin by pumpage, resulting in groundwater storage depletion of 453,300 acre-ft. Agricultural pumpage was the largest discharge in the SACIM. Groundwater pumping resulted in simulated groundwater levels declining by more than 100 to 150 ft relative to initial groundwater level conditions. Declines in groundwater levels depended on the layer and groundwater subarea. The decline in groundwater levels resulted from the depletion of groundwater storage. The simulated decline in groundwater levels resulted in simulated decreases in natural discharge from the SACVW and simulated reductions of groundwater inflow to Barka Slough.

References Cited

Allander, K.K., Niswonger, R.G., and Jeton, A.E., 2014, Simulation of the Lower Walker River Basin hydrologic system, west-central Nevada, using PRMS and MODFLOW models: U.S. Geological Survey Scientific Investigations Report 2014–5190, 93 p. [Available at https://doi.org/10.3133/sir20145190.]

Allen, R.G., Pereira, L.S., Raes, D., and Smith, M., 1998, Crop evapotranspiration—Guidelines for computing crop water requirements: Rome, Italy, —FAO Irrigation and Drainage Paper 56. v. 300, no. 9, p. D05109.

Anderson, M.R., and Woessner, W.W., 1992, Applied groundwater modeling simulation of flow and advective transport: San Diego, Calif., Academic Press, 381 p.

Bright, D.J., Nash, D.B., and Martin, P., 1997, Evaluation of ground-water flow and solute transport in the Lompoc area, Santa Barbara County: U.S. Geological Survey Water-Resources Investigations Report 97–4056, 113 p. [Available at https://doi.org/wri974056.]

Brush, C.F., Belitz, K., and Phillips, S.P., 2004, Estimation of a water budget for 1972–2000 for the grasslands area, central part of the western San Joaquin Valley, California: U.S. Geological Survey Scientific Investigations Report 2004–5180, 51 p. [Available at https://doi.org/10.3133/sir20045180.]

California Department of Water Resources, 2016, California's groundwater, working toward sustainability: California Department of Water Resources Bulletin 118, Interim Update 2016, accessed May 23, 2018, at https://www.water.ca.gov/Programs/Groundwater-Management/Bulletin-118.

California Department of Water Resources, 2021a, SGMA Basin Prioritization Dashboard: accessed September 16, 2021, at https://gis.water.ca.gov/app/bp-dashboard/final/.

California Department of Water Resources, 2021b, Sustainable Groundwater Management Act (SGMA): accessed September 16, 2021, at https://water.ca.gov/Programs/Groundwater-Management/SGMA-Groundwater-Management.

California Irrigation Management Information System, 2017a, CIMIS station reports: accessed June 26, 2017, at https://cimis.water.ca.gov/WSNReportCriteria.aspx.

California Irrigation Management Information System, 2017b, CIMIS spatial reports: accessed October 10, 2017, at https://cimis.water.ca.gov/SpatialData.aspx.

California Irrigation Management Information System, 2020, CIMIS overview: accessed October 26, 2020, at https://cimis.water.ca.gov/.

County of Santa Barbara, 2010, Los Alamos community plan update, final environmental impact report: v. II, Appendices, 127 p., accessed August 30, 2021, at https://www.countyofsb.org/plndev/policy/communityplans/losalamos.sbc.

Cromwell, G., Densmore, J.N., Sweetkind, D.S., Engott, J.A., Seymour, W., Larsen, J.D., and Ely, C.P., 2022, Hydrogeologic characterization of the San Antonio Creek Valley watershed, Santa Barbara County, California: U.S. Geological Survey Scientific Investigations Report 2022–5001, 129 p. [Available at https://doi.org/10.3133/sir20225001.]

Descheneaux, R.V., 1975, New water wells in San Antonio watershed: Vandenberg Air Force Base Environmental Impact Report, 4392d Civil Engineering Squadron, 19 p.

Doherty, J., 2010, PEST, model-independent parameter estimation—User manual (5th ed., with slight additions): Brisbane, Australia, Watermark Numerical Computing.

Doherty, J.E., and Hunt, R.J., 2010, Approaches to highly parameterized inversion—A guide to using PEST for groundwater-model calibration: U.S. Geological Survey Scientific Investigations Report 2010–5169, 59 p. [Available at https://doi.org/10.3133/sir20105169.]

Drost, B.W., Ely, D.M., and Lum, W.E., II, 1999, Conceptual model and numerical simulation of the ground-water flow system in the unconsolidated sediments of Thurston County, Washington: U.S. Geological Survey Water-Resources Investigations Report 99–4165, 106 p. [Available at https://doi.org/10.3133/wri994165.]

Ely, C.P., Cromwell, G., Sweetkind, D.S., Larsen, J.D., Koehl, C.A., and O'Leary, D.R., 2022, Data release of hydrogeologic data from the San Antonio Creek Valley watershed, Santa Barbara County, California, 2015–2019: U.S. Geological Survey data release available at https://doi.org/10.5066/P9AD7DL8.

Ely, D.M., and Kahle, S.C., 2012, Simulation of groundwater and surface-water resources and evaluation of water-management alternatives for the Chamokane Creek basin, Stevens County, Washington: U.S. Geological Survey Scientific Investigations Report 2012–5224, 74 p. [Available at https://doi.org/10.3133/sir20125224.]

Freeze, R.A., and Cherry, J.A., 1979, Groundwater: Englewood Cliffs, N.J., Prentice Hall, 604 p.

Gardner, M.A., Morton, C.G., Huntington, J.L., Niswonger, R.G., and Henson, W.R., 2018, Input data processing tools for the integrated hydrologic model GSFLOW: Environmental Modelling & Software, v. 109, p. 41–53. [Available at https://doi.org/10.1016/j.envsoft.2018.07.020.]

Harbaugh, A.W., 2005, MODFLOW-2005—The U.S. Geological Survey modular ground-water model—The ground-water flow process: U.S. Geological Survey Techniques and Methods 6–A16. [Available at https://doi.org/10.3133/tm6A16.]

Henson, W.R., Medina, R.L., Mayers, C.J., Niswonger, R.G., and Regan, R.S., 2013, CRT—Cascade routing tool to define and visualize flow paths for grid-based watershed models: U.S. Geological Survey Techniques and Methods 6–D2, 28 p. [Available at https://doi.org/10.3133/tm6D2.]

Hill, M.C., 1998, Methods and guidelines for effective model calibration: U.S. Geological Survey Water-Resources Investigations Report 98–4005, 90 p. [Available at https://doi.org/10.3133/wri984005.]

Hill, M.C., Banta, E.R., Harbaugh, A.W., and Anderman, E.R., 2000, MODFLOW-2000, the U.S. Geological Survey modular ground-water model—User guide to the observation, sensitivity, and parameter-estimation processes and three post-processing programs: U.S. Geological Survey Open File Report 2000–184, 210 p. [Available at https://doi.org/10.3133/ofr00184.]

Howes, D.J., Fox, P., and Hutton, P.H., 2015, Evapotranspiration from natural vegetation in the central valley of California—Monthly grass reference-based vegetation coefficients and the dual crop coefficient approach: Journal of Hydrologic Engineering, v. 20, no. 10, p. 04015004-1–04015004-17.

Hutchinson, C.B., 1980, Appraisal of ground-water resources in the San Antonio Creek Valley, Santa Barbara County, California: U.S. Geological Survey Open File Report 80–750, 48 p. [Available at https://doi.org/10.3133/ofr80750.]

Konikow, L.F., Hornberger, G.Z., Halford, K.J., and Hanson, R.T., 2009, Revised multi-node well (MNW2) package for MODFLOW ground-water flow model: U.S. Geological Survey Techniques and Methods 6–A30, 67 p. [Available at https://doi.org/10.3133/tm6A30.]

LANDFIRE, 2014, Existing vegetation type layer, LANDFIRE 1.4.0: U.S. Department of the Interior, U.S. Geological Survey, accessed March 27, 2017, at https://landfire.cr.usgs.gov/viewer/.

Markstrom, S.L., Regan, R.S., Hay, L.E., Viger, R.J., Webb, R.M.T., Payn, R.A., and LaFontaine, J.H., 2015, PRMS-IV, the precipitation-runoff modeling system, version 4: U.S. Geological Survey Techniques and Methods 6–B7, 158 p. [Available at https://doi.org/10.3133/tm6B7.]

Markstrom, S.L., Niswonger, R.G., Regan, R.S., Prudic, D.E., and Barlow, P.M., 2008, GSFLOW-coupled ground-water surface-water flow model based on the integration of the precipitation-runoff modeling system (PRMS) and the modular ground-water flow model (MODFLOW-2005): U.S. Geological Survey techniques and Methods 6–D1, 240 p. [Available at https://doi.org/10.3133/tm6D1.]

Martin, P., 1985, Development and calibration of a two-dimensional digital model for the analysis of the ground-water flow system in the San Antonio Creek Valley, Santa Barbara County, California: U.S. Geological Survey Water-Resources Investigations Report 84–4340, 68 p. [Available at https://doi.org/10.3133/wri844340.]

Muir, K.S., 1964, Geology and ground water of San Antonio Creek Valley, Santa Barbara County, California: U.S. Geological Survey Water Supply Paper 1664, 53 p. [Available at https://doi.org/10.3133/wsp1664.]

National Centers for Environmental Information, 2019, Global historical climatology network—Daily, ver. 3: accessed April 2, 2019, at https://www.ncei.noaa.gov/access/search/data-search/daily-summaries.

Nishikawa, T., ed., 2018, Santa Barbara and Foothill groundwater basins geohydrology and optimal water resources management—Developed using density dependent solute transport and optimization models: U.S. Geological Survey Scientific Investigations Report 2018–5059, variously paged. [Available at https://doi.org/10.3133/sir20185059.]

Niswonger, R.G., 2020, An agricultural water use package for MODFLOW and GSFLOW: Environmental Modelling & Software, v. 125, 16 p. [Available at https://doi.org/10.1016/j.envsoft.2019.104617.]

Niswonger, R.G., and Prudic, D.E., 2005, Documention of the streamflow routing (SFR2) package to include unsaturated flow beneath streams—A modification to SFR1: U.S. Geological Survey Techniques and Methods 6–A13, 48 p. [Available at https://doi.org/10.3133/tm6A13.]

Niswonger, R.G., Panday, S., and Ibaraki, M., 2011, A Newton formulation for MODFLOW-2005: U.S. Geological Survey Techniques and Methods 6–A37, 44 p. [Available at https://doi.org/10.3133/tm6A37.]

Niswonger, R.G., Prudic, D.E., and Regan, R.S., 2006, Documentation of the unsaturated-zone flow (UZF1) package for modeling unsaturated flow between the land surface and the water table with MODFLOW-2005: U.S. Geological Survey Techniques and Methods 6–A19, 62 p. [Available at https://doi.org/10.3133/tm6A19.]

PRISM Climate Group, 2013, 30-year normals: PRISM Climate Group database, Oregon State University, accessed February 16, 2017, at https://prism.oregonstate.edu/.

Regan, R.S., and LaFontaine, J.H., 2017, Documentation of the dynamic parameter, water-use, stream and lake flow routing, and two summary output modules and updates to surface-depression storage simulation and initial conditions specification options with the precipitation-runoff modeling system (PRMS): U.S. Geological Survey Techniques and Methods 6–B8, 60 p. [Available at https://doi.org/10.3133/tm6B8.]

Regan, R.S., Markstrom, S.L., and LaFontaine, J.H., 2020, PRMS version 5.1.0—Precipitation-runoff modeling system (PRMS): U.S. Geological Survey Software Release, May 01, 2020.

Regan, R.S., and Niswonger, R.G., 2021, GSFLOW version 2.2.0—Coupled groundwater and surface-water flow model: U.S. Geological Survey Software Release, February 18, 2021.

Reitz, M., Sanford, W.E., Senay, G.B., and Cazenas, J., 2017, Annual estimates of recharge, quick-flow runoff, and evapotranspiration for the contiguous U.S. using empirical regression equations: Journal of the American Water Resources Association, v. 53, no. 4, p. 961–983. [Available at https://doi.org/10.1111/1752-1688.12546.]

Sanford, W.E., and Selnick, D.L., 2012, Estimation of evapotranspiration across the conterminous United States using a regression with climate and land-cover data: Journal of the American Water Resources Association, v. 49, no. 1, p. 217–230. [Available at https://doi.org/10.1111/jawr.12010.]

Santa Barbara County, 2019, Daily rainfall: accessed March 24, 2019, at http://www.countyofsb.org/pwd/dailyrain.sbc.

Snyder, R.L., Lanini, B.J., Shaw, D.A., and Pruitt, W.O., 1994, Using reference evapotranspiration and crop coefficients to estimate crop evapotranspiration for agronomic crops, grasses, and vegetables: Cooperative Extension University of California Division of Agriculture and Natural Resources Leaflet 21427, 12 p., at https://cimis.water.ca.gov/Content/PDF/21427-KcAgronomicGrassandVeg.pdf.

Snyder, R.L., Orang, M., Bali, K., and Eching, S., 2014, Basic irrigation scheduling (BIS): Regents of the University of California, accessed April 20, 2020, at http://biomet.ucdavis.edu/irrigation_scheduling/bis/BIS.htm.

Tetra Tech, Inc., 2012, Final historical water balance of the San Antonio groundwater basin: Tetra Tech Inc., Pasadena, California, prepared for Vandenberg Air Force base, California, 82 p.

Tetra Tech, Inc., 2013, Final groundwater model of the San Antonio basin: Tetra Tech Inc., Santa Maria, California, prepared for Vandenberg Air Force base, California, 129 p.

Tikhonov, A.N., and Arsenin, V.Y., 1977, Solution of ill-posed problems: V.H. Winston, Washington D.C., 258 p.

U.S. Census Bureau, 2010, Explore Census Data: accessed September 11, 2019, at https://data.census.gov/cedsci/.

U.S. Department of Agriculture, 2016, Soil survey geographic (SSURGO) database: U.S. Department of Agriculture, Natural Resources Conservation Service, accessed November 14, 2016, at https://websoilsurvey.sc.egov.usda.gov/.

U.S. Geological Survey, 2013, National elevation dataset: accessed January 19, 2017, at https://viewer.nationalmap.gov/basic/.

U.S. Geological Survey, 2016, National hydrography dataset (ver. USGS National Hydrography Dataset Best Resolution (NHD) for Hydrologic Unit (HU) 8-18060009 (published 20161230)): accessed January 19, 2017, at https://www.usgs.gov/core-science-systems/ngp/national-hydrography/access-national-hydrography-products.

U.S. Geological Survey, 2021, USGS water data for the Nation: U.S. Geological Survey National Water Information System database, accessed August 31, 2021, at https://doi.org/10.5066/F7P55KJN.

Welter, D.E., White, J.T., Hunt, R.J., and Doherty, J.E., 2015, Approaches in highly parameterized inversion—PEST++ version 3, a Parameter ESTimation and uncertainty analysis software suite optimized for large environmental models: U.S. Geological Survey Techniques and Methods 7–C12, 54 p. [Available at https://doi.org/10.3133/tm7C12.]

Western Regional Climate Center, 2017, RAWS sites: accessed October 17, 2017, at https://wrcc.dri.edu/wraws/scaF.html.

White, J., Fienen, M., Barlow, P., and Welter, D., 2018, A tool for efficient, model-independent management optimization under uncertainty: Environmental Modelling & Software, v. 100, p. 213–221. [Available at https://doi.org/10.1016/j.envsoft.2017.11.019.]

Williams, L.E., 2001, Irrigation of winegrapes in California: accessed May 6, 2020, at https://www.yumpu.com/en/document/view/25179133/irrigation-of-winegrapes-in-california-by-larry-williams.

Woodring, W.P., and Bramlette, M.N., 1950, Geology and paleontology of the Santa Maria district, California: U.S. Geological Survey Professional Paper 222, 185 p., 23 pls. [Available at https://doi.org/10.3133/pp222.]

Xian, G., Homer, C., Dewitz, J., Fry, J., Hossain, N., and Wickham, J., 2011, The change of impervious surface area between 2001 and 2006 in the conterminous United States: Photogrammetric Engineering and Remote Sensing, v. 77, no. 8, p. 758–762.

For more information concerning the research in this report, contact the

Director, California Water Science Center
U.S. Geological Survey
6000 J Street, Placer Hall
Sacramento, California 95819
https://www.usgs.gov/centers/ca-water/

Publishing support provided by the U.S. Geological Survey
Science Publishing Network, Sacramento Publishing Service Center

ISSN 2328-0328 (online)
https://doi.org/10.3133/sir20215139